Separation of proteins
by
simulated moving bed
chromatography

Joukje Houwing

Separation of proteins by simulated moving bed chromatography

Proefschrift

ter verkrijging van de graad van doctor
aan de Technische Universiteit Delft,
op gezag van de Rector Magnificus prof. dr. ir. J.T. Fokkema,
voorzitter van het College voor Promoties,
in het openbaar te verdedigen op dinsdag 10 juni 2003 om 16:00 uur

door Joukje HOUWING

doctorandus in de scheikunde en scheikundig ingenieur
geboren te Gorredijk

Dit proefschrift is goedgekeurd door de promotoren:
Prof. dr. ir. L.A.M. van der Wielen
Prof. ir. K.Ch.A.M. Luyben

Samenstelling promotiecommissie:
Rector Magnificus, voorzitter
Prof. dr. ir. L.A.M. van der Wielen, Technische Universiteit Delft, promotor
Prof. ir. K.Ch.A.M. Luyben, Technische Universiteit Delft, promotor
Prof. dr. ir. G.W.K. van Dedem, Technische Universiteit Delft
Prof. dr. ir. J.T.F. Keurentjes, Technische Universiteit Eindhoven
Prof. dr. ir. P.J. Jansens, Technische Universiteit Delft
Prof. dr. ir. R.M. Boom, Wageningen University
Prof. dr.-ing H. Schmidt-Traub, Universität Dortmund, Duitsland

Reserve commissielid:
Prof. dr. ir. J.J. Heijnen, Technische Universiteit Delft.

Ing. H.A.H. Billiet heeft als begeleider in belangrijke mate aan de totstandkoming van dit proefschrift bijgedragen.

Het in dit proefschrift beschreven onderzoek werd uitgevoerd aan het Kluyverlaboratorium voor Biotechnologie, Julianalaan 67, 2628 BC Delft.

Het onderzoek werd mede mogelijk gemaakt door een financiële bijdrage van het ministerie van Economische Zaken, in het kader van het innovatief onderzoeksprogramma milieutechnologie-preventie (IOP-MP).

ISBN 90-6464-943-X.

Contents

1. Introduction 7
2. Mass transfer effects during separation of proteins in SMB by size exclusion 17
3. Azeotropic phenomena during separation of dilute mixtures of proteins by simulated moving bed chromatography 45
4. Optimization of azeotropic protein separations in gradient and isocratic ion exchange SMB 51
5. Positioning of salt gradients in ion exchange SMB 75
6. Effect of salt gradients on the separation of dilute mixtures of proteins by ion exchange in SMB 101
7. A generalized approach for flow selection in SMB: separation of concentrated protein mixtures by gelfiltration 131

Outlook 159

Summary 163

Samenvatting 167

Dankwoord 171

Curriculum Vitae 173

Publicaties 175

1

Introduction

Conventional chromatography: the problem

Where would biotechnologists and pharmacist be without liquid chromatography? Column liquid chromatography can help in separation of almost any mixture of components, to yield pure proteins, peptides, or synthetical formulae for application in e.g. food and pharma. This versatility is a result of many ways to establish a difference in affinity of components for a sorbent phase. The affinity can be based on size, charge or hydrophobicity, and can frequently be modulated by the addition of solvents (in reversed phase chromatography) or salts (in ion exchange or hydrophobic interaction chromatography). Furthermore, there are many sorbents available, each with its own specific application area.

Although almost any separation is technically feasible, the efficiency of conventional fixed bed chromatography may be (too) low for industrial application. Current process scale chromatographic separations suffer from a few drawbacks:

- the sorbent inventory is high, which implies high costs, as the sorbents are costly (approximately 0.5 €/mL);
- the use of (salty) buffers is large, which is very undesired with respect to environmental, as well as cost aspects;
- products can only be harvested in a diluted form, which imposes the requirement for further processing.

These drawbacks are inherent to the current operation of chromatography. Chromatography columns are operated batch-wisely, which involves a small loading time, combined to a large time to elution. Meanwhile, mass transfer and equilibrium effects lead to the broadening of bands and the dilution of the separating fractions.

This observation formed an important argument for the startup of the Ph-D project on “More Efficient Process Chromatograpy”, which was carried out at Groningen State University (by Jaap Bosma and Hans Wesselingh) and Delft University of Technology.

More efficient chromatographic methods

In literature, a few methods to improve chromatographic efficiency are described. Some promising examples are:

- displacement chromatography;
- two way chromatography;

- recycle chromatography;
- simulated moving bed chromatography.

In *displacement chromatography* (Horváth *et al*., 1981; Subramanian *et al.*, 1988, Brooks and Cramer, 1992), a displacer is introduced after the feed injection. The displacer has a high affinity towards the chromatography resin, which results in the development of an “isotachic train”, and array of narrow, highly concentrated peaks of the pure components in order of their affinity. The displacement train is a result of the roll-up effect that takes place when species interfere.
Although displacement chromatography produces very pure and concentrated products, it has some severe drawbacks. One drawback is that the bands in the isotachic train are very narrow, which makes the harvest of the pure products a non-trivial task. A second drawback is the need to introduce an additional, strongly adsorbing species, which is undesired as it is hard to be removed from the resin.

In *two way chromatography* (Bailly and Tondeur, 1981), displacement effects are exploited as well. In two way chromatography, there is no addition of an additional displacing species. By the alternation of the direction of flow, the more retained species in the feed serve as the displacer for the less retained species. Two way chromatography may lead to an elevation of the concentration. However a serious drawback is that it is by far too complex for separation of a multicomponent mixture.

The important feature of *recycle chromatography* (Bailly and Tondeur, 1982) is that products are harvested from the column before complete resolution has taken place. Only the pure fronts and tails of the peaks are collected, whereas the “unseparated” fraction leaving the column is mixed with fresh feed and re-supplied to the column. This way of operation minimizes the losses of feed as the result of improper resolution, however, at the expense of column volume due the reintroduction of the (diluted) recycle. A second drawback is the possible accumulation of undesired components, which is feared in pharmaceutical applications.

In *Simulated Moving Bed (SMB) chromatography*, not only the liquid, but also the resin is (simulated to) be in motion (Ballanec and Hotier, 1993). This countercurrent contact allows the continuous fractionation of a feed in two product fractions. The countercurrent operation assures a high driving force towards mass transfer. In the SMB, it is sufficient when the products exist in pure form only at the product outlet ports. All these processes lead to a very efficient use of resin. As a result of the low dilution of products, the consumption of eluent can be reduced compared to fixed bed chromatography. In the SMB system, the feed is continuously recycled in the system. This is advantageous from an efficiency point of view; however, it makes distinction of separate batches impossible. This was initially seen as a drawback of the technology in pharmaceutical applications.

Based on these considerations, we have decided to study the use of simulated moving bed chromatography. In the SMB, it seems to be possible to reduce both resin inventory and eluent consumption and maintain a high product concentration at the same time. This is not possible using the other "more efficient" options, which lead to improvement at only one of these points. Further advantages of SMB over the other options are that SMB is applicable to large scale processes and does not involve any additional species that are hard to recover.

A short history of simulated moving bed chromatography

Already in the early 1960's simulated moving bed systems were developed. The pioneering patent of Broughton of UOP (Broughton, 1961) describes the setup of the SMB system, and its application in petrochemical industry. Since then, the technique found several large scale applications, for instance in fractionation of saccharides (e.g. separation of glucose and fructose), xylenes, olefins and paraffins (Johnson and Kabza, 1993). The SMB according to the most used Sorbex layout is schematically depicted in Figure 1. It consists of four sections, which are numbered I through IV. The liquid and sorbent move countercurrently, as is indicated by arrows in the figure. Both liquid and sorbent are recycled. At the "center" of the system, a feed (F) is introduced. The desorbent (D), introduced at the bottom, serves for regeneration of the column. The more retained components in the feed are predominantly transported in their sorbed form, and move downwards along with the resin. They are harvested in the extract product. The less retained components move upwards along with the liquid. They are harvested in the raffinate product. The direction of movement is determined by the ratio of the liquid to sorbent flow rate. A high ratio results in upward movement of the components.

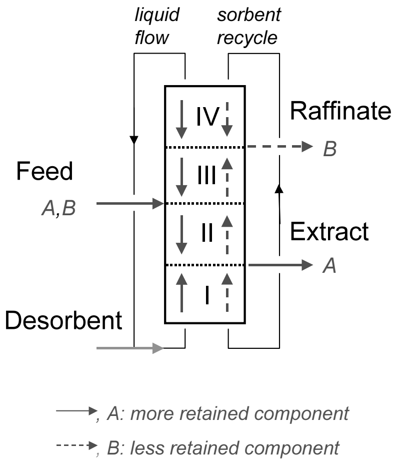

Figure 1. Schematic representation of SMB.

Actually, we just described a True Moving Bed system, a system where both liquid and sorbent move. In chromatography systems, the sorbent cannot move, since this devastates resolution. The movement of the sorbent is simulated instead. This is done by dividing the sorbent bed in small fractions, to the size of one column. Thus, the system consists of (say) twelve interconnected columns. Once per switch interval, the sorbent is moved one column in the opposite direction of liquid movement, thus simulating downward sorbent movement. Usually, three or four columns per section are sufficient to simulate the countercurrent movement (Hidajat *et al.*, 1986). After a number of cycles, the SMB is at a cyclic steady state: the profiles in the columns do not change going from one switch to another.

The SMB only functions properly when the ratio of liquid to sorbent flow rate has been chosen properly. Only then, complete separation, that is when there is a pure extract of the more retained component as well as a pure raffinate of the less retained component, can be achieved. The design of systems obeying linear isotherms, such as in separation of glucose and fructose, is relatively easy (Ruthven and Ching, 1989). However, the design of a separation with non-linear isotherms is much more complicated. That is why the new developments in SMB technology have only been initiated in the late 1980's, after development of fast computers.

Since then, robust design procedures have been developed for systems obeying Langmuir and Stoichiometric isotherms. The basis of these design procedures lies in wave theory (Helfferich and Klein, 1970, Rhee *et al.*, 1970, 1971). The currently most used procedure for flow selection in SMB has been developed by Morbidelli and coworkers (Storti *et al.*, 1989, 1993). This method is also termed "triangle theory", as a reference to the triangularly shaped regions that form the "working area". Other procedures have been described as well (Ma and Wang, 1997, Hashimoto *et al.,* 1988; Ruthven and Ching, 1989). Also, much attention has been paid to the computation of the profiles and performance of the SMB at given settings (Ruthven and Ching, 1989; Zhong and Guiochon, 1994, 1996; Yun *et al.,* 1997).

Research Challenges

At the start of this project, only few applications of SMB in biotechnology were described in literature; e.g. Maki *et al.,* (1987), Hashimoto *et al.,* (1988), Huang et al., (1988), Adachi (1994), Gottschlich *et al.,* (1996), Van Walsem and Tompson (1997). Most of these considered a rather experimental setup, without the application of a robust design procedure. This defined the niche to position the current project in. The aims of this project were defined as:

- demonstrate the possibility of fractionation of mixtures of proteins by Simulated Moving Bed chromatography;
- develop methods for flow selection of the specific separations;
- optimize the fractionation processes.

The use of a gradient in salt concentration in the SMB was defined as a promising option for further improvement of ion exchange SMB processes.

Model system

The developed theories needed to be verified by experiments, using a model system. First, we opted for an industrially relevant model separation, i.e. the production of Human Serum Albumin (HSA). This protein is present in concentrations up to 60 g/L in the human blood, where it is responsible for the maintenance of the osmotic value of the blood. It also serves as a transport protein. In case of severe blood loss, HSA has to be replenished by infusion. Hence, the world market in HSA is large; it was estimated at 400 tons/year in 1998 (Kerry-Williams *et al.*, 1998). HSA for infusion purposes is currently obtained from human blood donation. However, this carries a hazard for viral infections, such as hepatitis and HIV. Hence, there is a tendency towards the recombinant production of HSA, as exemplified by the activities of Delta Biotechnology and the Japanese Green Cross (Goodey *et al.*, 1996; Kobayashi *et al.*, 1996).

The recombinant HSA used in this project was produced in fed batch fermentations of recombinant *Pichia pastoris* (De Hulster, 1997). The moss-green fermentation broth indeed contained *r*HSA, but also many other components which were not identified. The latter resulted in multiple peaks during chromatography and a time-consuming and troublesome quantitative analysis by capillary electrophoresis (Jacobs, 1998). As these were severe drawbacks that impeded the progress of the project, it was decided to leave the *r*HSA model system, and use a synthetic mixture of BSA (the bovine analog of HSA) and horse myoglobin as the model solution during the remainder of the project. The advantages of this model protein mixture are the relatively low price, the availability and the easy spectrophotometric detection.

Outline of this thesis

This research on simulated moving bed systems was started on size exclusion chromatography, for its relative ease of the design in terms of the liquid and solid flow rate ratios. However, it was hard to obtain complete separation, since mass transfer effects play an important role at the low diffusivity of the large protein molecules in combination with the large sorbent particles used in the experiments. Chapter 2 describes the results and considers the optimization of the particle size in SMB.

The subsequent chapters describe the separation of mixtures of proteins by ion exchange SMB. In chapter 3, the concept of a salt gradient SMB is introduced and the procedure for its design, based on the “triangle theory” of Morbidelli and coworkers is addressed. Also, the azeotropic situations that may occur by choosing incorrect concentrations of salt in the desorbent and feed solution are described.

The azeotrope is also the subject of chapter 4. The salt concentrations in the feed and the desorbent entering the gradient SMB and the flow rate ratios are optimized with respect to industrial optimization functions, such as throughput, desorbent consumption and salt consumption.

Chapter 5 addresses the experimental formation of the salt gradient in the SMB. Sodium chloride interacts with the ion-exchange resin used (Q-Sepharose FF) at the applied high salt concentration, which asks for an additional design step.

The subsequent chapter (chapter 6) describes the experimental verification of the salt gradient SMB, in particular the ion exchange separation of dilute mixtures of BSA and myoglobin, using sodium chloride gradients on Q-Sepharose FF.

In the final chapter (chapter 7), a general procedure is developed for selection of flow rate ratios for SMB separation of binary mixtures with arbitrary (convex or concave) isotherms. It is applied to the separation of proteins by size exclusion chromatography from concentrated feed solutions, where isotherms are no longer linear.

The thesis concludes by a summary in English, and a summary in Dutch.

Literature

Adachi, S., “Simulated moving bed chromatography for continuous separation of two components and its application to bioreactors”, *J. Chromatogr.*, **658**, 271 (1994).

Bailly, M. and D. Tondeur, “Two-way chromatography: flow reversal in non-linear preparative liquid chromatography,” *Chem. Eng. Sci.*, **36**, 455 (1981).

Bailly, M. and D. Tondeur, “Recycle optimization in non-linear productive chromatography I Mixing recycle with fresh feed”, *Chem. Eng. Sci.*, **37**, 1199 (1982).

Ballanec, B. and G. Hotier, “From batch to simulated countercurrent chromatography,” In: *Preparative and production scale chromatography,* G. Ganetsos and P.E. Barker (eds.), Marcel Dekker, New York (1993).

Brooks, C.A. and S.M. Cramer, “Steric mass-action ion-exchange: displacement profiles and induced salt gradients,” *A.I.Ch.E. J.*, **38**, 1969, (1992).

Broughton, US patent 02985589 (1961).

Goodey, A.R., D. Sleep, H. van Urk, S. Berenzenko, J.R. Woodrow, R.A. Johnson, P.C. Wood, S.J. Burton and A.V. Quirk, “Process of high purity albumin production”, International patent WO 96/37515 (1996).

Gottschlich, N., S. Weidgen and V. Kasche, “Continuous biospecific affinity purification of enzymes by simulated moving bed chromatography:

Theoretical description and experimental results," *J. Chromatogr.*, **719**, 267, (1996).

Hashimoto, K., S. Adachi and Y. Shirai, "Continuous desalting of proteins with a simulated moving bed adsorber", *Agric. Biol. Chem*., **52**, 2161 (1988).

Helfferich, F.G. and G. Klein, "Multicomponent chromatography: theory of interference," Marcel Dekker, New York (1970).

Hidajat, K., C.B. Ching and D.M. Ruthven, "Simulated countercurrent adsorption processes: a theoretical analysis of the effect of subdividing the adsobent bed," *Chem. Eng. Sci.,* **41**, 2953 (1986).

Horváth, C., A. Nahum and J.H. Frenz, "High performance displacement chromatography," *J. Chromatogr.,* **218**, 365 (1981).

Huang, S.H., W.S. Lee and C.K. Lin, "Enzyme separation and purification using improved simulated moving bed chromatography," in: *Horizontals of biochemical engineering*, S. Aiba (ed), Oxford university press (1988).

Hulster, de A.F., "Development of a fed-batch fermentation protocol for high-cell-density cultivation of recombinant Pichia pastoris, Human Serum Albumin production", internal report ref. 9610, BIRD Engineering BV, Delft (1997).

Jacobs, L., "Large scale production of recombinant HSA with the yeast *Pichia pastoris*," final report TwAiO –project, Delft University of Technology (1998).

Johnson, J.A. and R.G. Kabza, "Sorbex: industrial-scale adsorptive separation," In: *Preparative and production scale chromatography,* G. Ganetsos and P.E. Barker (eds.), Marcel Dekker, New York (1993).

Kerry-Wiliams, S.M., S.C. Gilbert, L.R. Evans and D.J. Ballance, "Disruption of the *Saccharomyces cerevisiae YAP3* gene reduces the proteolytic degradation of secreted recombinant human serum albumin," *Yeast*, **14**, 161 (1998).

Kobayashi, K., K. Tomomitsu, S. Kuwae, T. Ohya, T. Ohda and T. Omura, "Process for producing proteins," EP 0 736 605 A1 (1996).

Ma, Z. and N.-H. L. Wang, "Standing wave analysis of SMB chromatography: linear systems," *A.I.Ch.E. J.*, **43,** 2488 (1997).

Maki, H., H. Fukuda and H. Morikawa, "The separation of glutathione and glutamic acid using a simulated moving bed adsorber system," *J. Ferment. Technol.*, **65**, 61 (1987).

Rhee, H.-K., R. Aris and N.R. Amundson, "On the theory of multicomponent chromatography," Phil. Trans. Roy. Soc. Lond. A., **267**, 419, (1970).

Rhee, H.-K., R. Aris and N.R. Amundson, “Multicomponent adsorption in continuous countercurrent exchangers,” *Phil. Trans. Roy. Soc. Lond. A.*, **269,** 187 (1971).

Ruthven, D.M. and C.B. Ching, “Countercurrent and simulated countercurrent adsorption separation processes,” *Chem. Eng. Sci.*, **44**, 1011 (1989).

Subramanian, G., M.W. Phillips and S.M. Cramer, “Displacement chromatography of biomolecules,” *J. Chromatogr.* **493**, 341 (1988).

Storti, G., M. Masi, S. Carrà and M. Morbidelli, “Optimal design of multicomponent countercurrent adsorption separation processes involving non-linear equilibria,” *Chem. Eng. Sci.*, **44**, 1329 (1989).

Storti, G., M. Mazzotti, M. Morbidelli and S. Carrà, “Robust design of binary countercurrent adsorption separation processes,” *A.I.Ch.E. J.*, **39**, 471 (1993).

Van Walsem H.J. and M.C. Thompson, “Simulated moving bed in the production of lysine,” *J. Biotechnol.*, **59**, 127 (1997).

Yun, T., G. Zhong and G. Guiochon, “Experimental study of the influence of the flow rates in SMB chromatography”, *A.I.Ch.E. J.*, **41**, 2970 (1997).

Zhong, G.M. and G. Guiochon, “Theoretical analysis of band profiles in non-linear ideal countercurrent chromatography”, *J. Chromatogr.*, **688**, 1 (1994).

Zhong, G.M. and G. Guiochon, “Analytical solution for the linear ideal model of simulated moving bed chromatography”, *Chem. Eng. Sci.,* **51**, 4307 (1996).

2

Mass transfer effects during separation of proteins in SMB by size exclusion

Abstract

The chromatographic fractionation of proteins by size exclusion chromatography in Simulated Moving Bed (SMB) is studied. During experimental fractionation of a mixture of Bovine Serum Albumin (BSA) and myoglobin on Sepharose Big Beads, mass transfer effects are shown to limit the performance of the SMB. The internal profiles as well as the extract and raffinate compositions are well described by a steady state equivalent TMB model that incorporates mass transfer effects.

The selection of the particle size in SMB is a trade off between productivity and mass transfer. Based on the equivalent TMB model, the optimum particle size and configuration of the SMB can be selected, at which preset performance criteria (purity, recovery) are met at specified flow rate ratios, total column length and pressure drop. For the current feed and apparatus, an optimal particle size of approximately 145 μm is calculated for achievement of purities and overall recoveries of 95%.

This paper has been published in: *A.I.Ch.E. J.* **49**, 665 (2003).

Introduction

In the production of biopharmaceutical proteins, size exclusion chromatography is a common method of choice as one of the last steps in purification. For example in the purification of recombinant Human Serum Albumin (*r*HSA), size exclusion is used for removal of dimeric forms as well as degradation fragments of HSA from the monomeric product (Berezenko *et al.*, 1996). Conventional size exclusion chromatography is a technique of low efficiency, which is predominantly caused by the limited selectivity of the resin material for the target protein or contaminants. To achieve a sufficiently high resolution at the small differences in distribution coefficients of the solutes to be separated, the ratio of sorbent material to feed volume is large. Only a diluted product can often be obtained. In order to obtain the required purity at a reasonable yield, recycling of product fractions may be needed. This further increases eluent and resin consumption.

Obviously, there is a need for more efficient size exclusion based processes. Simulated Moving Bed (SMB) technology seems an attractive alternative for these tedious separations. By SMB technology, a continuous feed is fractionated in two (or more) product streams, as is schematically depicted in Figure 1.

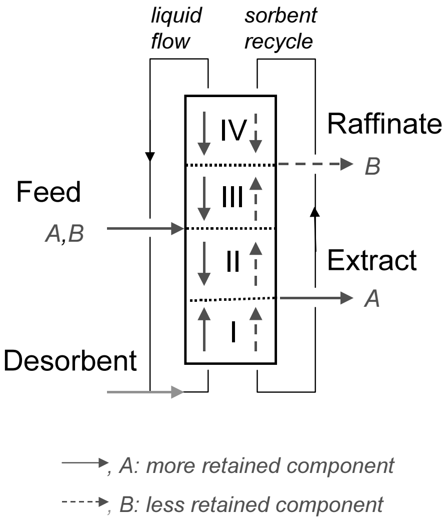

Figure 1. Schematic representation of SMB system. Arrows indicate the direction of movement of components.

In general, reduced sorbent and solvent needs compared to fixed bed chromatography have been reported (Ballanec and Hotier, 1993; Cavoy *et al.* 1997). Recently, the use of SMB technology has gained an increased interest for purification of various fine chemicals and biotechnology products. Examples of recent studies are the separation of enantiomers (Pais *et al.*, 1997; Cavoy *et al.*, 1997), amino acids (Wu *et al.*, 1998, Van Walsem and Thompson, 1997) and proteins (Houwing *et al.*, 1999; Gottschlich and Kasche, 1997). So far, size exclusion chromatography in SMB has only been reported for the fractionation of dextran polymers (Ruthven and Ching, 1989) as well as for the desalination of a single protein feed stream (Hashimoto, 1988).

A satisfactory performance of the SMB in terms of product purity can only be achieved after proper selection of the liquid and solid flow rates. Methods for selection of the liquid to sorbent flow rate ratios usually rely on a local equilibrium approach. In case of linear adsorption isotherms, the analysis is simple and based on separation factors ($S=\Phi_S K/\Phi_L$) (Ruthven and Ching, 1989). The procedure relies on recognition of the direction of movement of every component in every section required for separation, as is shown in Figure 1. Movement in upward direction requires a separation factor exceeding unity, whereas downward motion needs separation factors below unity. In case of non-linear adsorption isotherms, a more involved analysis based on wave theory is usually performed (Storti *et al.,* 1989; Wu *et al.,* 1998). “Triangle theory”, the approach of the group of Morbidelli (e.g. Storti *et al.*, 1993), defines a region of complete separation. Only when the ratios of liquid to sorbent flow rates in section II and III (cf. Figure 1) are chosen inside this region (and provided sections are of sufficient length), a pure extract and a pure raffinate product may be harvested, i.e. complete separation can occur. The ratios of liquid-to-resin flow rates in the various sections of a TMB system, $m=\Phi_L/\Phi_S$, are related to the flow rates Φ^{SMB} and switch time τ in the corresponding SMB system by (Migliorini *et al.*, 1999):

$$m = \frac{\Phi^{SMB}\cdot\tau - V\varepsilon - V_d}{V(1-\varepsilon)} \qquad \textbf{(1)}$$

where V is the volume of one column, ε is the bed porosity and V_d is the dead volume per column.

Equilibrium theory thus gives the necessary criteria for design of the SMB. However, these criteria are not sufficient, because mass transfer and pressure drop limitations further restrict the operating window. In this study, we focus on the selection of the particle diameter. The optimal particle diameter holds a compromise between productivity, which is limited by the pressure drop and hence favored by large particles, and mass transfer efficiency, which is favored by small particles. In practice, SMB particle size selection is often based on prior knowledge of fixed bed separations. However, this may not result in an optimal particle size for SMB, as a result of column sizing restrictions in the SMB (Charton and Nicoud, 1995). It may be useful to use larger particles in the SMB of fixed column length, in order to achieve the required purity and recovery at a maximum productivity.

The effect of mass transfer resistances on the performance of the SMB has been shown in several papers. Storti *et al*. (1989) based their analysis on dimensionless Stanton numbers, and showed that a minimal Stanton number is required to obtain a given separation performance. Zhong and Guiochon (1997) based the analysis of the effect of mass transfer resistances on simulations of the simulated moving bed under linear conditions; they showed the effect on profiles inside the columns. Wu *et al.* (1998) showed that mass transfer effect should be incorporated into the design of an SMB system for separation of amino acid mixtures. In their approach, the mass transfer and dispersion factors are added to the flow rate ratios obtained from equilibrium analysis. Azevedo and Rodrigues (1999) showed the shrinking of the region of complete separation as a function of mass transfer effects in case of linear isotherms. The boundaries to the region of complete separation were calculated by repetitively taking an incremental increase in flow rate ratios, and verifying the complete separation at these settings by numerical simulation. Migliorini *et al.* (1999b) did a similar job for isotherms of the bi-Langmuir type, where contours of given purity were calculated by numerical simulation as a function of the column mass transfer efficiency.

The optimization of particle size in SMB has been described by Charton and Nicoud (1995). The optimal particle size is found at the optimum defined by the maximum overall pressure drop and the mass transfer efficiency. In the analysis, it is assumed that the number of columns per section is equal in all sections. For pressure drop calculations, an average velocity has been taken. This approach is only useful in case of “symmetric” separations, of components of similar diffusivity and feed solutions containing similar concentrations of the two solutes to be separated.

In this study, we have analyzed the optimization of the particle selection for SMB fractionation of a mixture of proteins, where mass transfer resistances are relatively large. The fractionation of Bovine Serum Albumin (BSA) and myoglobin (myo) has been taken as a model separation, and has been studied both by experiment and model. The importance of mass transfer effects on separation performance is illustrated in experiments in an SMB with a small number of columns, containing relatively large gel particles. In addition, an analysis based on Stanton numbers has been performed, in order to select the optimal particle size.

Theory

Fixed bed and TMB models

The profiles in conventional fixed bed columns as well as in TMB systems have been simulated numerically. The basis of our models is the one-dimensional mass balances for the liquid and sorbent phases:

$$\begin{aligned} \frac{\partial c}{\partial t} &= -v\frac{\partial c}{\partial x} + E\frac{\partial^2 c}{\partial x^2} - \beta \cdot k_o a \cdot (q_{eq} - q) \\ \frac{\partial q}{\partial t} &= v_s \frac{\partial q}{\partial x} + k_o a \cdot (q_{eq} - q) \end{aligned} \qquad \textbf{(2)}$$

where c and q are the liquid and solid phase concentration, respectively, q_{eq} is the solid phase concentration in equilibrium with c. In this paper, only linear equilibria will be considered, hence $q_{eq} = Kc$, where K is the distribution coefficient. Variables v and v_s are the liquid and solid phase interstitial velocities, x is the distance in the column, E is the axial dispersion coefficient, β is the phase ratio ($(1-\varepsilon)/\varepsilon$) and $k_o a$ is the overall mass transfer coefficient. In case of a conventional fixed bed column, the solids velocity (v_s) obviously equals zero.

Mass transfer between the two phases is described using a linear driving force approximation. In order to simplify the set of equations, the axial dispersion term ($E\ \partial^2 c/\partial x^2$) has been omitted from equation (2) and been implemented in the overall mass transfer coefficient according to Glueckauf (Ruthven, 1984). The definition of the mass transfer coefficient, as given by Carta and Stringfield (1992), reworked in our symbols is:

$$\frac{1}{k_o \cdot a} = \frac{2 d_p K \beta}{v} + \frac{d_p}{6} \cdot \left(\frac{K}{k_L} + \frac{1}{k_S} \right) \tag{3}$$

The first term represents dispersion, the second term represents the mass transfer resistance in the liquid film surrounding the particle and the third term represents the mass transfer resistance in the pore liquid. In this equation, both left- and right-hand side have been divided by the interfacial area $a=6/d_p$, where d_p is the particle diameter. The liquid side mass transfer coefficient k_L is calculated from dimensionless relations involving the liquid side Sherwood number (Guiochon *et al.*, 1994):

$$Sh_L = \frac{1.903}{\varepsilon} \cdot Re^{0.33} \cdot Sc^{0.33} \quad \text{where}$$
$$Sh_L = \frac{d_p k_L}{D}, \quad Re = \frac{\rho v d_p}{\eta} \quad \text{and} \quad Sc = \frac{\eta}{D\rho} \tag{4}$$

The diffusion coefficients are assumed to be $D_{BSA}=6 \cdot 10^{-11} \text{m}^2/\text{s}$ and $D_{myo}=10.8 \cdot 10^{-11} \text{m}^2/\text{s}$ (Laurent and Killander, 1964). Furthermore, η is the viscosity and ρ is the liquid (water) density.

The solid side mass transfer coefficient k_S is calculated in a similar way from the solid side Sherwood number ($k_S=D_S\, Sh_S / d_p$). Sh_S has been used as a fitting parameter. The intraparticle diffusion coefficient (D_S) was calculated from the free liquid diffusion coefficient (D), the radius of the protein (r_p) and the particle solids fraction (ϕ_f) as was shown by Vonk (1994):

$$\frac{D_S}{D} = \exp\left(-\phi_f^{\,0.5} \cdot \lambda\right) \quad \text{where} \quad \lambda = \frac{r_p}{r_f} \tag{5}$$

The fiber diameter was assumed to be 1.7 nm as described for Sepharose matrices by Vonk (1994). The protein radii were obtained from the Stokes-Einstein relation, which relates the free diffusivity in water to the solute equivalent sphere diameter. For BSA and myoglobin, the calculated radii are 3.64 nm and 1.99 nm, respectively.

In order to calculate the profiles in fixed bed pulse experiments, the analytical solution of the mass balance equation (2) derived by Carta and Stringfield (1992) is used. This model neglects accumulation in the liquid phase. As suggested by the authors, one column void volume is added to the elution volumes of the peaks in order to be able to account for liquid phase accumulation.

The steady state profiles in the equivalent TMB are predicted by an analytical solution of the TMB mass balance equations. The model, which is similar to that of Ruthven and Ching (1989), is shown in the appendix. The basic equation is the mass balance of the liquid. At steady state, the accumulation in the liquid phase is zero, so the equation reduces to:

$$v\cdot\frac{dc}{dx}+\beta k_0 a\cdot\left(Kc-q\right)=0 \tag{6}$$

The relation between the solid and liquid phase concentrations is obtained from the overall mass balance over a countercurrent column from the liquid inlet side (position x=0) to position x:

$$q-q_0=\frac{v}{\beta v_s}\cdot\left(c-c_0\right) \tag{7}$$

The combination of these two equations results in a differential equation that can be integrated analytically, to yield the profile of one section at known inlet concentrations. When four section balances are combined to the "node-equations", i.e. the mass balances over in- and outlet ports, all concentrations in the equivalent TMB can be calculated.

Optimization of separation performance

The model described in the previous paragraph can be used for optimization of the performance of the SMB. The performance is indicated in terms of purity (P_E and P_R), recovery (R_E, R_R, $R_{ov,A}$ and $R_{ov,B}$, where the latter two indicate the overall recovery of the components in both extract and raffinate) and productivity, the amount of feed processed per unit of system volume (Pr). In this paper, the following definitions of these will be used:

$$\begin{aligned}
&P_E=\frac{c_{A,E}}{c_{A,E}+c_{B,E}} && P_R=\frac{c_{B,R}}{c_{A,R}+c_{B,R}}\\
&R_E=\frac{\left(m_2-m_1\right)c_{A,E}}{\left(m_3-m_2\right)c_{A,F}} && R_R=\frac{\left(m_3-m_4\right)c_{B,R}}{\left(m_3-m_2\right)c_{B,F}}\\
&R_{ov,A}=1-\frac{m_4c_{A,W}}{\left(m_3-m_2\right)c_{A,F}} && R_{ov,B}=1-\frac{m_4c_{B,W}}{\left(m_3-m_2\right)c_{B,F}}\\
&Pr=\frac{\Phi_F}{V_{tot}}=\frac{(m_3-m_2)v_s(1-\varepsilon)}{L_{tot}}
\end{aligned} \tag{8}$$

In equation (8), A is the more retained component and B is the less retained component, and the subscripts *E, F, R* and *W* denote the extract, feed, raffinate and waste, respectively. The variable L_{tot} represents the added column length.

In the following we will use the TMB model to optimize the purity and recovery as well as the productivity. In this analysis, it is assumed that the equilibrium- and mass transfer coefficients do not change when the sorbent particle is increased or reduced in size (Charton and Nicoud, 1995). Furthermore, we will only use TMB situations, i.e. where column lengths can have any value and are not restricted to an integer number of columns, such as in the SMB.

Optimization of purity and recovery

In the TMB model, only the Stanton numbers influence performance as soon as the flow rate ratios have been fixed. In order to obtain the system configuration (i.e. the lengths of the four sections) that result in a given purity and recovery, the Stanton number needs to be adjusted. This is conveniently done by varying the lengths of the four sections independently in the model, while keeping the variables m, d_p, v_s constant, until the imposed purity and (overall) recovery are met.

Optimization of productivity

As is clear from equation (8), the productivity is determined by the solids interstitial velocity v_s. This velocity is limited by the particle diameter. One the one hand, pressure drop restrictions only allow a high velocity at large particle diameters. On the other hand, mass transfer effects only allow a high velocity at small particle diameters. Obviously, there is a trade off, as is the case in conventional fixed bed chromatography.

For calculation of the **productivity limited by pressure drop**, we assume that the pressure drop per meter limits the flow rate applied in the SMB. The pressure drop per meter under laminar flow conditions is given by the Blake-Kozeny equation:

$$\Delta P / L = 170 \frac{\beta^2 \eta v_{\max}}{d_p^{\,2}} \tag{9}$$

The maximum productivity with respect to pressure drop is then calculated by combining eq. (8) and (9). The relation between v_{max} and v_s is obtained from eq.

(1). The resulting relation for the maximum productivity determined by pressure drop, at known total length is:

$$Pr_{\Delta p} = \left(\frac{(m_3 - m_2)}{\beta m_{\max} + 1 + \frac{V_d}{V\varepsilon}} \right) \cdot \frac{\varepsilon}{L_{tot}} \cdot \frac{\Delta P/_{L} \cdot d_p^{\,2}}{170\,\eta\beta} \tag{10}$$

It is assumed that the ratio of extra-column dead volume to column volume is constant, and independent of the system size.

The calculation of the **productivity limited by mass transfer effects,** is a matter of optimization of the Stanton numbers. In this case, a total column length is imposed, as are the purities and the overall recoveries of the two components (cf. equation (8)). At fixed values of m and d_p, there are five unknown variables (length of four sections and solids velocity), and five (implicit) equations (two for purity, two for recovery, one for total length). These can be solved using the TMB model. The calculation is repeated for various particle sizes.

As in conventional fixed bed chromatography, the **optimum particle size** is found by equating the maximum productivity defined by mass transfer limitations and defined by pressure drop limitations.

Experimental

SMB setup

The **laboratory-scale SMB** used in the experiments was built by the workshop of the Kluyver Laboratory. Four Shimadzu LC8a pumps are used for control of the desorbent, extract, feed and raffinate streams. These pumps are controlled by a Shimadzu LC10a system controller. The positions of the feed and effluent streams in the system are controlled by four twelve-port valves (Valco). Unidirectional flow is established by connection of the recycle stream to open air, analogous to Priegnitz (1996). A 24-port valve (Valco) serves for this purpose. In our experiments, the liquid waste stream was not recycled to the desorbent stream for further reduction of eluent. Valves were controlled by in-house developed computer software.

The **dead volume** connected to each individual column in the SMB system was 0.39±0.01 mL per column. This value is de difference between the residence times of pulses of dextran blue, tryptophan, BSA and myoglobin on 8 separate columns, and the same columns assembled in the SMB. The method for pulse residence time determination is given below.

In order to **monitor the actual flow rates** in the SMB system, samples of the extract, raffinate and waste streams were weighed.

Methods

For **preparation of the SMB-columns**, the matrix was packed in 1 cm diameter Omnifit glass columns at increasing flow rates up till 10 mL/min, resulting in columns of 8.9 cm length, 6.9 mL volume. The beds have a void fraction of 0.39 as was determined by dextran blue pulses. The packing quality of the columns was checked by pulses of dextran blue (Pharmacia Biotech Benelux) and tryptophan (Merck, Darmstadt). The retention times were 2.70±0.12 mL and 7.87±0.13 mL respectively. For preparation of a column for pulse experiments, a similar procedure was used. Packing was continued up till 6.5 mL/min, resulting in a column of 9.6 cm length.

Single column **pulse experiments** were performed on an FPLC system controlled by Unicorn version 2.01 (Amersham Pharmacia Biotech Benelux). Pulses of 100 μL containing 10 g/L protein were injected. Phosphate buffer was used as eluent. Various flow rates between 0.5 and 4 mL/min were used.

Off line **determinations of the concentrations of the proteins** were performed on a PDA spectrophotometer (HP 8435e UV-VIS spectroscopic system, Hewlett Packard). In addition, the concentrations of the two proteins were monitored by an in-line Shimadzu SPD-M10Avp Photo-diode array detector, operated under Class- VP-software (version 4.2, Shimadzu).

Using single-component calibration curves, the concentrations of myoglobin and BSA were calculated from the absorption at 405 and 280 nm. The absorption at 405 nm is attributed to myoglobin, since BSA absorption is negligible at that wavelength. From the absorption at 280 nm and the known concentration of myoglobin, the concentration of bovine serum albumin was calculated.

The **particle void fraction** was determined by weight. The density of a settled bed of particles was determined by weighing a measuring cylinder without (w_m) and with a gel slurry (w_s), with the slurry volume of water (w_{ws}) and with water of a volume equal to the settled bed volume (w_{wb}). The settled bed density ρ_s was calculated from:

$$\rho_b = \frac{w_s - w_m - w_{ws} + w_{wb}}{w_{wb} - w_m} \cdot \rho$$

The density of Big Beads was thus determined to be 1050 kg/m^3. The dry weight of the settled bed (dw_b) was determined in duplicate by drying at 105 °C for 2 hours. The obtained value, 63.8 g/L agrees well with the value of 63.4 g/L bed given by the manufacturer (Kon, personal communication). The fraction of fibers in the sorbent sphere (ϕ_f) was calculated from the above data with:

$$\rho_b = \varepsilon_{sb}\,\rho + (1-\varepsilon_{sb})(1-\phi_f)\rho + dw_b$$

where the porosity of the settled bed was estimated as 0.39. The thus obtained fraction of fibers was 0.022 mL fiber/mL sorbent sphere.

Materials

An underivatised Sepharose Big Beads **matrix**, which was a kind gift from Amersham Pharmacia Biotech Benelux, was used. This matrix with an average particle diameter of 200 μm is made of highly cross-linked agarose.

In all experiments, a 10 mM phosphate **buffer**, pH 7 containing 0.1 M NaCl was used as eluent. In the SMB experiments a feed solution containing 1 g/L myoglobin from horse heart (Sigma cat no. M1882, >90% pure) and 5 g/L Bovine Serum Albumin (Sigma, cat no. A7906) was used.

Results

Pulse experiments

Both the position and the shape of the response to pulse experiments were a strong function of the applied liquid velocity (see Figure 2 for BSA experiments). This supports the hypothesis that mass transfer resistances play an important role in the size exclusion of proteins on such large diameter particles and at high liquid velocities. Best fits of the analytical solution to the chromatograms were obtained when K_{myo}=0.88, K_{BSA}=0.65, and Sh_s=6.64. The best fits have been determined by the sum of the sum of squared errors SSE

(=$\Sigma(c_{measured}-c_{model})^2$) of all experiments. Figure 2 shows a comparison of the normalized experimental chromatograms and model predictions at a flow rate of 1 mL/min as an example. At higher flow rates, the accuracy of the prediction decreased; the SSE increased from 0.003 at a liquid flow rate of 1 mL/min to 0.09 at a liquid flow rate of 4 mL/min. At the high flow rates, the mass transfer effects were overpredicted by the model.

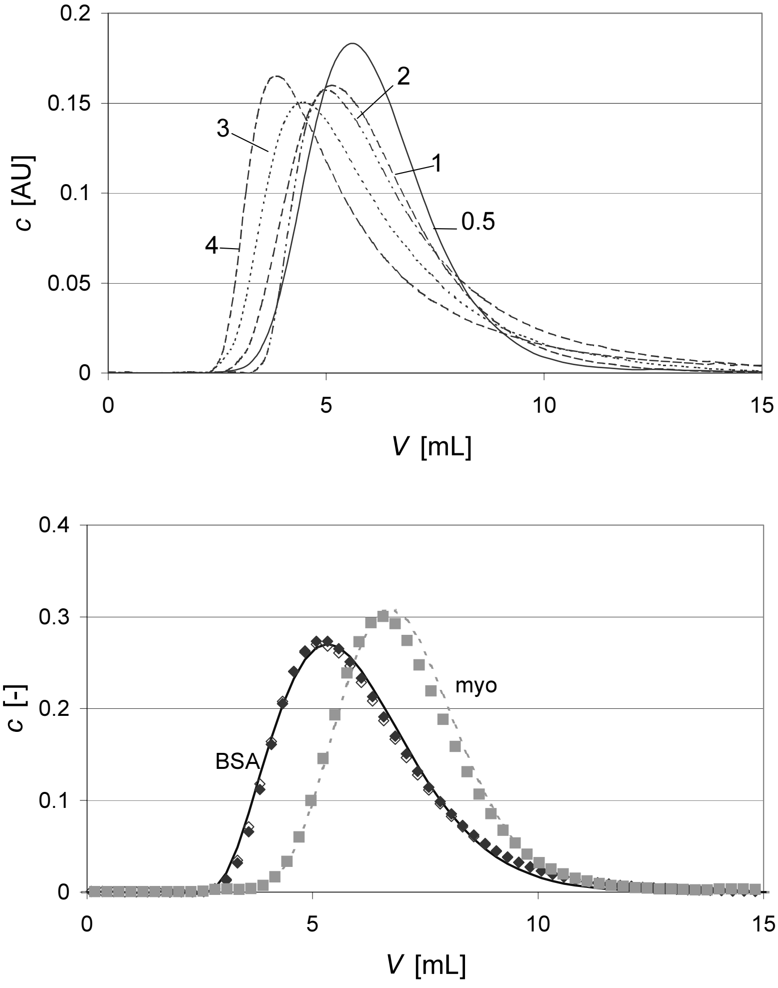

Figure 2. Top: Variations in experimental peak shape of pulses of BSA at different liquid velocities. Numbers indicate flow rates in mL/min. Bottom: Example of simulated pulse chromatograms at 1 mL/min calculated from analytical solution. Parameters used in simulation: K_{BSA}=0.65; K_{myo}=0.88; Shs=6.6.

SMB experiments

In neither of the five SMB experiments, of which the conditions are shown in Table I and Figure 3, 100% purity of either of the two products, was obtained (cf. Table I). Complete separation was expected in experiment II, III and IV, as these experiments were chosen well inside the ‘triangle of complete separation’ as is shown in Figure 3. This clearly reflects the effects of mass transfer limitations.

Table I. Experimental conditions, outlet concentrations and calculated purities.

Experiment	I	II	III	IV	V
m_1	1.02	1.02	1.02	1.02	1.02
m_2	0.62	0.66	0.72	0.78	0.84
m_3	0.66	0.70	0.76	0.82	0.88
m_4	0.33	0.31	0.30	0.31	0.31
c_{myo} Extract [g/L]	0.09	0.10	0.11	0.10	0.09
c_{BSA} Extract [g/L]	0.22	0.17	0.12	0.10	0.07
c_{myo} Raffinate [g/L]	0.00	0.01	0.01	0.02	0.04
c_{BSA} Raffinate [g/L]	0.28	0.31	0.31	0.34	0.35
c_{myo} Waste [g/L]	0.00	0.00	0.00	0.00	0.00
c_{BSA} Waste [g/L]	0.01	0.01	0.00	0.01	0.01
Purity Extract	0.30	0.38	0.47	0.50	0.54
Purity Raffinate	0.99	0.98	0.96	0.94	0.90

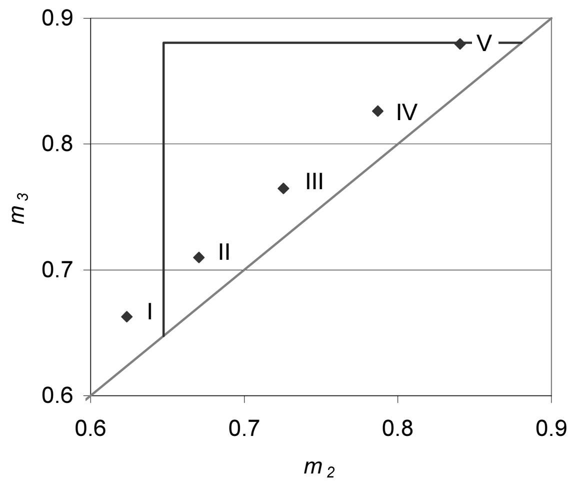

Figure 3. Position of experimental points (σ) relative to the region of complete separation for myoglobin and BSA. Roman numbers refer to experiment numbers in Table I.

Large mass transfer resistances result in broadening of the fronts between loaded and unloaded parts of the column. Hence, the tail of the desorptive front of BSA can extend beyond the extract outlet and result in a contamination of the extract stream with BSA. This is seen in Figure 4, which compares the measured concentrations leaving each column at the half of the cycle time (Ruthven and Ching, 1989) and the model predictions of the profile for experiment III.

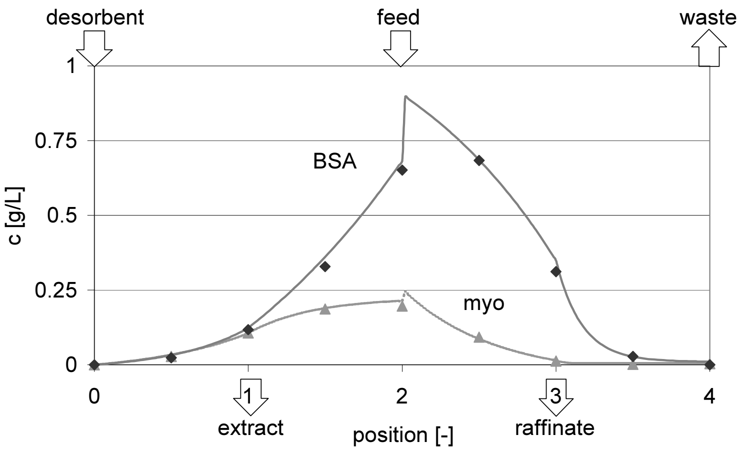

Figure 4. Experimental (symbols) and simulated (lines) concentration profiles along the laboratory scale SMB in experiment III.

Even though the harvested products are not pure, enrichment does occur. This illustrated by the concentration ratio of BSA to myoglobin. The feed solution contained 5 g/L BSA and 1 g/L myoglobin, a BSA to myoglobin ratio of 5. The extract is enriched in myoglobin, as shown by a decrease of this ratio to 1 in Figure 4. The raffinate is enriched in BSA, as shown by an increase of the ratio to 40.

The tendencies in the relation between variation in flow rate ratios and separation performance of the mass transfer limited size-exclusion-SMB agreed qualitatively with the expected SMB behavior. For instance, a simultaneous increase of the flow rate ratio in sections II and III results in an increased recovery of both components in the raffinate product and a decreased recovery of both proteins in the extract product. This is expected, since the upward transport of both BSA and myoglobin is favored by increasing flow rate. The quantitative agreement between experimental and predicted performance is good, as can be seen in Figure 5, which shows a comparison of the predicted and experimental recoveries as calculated from on-line analysis at steady state in the five experiments as a function of m_2.

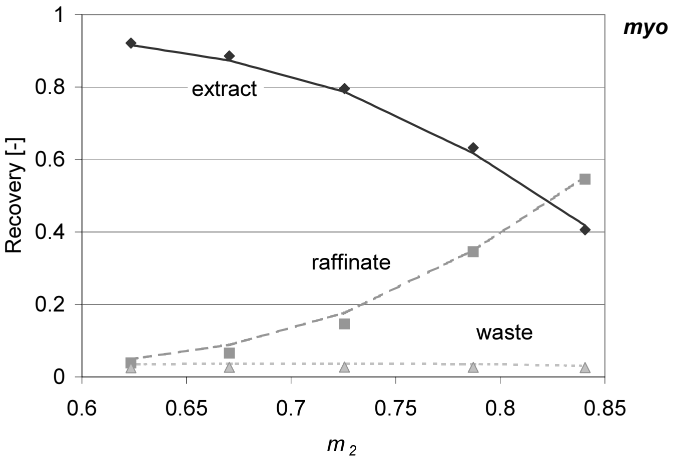

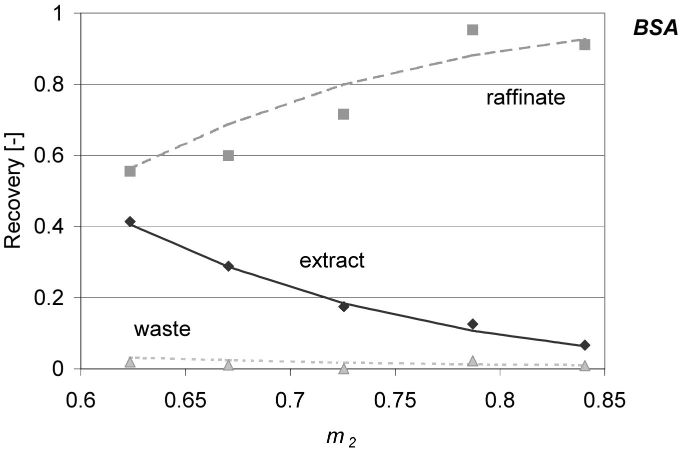

Figure 5. Recovery of myoglobin (top) and BSA (bottom) in extract, raffinate and waste streams. Symbols represent experimental values, lines indicate model predictions.

Optimization of purity and recovery

Obviously, the experimental Stanton numbers have been too low for attainment of complete separation. The Stanton numbers that are required to obtain a given purity and recovery were calculated using the TMB model. Arbitrarily, the extract and raffinate purity and overall recovery of both BSA and myoglobin have been chosen at 95%. The particle diameter and solids interstitial velocity were kept constant at the experimental values of 200 μm and 0.0013 m/s, respectively. At these constant values, only the column lengths per section determine the Stanton number; hence we only represented the section lengths calculated per experiment in Figure 6. This figure lacks data on experiment I, as this point has been chosen too far outside the region of complete separation to obtain the given purity and recovery using any combination of column lengths. In this case, equilibrium (rather than mass transfer) prohibits the attainment of complete separation.

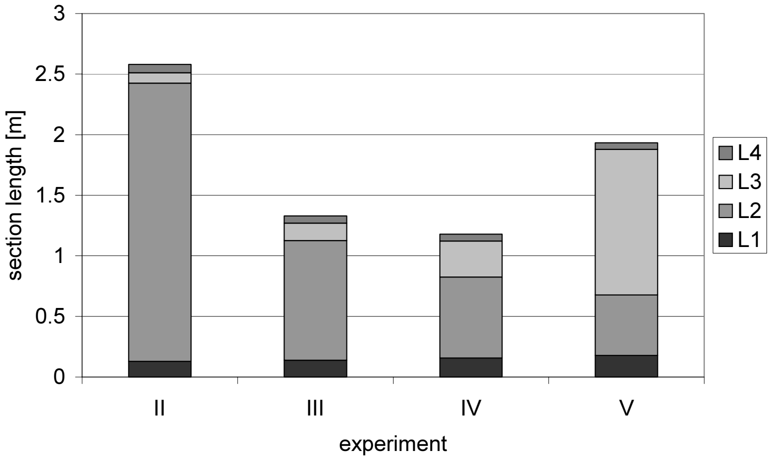

Figure 6. Optimal column length for achieving P_E=P_R=$R_{ov,A}$=$R_{ov,B}$=95%, d_p=200 μm, v_s=0.0013 m/s.

The figure shows that in all experiments, a rather short section I and IV will suffice. This agrees with the choice of the operating point, which is rather far from the respective boundaries. Section II and III require more length. It is seen that, travelling from experiment II to experiment V, the calculated required length of section II is decreased and the length of section III is increased. This is expected, as the operating points drift away from the m_2-boundary and more and more approach the m_3-boundary. The total length is minimal in experiment IV. This operating point is well inside the triangle, and closer to the m_3-boundary than to the m_2-boundary. This asymmetry reflects the asymmetric feed concentrations chosen; the change in concentration of BSA, with a feed concentration of 5 g/L, is much higher than that of myoglobin, with a feed concentration of 1 g/L.

Note that the analysis per section is not included in the procedure described by Charton and Nicoud (1995). This might lead to an unnecessary high efficiency of sections I, III and IV, or a too low efficiency in section II.

Optimization of productivity

For optimization of productivity as a function of the particle diameter, the system variables (total column length and maximum pressure drop), as well as the performance parameters are set at a chosen value. In practice, these are enforced by the available SMB system, or the requirements on the products. Essentially, this is an economic optimization. In this paper, we only optimized productivity as such, as the economic optimization contains many (company)specific figures. In this paragraph, the results are shown of optimization of the particle size with variable system length (Figure 7A), variable maximum allowed pressure drop per meter (Figure 7B) and variable separation performance (Figure 7C). This is done in order to sketch the variance in the optimal particle size. In all calculations, the m-values of experiment III were used. The base case was the situation with a total system length of 1 m, a pressure drop of 10^5 Pa/m and $P_E=P_R=R_{ov,A}=R_{ov,B}=95\%$. In the base case, the optimum particle diameter equaled 145 μm, which is indeed much smaller than the experimental 200 μm. In the base case, the optimal distribution of column length per section $L_1 : L_2 : L_3 : L_4$ was 1.05 : 7.42 : 1.09 : 0.45. These figures did not change very much in comparison to the values shown in Figure 6 upon changing the particle diameter. This is due to the fact that the resistance to mass transfer is predominantly in the solid phase; the third term in equation (3) is approximately 50 times as large as the first and second term. Hence, the Stanton number is proportional to $L/(v_s{\cdot}d_p^2)$. Constant Stanton numbers (required for a constant separation performance) are achieved when v_s is proportional to d_p^2, without changing the length per section.

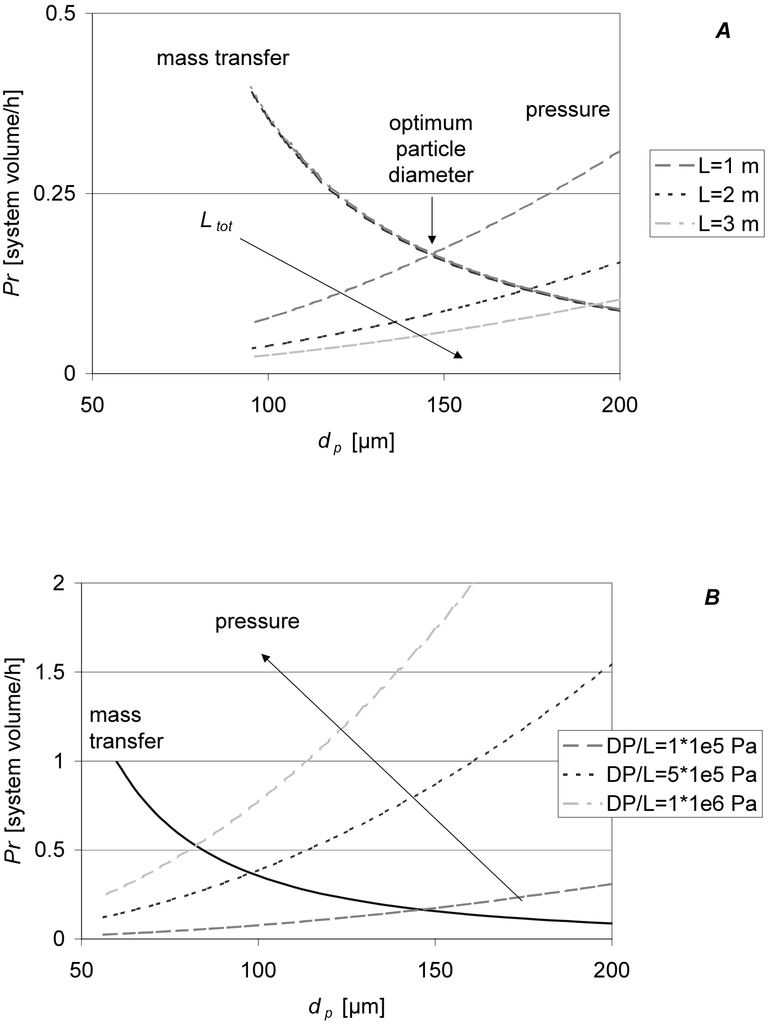
A
0.5
0.25
0
Pr [system volume/h]
mass transfer
optimum particle diameter
pressure
L tot
L=1 m
L=2 m
L=3 m
50
100
150
200
d p [μm]
B
2
1.5
1
0.5
0
Pr [system volume/h]
pressure
mass transfer
DP/L=1*1e5 Pa
DP/L=5*1e5 Pa
DP/L=1*1e6 Pa
50
100
150
200
d p [μm]

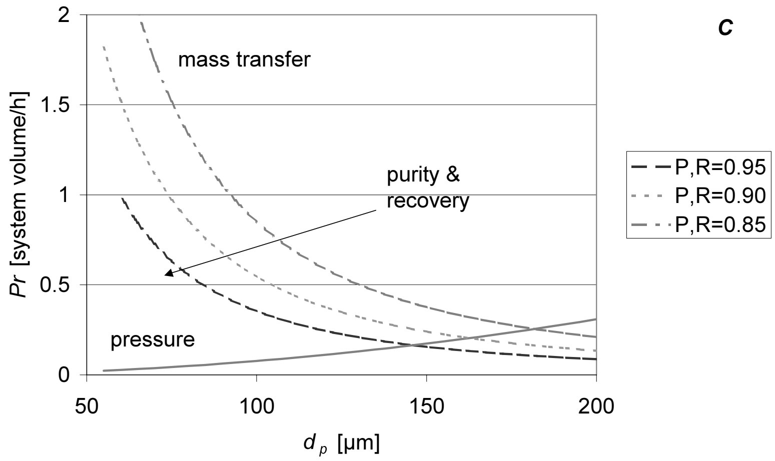

Figure 7. Optimization of throughput as a function of particle size at conditions of experiment III. A: effect of total length; B: effect of pressure drop; C: effect of purity and recovery requirements.

When the total system length is varied, the productivity determined by mass transfer is almost invariable. This again is a result of the mass transfer resistance being predominantly at the solids side of the particle. Stanton is then constant when the ration L/v_s is constant. According to equation (8), productivity is then also constant. The productivity as limited by the pressure drop does depend on the system length, as suggested by equation (10). The combination of the two effects is that the optimum particle size shifts to increased values upon increasing the system length.

When the maximum allowed pressure drop is increased, the optimum particle size is shifted to smaller particles, for obvious reasons.

The change of the purity requirements to lower values leads to a shift of the optimum particle size to larger particles. This is expected, as lower Stanton values are sufficient to reach the given performance.

Conclusions

SMB systems can be used for the fractionation of two proteins by size exclusion chromatography. In experiments with an aqueous feed stream containing BSA and myoglobin, the obtained extract streams were enriched in myoglobin and the raffinate streams were enriched in BSA. Equilibrium theory has been used to define the conditions for complete separation (Triangle Theory), but no complete separation has been observed. Clearly, this is due to slow mass transfer of macromolecules such as proteins in porous matrices. The experimental concentration profiles agree well with those calculated with a steady state true moving bed model, using a linear driving force approximation for description of mass transfer.

SMB-systems, optimized with respect to productivity per resin volume per time and eluent consumption, operate under mass transfer limitation. This should be taken into account to define the proper operating conditions. There are minimum values for the Stanton numbers in each of the sections of an SMB-system required to obtain a given purity and recovery. These minimum Stanton numbers can be identified using an equivalent TMB model, after selection of the purity of the extract and raffinate product and the overall recovery of the two proteins. Column length per section, liquid velocity and particle size can be selected in such a way that these criteria on Stanton numbers are met.

The productivity at the *m*-values of experiment III has been optimized with respect to particle diameter. In the “base case”, where the total length equals 1 m, the maximum pressure drop is 10^5 Pa/m and $P_E=P_R=R_{ov,A}=R_{ov,B}=95\%$, the optimum particle size is 145 µm, and the distribution of column lengths $L_1 : L_2 : L_3 : L_4$ is 1.05 : 7.42 : 1.09 : 0.45. The optimum particle diameter shifts to smaller particle size as the pressure drop is increased, purity and recovery requirements are increased, or the total column length is decreased. These figures show that the equivalent TMB model can well be used for optimization of performance criteria. It should be noted that in practical systems, the optimization is an economical one; however, by changing the objective function, the TMB model can also be used for that purpose.

Acknowledgements

The Dutch Ministry of Economic Affairs is gratefully acknowledged for the financial support in the framework of the IOP Milieutechnologie (Preventie) program. Amersham Pharmacia Biotech is acknowledged for the gift of gel materials.

Notation

A	column area	[m^2]
a	solid-liquid interfacial area	[1/m]
c	liquid phase concentration	[g/L]
D	diffusion coefficient	[m^2/s]
D_p	effective diffusion coefficient in sorbent pores	[m^2/s]
d_p	particle diameter	[m]
E	dispersion coefficient	[m^2/s]
K	distribution coefficient	[-]
k_o	overall mass transfer coefficient	[m/s]
L	column length	[m]
L_s	section length	[m]
m	flow rate ratio [Φ_L/Φ_S]	[-]
Pe	Peclet number [vL/E]	[-]
Pr	productivity	[system volume/h]
q	solid phase concentration	[g/L]
r_f	fiber radius	[nm]
r_p	Stokes radius of protein	[nm]
S	Separation factor [$\Phi_S K/\Phi_L$]	[-]
Sc	Schmidt number [$\eta/D\rho$]	[-]
St	Stanton number [$k_o a L_s/v_s$]	[-]
t	time	[s]
u	superficial velocity	[m/s]
v	interstitial velocity	[m/s]
v_s	solid phase interstitial velocity	[m/s]
V	column volume	[m^3]
V_d	dead volume per column	[m^3]
V_{tot}	total system volume	[m^3]
x	distance	[m]
z	dimensionless distance [x/L]	[-]

β	phase ratio [$(1-\varepsilon)/\varepsilon$]	[-]
ε	porosity	[-]
ϕ_f	particle solids fraction	[-]
λ	aspect ratio	[-]
η	viscosity	[Pa·s]
ρ	density	[kg/m^3]

θ	dimensionless time	[-]
τ	switch time	[s]
Φ	volumetric flow rate	[m^3/s]

Literature

Azevedo, D.C.S. and A.E. Rodrigues, "Design of a simulated moving bed in the presence of mass-transfer resistances," *A.I.Ch.E. J.*, **45,** 956 (1999).

Ballanec, B. and G. Hotier, "From batch to simulated countercurrent chromatography," In: *Preparative and production scale chromatography,* G. Ganetsos and P.E. Barker (eds.). Marcel Dekker, New York (1993).

Berezenko, S., A.V. Quirk, P.C. Wood, J.R. Woodrow, D. Sleep; H. van Urk, S.J. Burton, J. Stephen, A.R. Goodey, R.A. Johnson, "Process of high purity albumin production," World Patent application WO 9637515 (1996).

Cavoy, E., M.-F. Deltent, S. Lehoucq and D. Miggiano, "Laboratory-developed simulated moving bed for chiral drug separations. Design of the system and separation of Tramadol enantiomers," *J. Chromatogr.*, **769**, 49 (1997).

Carta, G. and W. B. Stringfield, "Analytic solution for volume-overloaded gradient elution chromatography," *J. Chromatogr.*, **605**, 151 (1992).

Charton, F. and R. Nicoud, "Complete design of a simulated moving bed," *J. Chromatogr.*, **702**, 97 (1995).

Gottschlich, N. and V. Kasche, "Purification of monoclonal antibodies by simulated moving bed chromatography," *J. Chromatogr.*, **765**, 201 (1997).

Guiochon, G., S. Golshan-Shirazi and A.M. Katti, *Fundamentals of preparative and nonlinear chromatography.* Academic Press, Boston (1994).

Hashimoto, K., S. Adachi and Y. Shirai, "Continuous desalting of proteins with a simulated moving bed adsorber," *Agric. Biol. Chem.*, **52**, 2161 (1988).

Houwing, J., H.A.H. Billiet, J.A. Wesselingh and L.A.M. van der Wielen, "Azeotropic phenomena during separation of dilute mixtures of proteins by simulated moving bed chromatography," *J. Chem. Technol. Biotechnol.*, **74**, 213 (1999).

Laurent, T.C. and J. Killander, "A theory of gel filtration and its experimental verification," *J. Chromatogr.*, **14**, 317 (1964).

Migliorini, C., M. Mazzotti and M. Morbidelli, "Simulated moving bed units with extra-column dead volume," *A.I.Ch.E. J.*, **45**, 1411 (1999).

Migliorini, C., A. Gentilini, M. Mazzotti and M. Morbidelli, “Design of simulated moving bed units under nonideal conditions,” *Ind. Eng. Chem. Res.*, **38**, 2400 (1999b).

Pais, L.S., J.M. Loureiro and A. Rodrigues, “Separation of 1,1-bi-2-naphtol enantiomers by continous chromatography in Simulated Moving Bed,” *Chem. Eng. Sci.*, **52**, 245 (1997).

Priegnitz J.W., “Small scale simulated moving bed separation process,” US patent 5,565,104 (1996).

Ruthven, D.M., “Adsorption and adsorption processes,” Wiley, New York (1984).

Ruthven, D.M. and C.B. Ching, “Countercurrent and simulated countercurrent adsorption separation processes,” *Chem. Eng. Sci.*, **44**, 1011 (1989).

Storti, G., M. Masi, S. Carrà and M. Morbidelli, “Optimal design of multicomponent countercurrent adsorption separation processes involving nonlinear equilibria,” *Chem. Eng. Sci.*, **44**, 1329 (1989).

Storti, G., M. Mazzotti, M. Morbidelli and S. Carrà, “Robust design of binary countercurrent adsorption separation processes,” *A.I.Ch.E. J.*, **39**, 471 (1993).

Vonk, P. *Diffusion of large molecules in porous structures.* Ph-D thesis Groningen State University (1994).

Van Walsem, H.J. and M.C. Thompson, “Simulated moving bed in the production of lysine,” *J. Biotechnol.,* **59**,127 (1997).

Wu, D.-J., Y. Xie and N.H.L. Wang, “Design of simulated moving bed chromatography for amino acid separations,” *Ind. Eng. Chem. Res.*, **37**, 4023 (1998).

Zhong, G. and G. Guiochon, “Simulated moving bed chromatography. Effects of axial dispersion and mass transfer under linear conditions,” *Chem. Eng. Sci.*, **52**, 3117 (1997).

Appendix: steady state TMB model

In case of linear equilibria, the profiles in a True Moving Bed at steady state can be calculated analytically (cf. Ruthven and Ching, 1989). Let us consider one section of the true moving bed. Since the TMB is at steady state, all accumulation terms cease. When axial dispersion is integrated in the (linear driving force) mass transfer term, such as in eq. (3), the mass balance over the liquid phase at position x in the section reduces to:

$$v \cdot \frac{dc}{dx} + \frac{1-\varepsilon}{\varepsilon} \cdot k_o a \cdot (Kc - q) = 0 \qquad \textbf{(A 1)}$$

In our calculations, the mass transfer coefficient is related to the SMB interstitial velocities. The solid and liquid phase concentrations can be related via a balance relating the concentrations c and q at position x to the concentrations c_0 and q_0 at the liquid inlet side of the section (i.e. the bottom; position x=0):

$$q - q_0 = \frac{\varepsilon}{1-\varepsilon} \frac{v}{v_s} \cdot (c - c_0) \qquad \textbf{(A 2)}$$

After substitution of Eq. A 2 in (A 1) and introduction of the dimensionless variables $St=k_o a L_s/v_s$ and $z=x/L_s$, and the separation factor, S, defined as $S=K\beta\ v_s/v$, the mass balance equation can be rewritten in dimensionless form:

$$\frac{dc}{dz} = -St \cdot \left[(S-1)c + c_0 - {}^{Sq_0}\!/_{K} \right] \qquad \textbf{(A 3)}$$

This equation can be integrated analytically, yielding an equation only containing concentration (c) and location (z) and the concentrations at the bottom of the section (q_0, c_0):

$$\frac{(S-1)c + c_0 - {}^{Sq_0}\!/_{K}}{(S-1)c_0 + c_0 - {}^{Sq_0}\!/_{K}} = \exp[St(1-S)z] \qquad \textbf{(A 4)}$$

A similar mass balance can be written for all four sections of the TMB.

The bottom concentrations can be obtained from the mass balances relations at points of mixing of streams, the “nodes”. These are:

$$\begin{aligned} q_0{}^{I} &= q_L{}^{IV} & c_0{}^{I} &= c^{D} \\ q_0{}^{II} &= q_L{}^{I} & c_0{}^{II} &= c_L{}^{I} \\ q_0{}^{III} &= q_L{}^{II} & c_0{}^{III} &= \frac{m_2}{m_3} c_L{}^{II} + \left(\frac{m_3 - m_2}{m_3} \right) c^{F} \\ q_0{}^{IV} &= q_L{}^{III} & c_0{}^{IV} &= c_L{}^{III} \end{aligned} \qquad \textbf{(A 5)}$$

Simulation of a TMB profile can then be done in two steps. The first step is to find the ten node concentrations ($c_0{}^{I}$, $c_0{}^{II}$, $c_0{}^{III}$, $c_0{}^{IV}$, $c_L{}^{IV}$, $q_0{}^{I}$, $q_0{}^{II}$, $q_0{}^{III}$, $q_0{}^{IV}$, $q_L{}^{IV}$). This is done by combining the mass balance (Eq. A 2) from the bottom (x=0) to the top (x=L) of the section with the node equations (Eq. A 5), e.g. for section I:

$$q_0{}^{II} = q_L{}^{I} = q_0{}^{I} + m_1\left(c_L{}^{I} - c_0{}^{I}\right) = q_0{}^{I} + m_1\left(c_0{}^{II} - c_0{}^{I}\right) \qquad \textbf{(A 6)}$$

The relation between c_0 and c_L is obtained from integration of the liquid balance (Eq. A 4) to z=1. For convenience, the latter is rewritten using two dummy variables f and g:

$$\begin{aligned} &(S-1)\,c_L = c_0\, f + q_0\, g \qquad \text{where} \\ &f = S\exp[St\cdot(1-S)] - 1 \qquad \text{and} \qquad g = \frac{S}{K}\{1 - \exp[St\cdot(1-S)]\} \end{aligned} \qquad \textbf{(A 7)}$$

Combination of four equations of type A 4 and four of type A 6 and the node balance over the desorbent inlet yields a set of 10 equations, which is, written in matrix form:

$$\begin{bmatrix} f_1 & g_1 & 1-S^{I} & 0 & 0 & 0 & 0 & 0 & 0 & 0 \\ m_1 & -1 & -m_1 & 1 & 0 & 0 & 0 & 0 & 0 & 0 \\ 0 & 0 & f_2 & g_2 & 1-S^{II} & 0 & 0 & 0 & 0 & 0 \\ 0 & 0 & m_2 & -1 & -m_2 & 1 & 0 & 0 & 0 & 0 \\ 0 & 0 & 0 & 0 & f_3h_1 & g_3 & 1-S^{III} & 0 & 0 & 0 \\ 0 & 0 & 0 & 0 & m_3h_1 & -1 & -m_3 & 1 & 0 & 0 \\ 0 & 0 & 0 & 0 & 0 & 0 & f_4 & g_4 & 1-S^{IV} & 0 \\ 0 & 0 & 0 & 0 & 0 & 0 & m_4 & -1 & -m_4 & 1 \\ m_1 & 0 & 0 & 0 & 0 & 0 & 0 & 0 & 0 & 0 \\ 0 & 1 & 0 & 0 & 0 & 0 & 0 & 0 & 0 & -1 \end{bmatrix} \bullet \begin{bmatrix} c_0{}^{I} \\ q_0{}^{I} \\ c_0{}^{II} \\ q_0{}^{II} \\ c_0{}^{III} \\ q_0{}^{III} \\ c_0{}^{IV} \\ q_0{}^{IV} \\ c_L{}^{IV} \\ q_L{}^{IV} \end{bmatrix} = \begin{bmatrix} 0 \\ 0 \\ 0 \\ 0 \\ -f_3h_2 \\ -m_3h_2 \\ 0 \\ 0 \\ 0 \\ 0 \end{bmatrix}$$

(A 8)

Where h_1=m_2/m_3 and h_2=(m_3-m_2)/m_3. Note that the separation factors as well as the Stanton numbers vary from section to section. After solving this set of equations by matrix inversion (for instance using commercial software such as Mathcad (MathSoft Corp.), the node concentrations are known.

The second step in calculation of the profile over the TMB is to calculate the concentrations at various positions (z) in the sections via Eq. A 4, where the node concentrations are used for c_0 and q_0. Thus, the procedure is completed.

3

Azeotropic phenomena during separation of dilute mixtures of proteins by simulated moving bed chromatography

Abstract

Recently, we have introduced the use of a salt gradient over a simulated moving bed system used for purification of proteins using ion exchange chromatography (Houwing *et al.,* 1997). This paper describes azeotropic phenomena in such a system, where complete separation of mixture of proteins is not possible at certain salt concentrations, due to a reversing selectivity. These phenomena impose additional restrictions on the selection of the flow rates in each of the sections of the simulated moving bed which are discussed.

This paper has been published in: J. Chem. Technol. Biotechnol. **74**, 213 (1999).

Introduction

During chromatographic purification of proteins, large streams of salt-containing waste are usually generated. Reduction of these streams is desirable for economic reasons and because more strict environmental regulations increasingly prohibit their disposal. Since reduction of the consumption of eluent as well as the resin inventory can be realized by the use of Simulated Moving Bed (SMB) chromatography (Ballanec and Hotier, 1993), we are investigating the use of SMB systems for purification of proteins by ion exchange chromatography.

In a simulated moving bed, a feed stream can be separated into two fractions by the simulated countercurrent movement of an adsorbent and a liquid stream (Ruthven and Ching, 1993). By correct selection of the ratio of liquid to solid flow rates in each of the sections, weakly retained components *(B)* move towards the raffinate outlet and strongly retained components *(A)* move towards the extract outlet, as is depicted schematically in Figure 1.

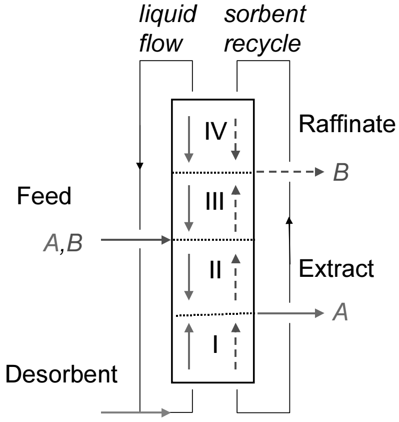

Figure 1. Schematic representation of a Sorbex type simulated moving bed. Arrows indicate the movement of components.

Recently, we have introduced a simulated moving bed system for separation of mixtures of proteins by ion exchange chromatography (Houwing *et al.,*1997). As in conventional column chromatography, an aqueous salt solution (e.g. NaCl) is used as a desorbent. Thus, the affinity of the protein for the sorbent in the lower sections of the SMB is reduced, resulting in smaller flow rates in these sections, as will be shown shortly. In the upper sections, the concentration of salt is lowered by the introduction of the feed stream with a lower salt content, leading to an increased affinity, which increases the possible flow rates in these sections. Overall, an increased productivity is obtained.

Protein isotherms

Ion exchange isotherms of proteins can often be described by a steric mass action (SMA) isotherm, as derived by Brooks and Cramer (1992). Every protein molecule is assumed to interact with the exchanger at z_p charges spread over the molecule. The “characteristic charge”, z_p, is usually only a fraction of the total number of charges. Moreover, exchange sites on the resin are shielded by binding of bulky protein molecules.

In case of dilute systems, the SMA-isotherm can be simplified to a linear equilibrium with a salt dependent equilibrium coefficient (Brooks and Cramer, 1992):

$$K = K_0 c_s^{-zp} \tag{1}$$

Where K_0 is a reference equilibrium coefficient and c_s is the concentration of salt.

In case of exchange of two components A and B the selectivity $S_{A,B}$ can be defined as the ratio of the two equilibrium coefficients:

$$S_{A,B} = \frac{K_A}{K_B} = \frac{K_{0,A}}{K_{0,B}} c_s^{zB-zA} \tag{2}$$

Thus, the selectivity is not a constant, but a function of the salt concentration. When $S_{A,B}$ exceeds unity, A is the more retained component; otherwise, B is the more retained component.

Azeotropy in simulated moving beds

The flows in a simulated moving bed for separation of dilute mixtures of proteins can be selected by construction of the region of complete separation, as has been shown by Morbidelli and co-workers (Storti *et al.,* 1993). The net flow of components, i.e. the ratio of the amount transported by the liquid to the amount transported by the resin is calculated using the salt dependent equilibrium coefficients. The salt concentrations in the sections are assumed to be independent of ion exchange and are calculated from a mass balance over the feed point.

A selectivity reversal in the simulated moving bed results in an azeotropic situation ($S_{A,B}$=1), where the mixture cannot be separated further. In that case, assuming that A is the more retained component in section II (see Figure 1), no combination of flow rates can be found that results in movement of A towards the extract port and B towards the raffinate port in section III; downward movement of A automatically results in downward movement of B, since B is the most retained component in section III.

The simulated moving bed can only lead to complete separation when the reversal of selectivity is avoided. Thus, additional boundaries on the region of complete separation are imposed by the correct direction of movement of the more retained component in section II and of the less retained component in section III.

Case study: separation of BSA and a yeast protein

Equilibrium coefficients of Bovine Serum Albumin (BSA), a yeast protein and sodium chloride on an anion exchanger (Q-Sepharose FF) have been determined in our laboratory according to the method described by Brooks and Cramer (1992). The selectivities ($S_{BSA/yeast\ protein}$) calculated by equation (2) are shown in Figure 2; the selectivity reverses at a salt concentration of 0.077 M NaCl.

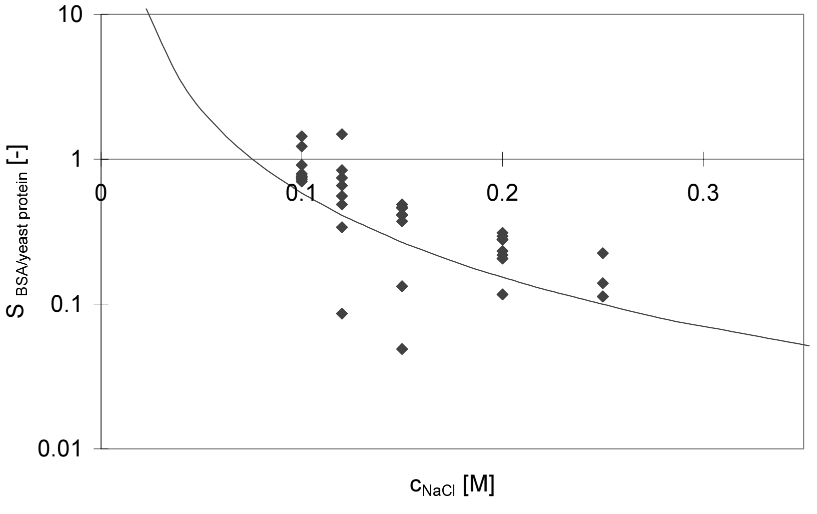

Figure 2. Selectivity of BSA and a yeast protein in a 10 mM acetate buffer, pH 5.4 on Q-Sepharose FF as a function of sodium chloride concentration.

The calculated region of complete separation in terms of the allowable flow rate ratios (m_j) is shown in Figure 3 in case of salt concentrations in desorbent and feed of 0.10 and 0.04 M, respectively. The additional boundary on the region imposed by correct movement of BSA in section III is indicated by “azeotropy line”. At increasing feed salt concentration, this line shifts to the left; when the feed concentration is over 0.077 M, the region of complete separation is no longer influenced. Simulations of an equivalent true countercurrent unit, using an equilibrium stage model as described in Ruthven and Ching (1993) have confirmed that complete separation inside the hatched region is indeed possible, but fails outside this triangle.

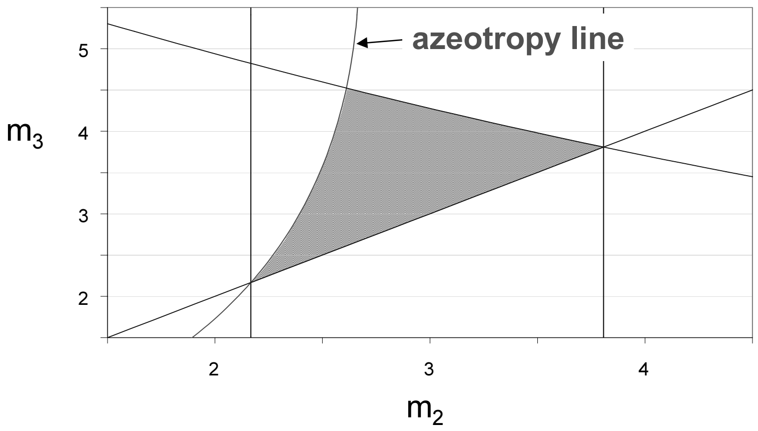

Figure 3. Region of complete separation of BSA and a yeast protein on Q-Sepharose FF. Only in the hatched region, complete separation is possible.

Future development

In this paper, we have focused on the selection flow rates in dilute mixtures of proteins. Currently, we are working on the experimental validation of this approach and its extension to the design of simulated moving beds for the separation of more concentrated (azeotropic) mixtures of proteins.

Acknowledgements

Financial support of the Dutch ministry of Economic Affairs through IOP-milieu Preventie is gratefully acknowledged.

Literature

Ballanec, B. and G. Hotier, "From batch to simulated countercurrent chromatography," In: *Preparative and production scale chromatography,* G. Ganetsos and P.E. Barker (eds.). Marcel Dekker, New York (1993).

Brooks, C.A. and S.M. Cramer, "Steric mass-action ion exchange: displacement profiles and induced salt gradients," *A.I.Ch.E. J.,* **38,** 1969 (1992).

Houwing, J., K.Ch.A.M. Luyben and L.A.M. van der Wielen, "Development of large scale purification process for recombinant HSA using SMB technology," *Proc. A.I.Ch.E. Annual Meeting, Los Angeles.* (1997).

Ruthven, D.M. and C.B. Ching, "Modelling of chromatographic processes," In: *Preparative and production scale chromatography,* G. Ganetsos and P.E. Barker (eds.). Marcel Dekker, New York (1993).

Storti, G., M. Mazzotti, M. Morbidelli and S. Carrá, "Robust design of binary countercurrent adsorption separation processes," *A.I.Ch.E. J.* **39**, 471 (1993).

4

Optimization of azeotropic protein separations in gradient and isocratic ion exchange SMB

Abstract

The separation of dilute binary mixtures of proteins by salt aided ion exchange SMB is optimized with respect to throughput, desorbent consumption and salt consumption. The optimal flow rate ratios are analytically determined via an adopted "triangle theory". Azeotropic phenomena are included in this procedure. The salt concentrations in the feed and recycled liquid are subsequently determined by numerical optimization.

The azeotropic separation of Bovine Serum Albumin (BSA) and a yeast protein is used to illustrate the procedure. Gradient operation of the SMB is generally preferred over isocratic operation. The separation of a feed of a salt concentration near c_{int}, the salt concentration where the selectivity reverses, is only possible in a gradient operated at concentrations above c_{int}. The consumption of desorbent and salt is always lower in the gradient SMB, especially at low feed salt concentrations where a complete liquid recycle is possible. The performance is best when a feed of low salt concentration is separated in a gradient with salt concentrations below c_{int}.

This paper has been published in: *J. Chromatogr. A* **994**, 189 (2002).

Introduction

More and more, Simulated Moving Bed (SMB) systems are used for the purification of various components on an industrial scale. Emerging applications are the separations of enantiomers using chiral stationary phases (Juza *et al.*, 2000, Schulte and Strube, 2001). The advantages of SMB over fixed bed chromatography are the reduced consumption of sorbent and solvent. Furthermore, often a higher purity can be obtained than in conventional fixed bed chromatography. A pure product can already be harvested from an SMB when there is a pure product in only a very small section of the unit, whereas this requires a fair column section in fixed bed separations (Ballanec and Hoitier, 1993).

Gradients in elution strength may further improve the efficiency of the SMB. By the use of different solvent compositions or physical conditions of the feed and desorbent streams, a situation of a high affinity of the solute for the matrix in the top sections (sections III and IV in Figure 1) and a low affinity in the bottom sections (sections I and II in Figure 1) is introduced. The situation of equal affinity in all four sections of the SMB will further be termed "isocratic operation". Several papers show that gradient operation may result in an increase of the throughput, i.e. the volume of feed loaded per column volume, and a reduction of the consumption of desorbent per feed volume compared to the isocratic situation.

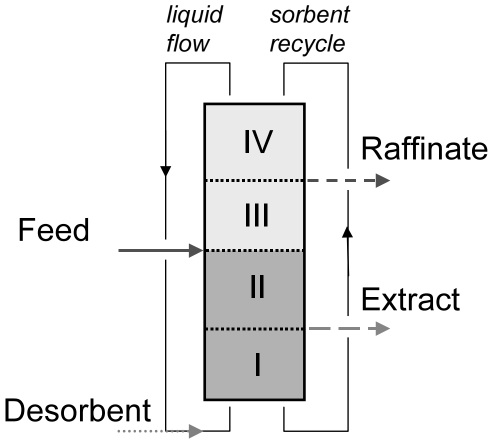

Figure 1. Schematic representation of gradient in SMB and numbering of sections therein. The desorbent is used for adjustment of volume and modulator concentration of the recycled stream. A dark color indicates a reduced affinity of the protein for the matrix.

Examples are temperature gradients during separation of sugars (Ching and Ruthven, 1986), pressure gradients in supercritical fluid chromatography (Mazzotti *et al*., 1997a), and methanol gradients in reversed phase separation of antibiotics (Jensen *et al.*, 2000). In the latter (unoptimized) example, the application of the gradient resulted in at least 50% reduction of solvent consumption and a twofold concentrating of the product compared to the isocratic SMB.

Houwing *et al.*, (1999, 2003) investigated the use of salt gradients during separation of dilute mixtures of proteins by ion exchange chromatography. An important observation was that no complete separation can be obtained at certain combinations of salt concentration in the desorbent and feed. This phenomenon was termed “azeotropy”. Similar to azeotropic situations such as observed in distillation processes, azeotropy in SMB is caused by a reversal of selectivity $S_{1,2}$, which is defined as:

$$S_{1,2} = \frac{q_1}{c_1} \cdot \frac{c_2}{q_2}$$

where q is the adsorbed phase concentration and c is the liquid phase concentration. When $S_{1,2}$ exceeds unity, component 1 is the more retained; when $S_{1,2}$ is below unity, component 2 is the more retained. In ion exchange of proteins, the selectivity is a function of the salt concentration. When using different salt concentrations in an SMB, the selectivity may exceed unity in the top sections and meanwhile be below unity in the bottom sections. No complete separation will occur under these conditions. Many examples of selectivity reversals during protein separations can be found in literature. Steric Mass Action (SMA) isotherms of (dilute mixtures) of proteins in ion exchange frequently lead to a reversal of selectivity as a function of salt concentration. A few examples thereof are the separation of α-chymotrypsinogen and cytochrome C (Brooks and Cramer, 1992), of horse and bovine cytochrome C (Natarajan *et al.*, 2000), and of α-lactalbumin and β-lactoglobulin (Freitag and Vogt, 2000).

In this paper, a procedure for optimization of the separation of dilute, azeotropic mixtures of proteins by ion exchange (IEX) in SMB systems is described. The considered optimization functions are:

- throughput: the volume of feed loaded per sorbent volume;
- desorbent consumption: the volume of desorbent required per volume of feed processed;

- salt consumption: the amount of salt required per volume of feed processed.

The procedure is based on primary selection of the optimal flow rate ratios, using an adaptation of “triangle theory” (Storti *et al.*, 1993), which includes azeotropy and is described in Houwing *et al.*, 1999. Secondly, the optimal salt concentrations in the lower sections (the inlet salt concentration) and the feed solution are optimized numerically. Thus, the chance to end up in a local optimum, which is substantial in similar systems with many variables, is reduced. The procedure is illustrated by taking the separation of dilute mixtures of Bovine Serum Albumin (BSA) and a yeast protein (yp) as an example.

Theory

Selection of flow rate ratios

The selection of the flow rate ratios *m* in a gradient SMB follows the “triangle theory” (Storti *et al.*, 1993); the procedure has been described in Houwing *et al.* (1999) and is summarized in Table I. The constraints on the flow rate ratios are given by the distribution coefficients ($K=q/c$) of the stronger (H) and weaker (L) binding component. These are a function of the salt concentration in the considered section. Furthermore, the addition of the feed dictates that m_3 exceeds m_2, the so called “positive feed” criterion.

Table I. Selection of flow rate ratios in gradient SMB.

$$\begin{array}{lclcl}
 & & m_1 & > & K_H(c_I) \\
K_H(c_I) & > & m_2 & > & K_L(c_I) \\
K_H(c_{III}) & > & m_3 & > & K_L(c_{III}) \\
K_L(c_{III}) & > & m_4 & &
\end{array}$$

In Table I, c_I and c_{III} represent the salt concentrations in sections I and III, respectively. The salt concentration c_I will furthermore be indicated as the “inlet salt concentration”, as it is the concentration that enters the system upon mixing of the recycle and the desorbent (Figure 1). The salt concentration in section III follows from the flow rates, the salt concentration of the feed and the inlet salt concentration via the mass balance over the point of feed introduction. When salt has no interaction with the sorbent, this balance reads:

$$c_{III} = \frac{m_2}{m_3}\left(c_I - c_F\right) + c_F \tag{1}$$

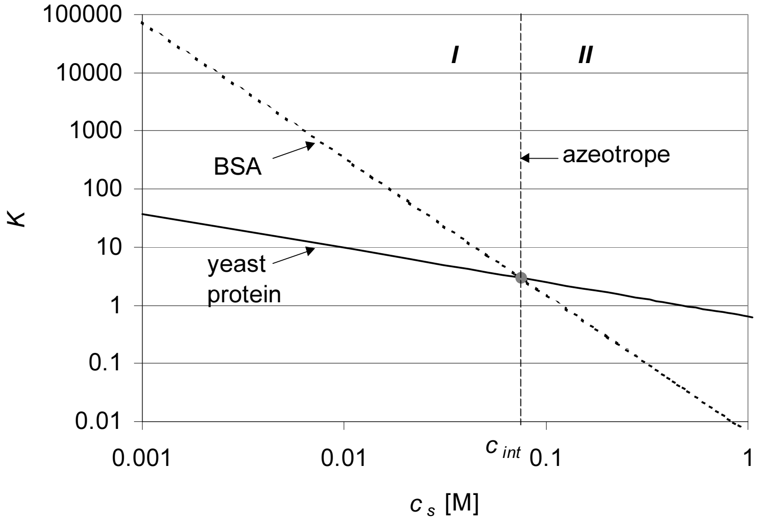

Figure 2. Intersecting plots of the distribution coefficients of BSA and a yeast protein on Q Sepharose FF at pH 5.4 in a 10 mM acetate buffer as a function of the salt (NaCl) concentration (from: Houwing *et al.*, 1999).

Azeotropic phenomena occur in the system shown in Figure 2, since the selectivity $S_{BSA,yp}$ exceeds unity at salt concentrations below the concentration of intersection (c_{int}), whereas it is below unity at concentrations exceeding c_{int}. This implies a salt aided SMB can only be operated properly in two regions: region I with salt concentrations below c_{int}, and region II with salt concentrations exceeding c_{int}, such as shown in Figure 2. Azeotropic phenomena can only be prevented by choosing the salt condition in section III in the same region as the salt concentration in section I. This is established by taking both limits on m_3 into account.

Table II. Mass action isotherm parameters of BSA and a yeast protein on Q-Sepharose FF, at pH 5.4 in a 10 mM acetate buffer with NaCl as described in Houwing *et al.* (1999).

component	BSA	yeast protein
K_0	$6.7 \cdot 10^{-3}$	0.64
z	2.35	0.59

Optimal flow rate ratios

Previous work on non-gradient SMB separation of components obeying a linear isotherm has shown that throughput is maximal and desorbent consumption is minimal when m_1 and m_2 are chosen near their lower limit, whereas m_3 and m_4 are chosen near their upper limit (Ruthven and Ching, 1989). The validity of this approach for the output functions considered in this paper has been tested. The results shown in Appendix I indicate that these flow rate ratios are indeed optimal for optimization of throughput and desorbent consumption. In some cases, optimization of the salt consumption may require a full numerical optimization of both flow rates and salt concentrations. This paragraph continues with the derivation of explicit relations for the optimal flow rate ratios in azeotropic SMB separations.

In an azeotropic situation, the choice of m_1 and m_4 is similar to that in non-azeotropic systems. The optimal values, close to the limiting values, are found by multiplication (m_1) or division (m_4) of the limits given in Table I by a factor α, which is chosen close to unity.

The optimal values of m_2 and m_3 are most conveniently found in a "region of complete separation" (Storti *et al.*, 1993). Only inside the triangular region enclosed by the lines defined by the constraints in Table I, the feed is separated into pure extract and raffinate fractions. Figure 3 shows the superposition of three such regions of complete separation in an SMB for fractionation of BSA and yeast protein operated in region II. As before, the maximum throughput (m_3-m_2) is obtained when m_2 is at the minimum value, whereas m_3 is at the maximum value. The term "optimal point" will further be used to indicate the corresponding point in the m_2-m_3 plane.

The optimal point is on the intersection of the $K_{BSA}(c_I)$ and $K_{yp}(c_{III})$ lines, i.e. point *X* in the isocratic situation. It shifts to increased m_3 upon decreasing the feed salt concentration, or increasing the desorbent concentration. The occurrence of azeotropy at these conditions is avoided by the use of the $K_{BSA}(c_{III})$ line. The three aforementioned lines intersect at point *Y* at a feed salt concentration $c_{F,Y}$. At that point, the salt concentration in section III equals c_{int}, because the distribution coefficients in section III are equal. The corresponding limiting m_3 equals the distribution coefficient of both components at c_{int}, and is further indicated as $m_{3,int}$. The feed and inlet salt concentration at this point *Y* are related via the feed mass balance (1), which is rewritten as:

$$c_{F,Y}\left(1-\frac{K_{BSA}}{c_{I,Y}{}^{zBSA}m_{3,int}}\right)=c_{int}-\frac{K_{BSA}c_{I,Y}}{c_{I,Y}{}^{zBSA}m_{3,int}} \qquad \textbf{(2)}$$

At a feed salt concentration below $c_{F,Y}$, azeotropic phenomena can only be avoided when m_2 exceeds the lower limit $K_{BSA}(c_I)$. Only then, the salt concentration in section III is (larger than) c_{int}. The optimal point is indicated by *Z* when the point of intersection of the $K_{yp}(c_{III})$ and $K_{BSA}(c_{III})$ lines is in between $K_{BSA}(c_I)$ and $K_{yp}(c_I)$, by *W* when it is on the intersection of $K_{yp}(c_I)$, $K_{yp}(c_{III})$ and $K_{BSA}(c_{III})$, and *V* when it is on the intersection of $K_{BSA}(c_{III})$ and $K_{yp}(c_I)$.
The feed and inlet salt concentration at W are related via:

$$c_{F,W}\left(1-\frac{K_{yp}}{c_{I,W}{}^{zyp}m_{3,int}}\right)=c_{int}-\frac{K_{yp}c_{I,W}}{c_{I,W}{}^{zyp}m_{3,int}}$$

Points *V* and *W* are not shown in Figure 3, because these do not occur during the separation of BSA and the yeast protein taken as an example.

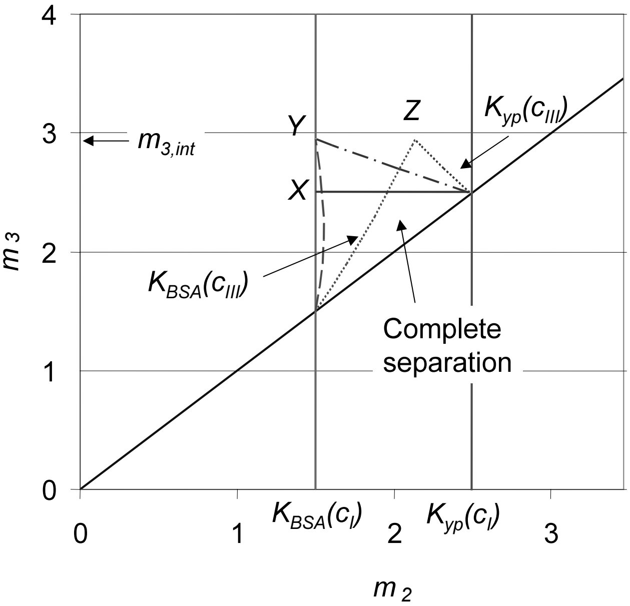

Figure 3. Superposition of three regions of complete separation during separation of BSA and a yeast protein in region II at c_I=0.1 M NaCl. Solid line: isocratic situation (c_F=0.1M NaCl), dash-dotted line: gradient at c_F=0.042 M NaCl, dotted line: gradient at c_F=0.01 M NaCl. Optimal points *X*, *Y* and *Z* are explained in the main text.

When the SMB is operated in region I, no azeotropy can occur. The optimal point is invariably at *X*, whereas the value of m_3 at the optimal point increases at decreasing salt concentration of the feed.

Table III summarizes the explicit equations on the optimal points that are required in analytical optimization. In appendix II, we have shown that the gross shape of the region of complete separation and the occurrence of one optimal point, that can be at *V*, *W*, *X*, *Y*, and *Z*, is general and holds for any mass action isotherm. Thus, Table III is also generally applicable.

Table III. Location of the optimal point.

operation in region	*criteria*		*optimal point*	m_2	m_3
I	$c_F<c_{int}$		X	$K_{yp}(c_I)$	$K_{BSA}(c_{III})$
II	$c_F<c_{int}$	$c_F<c_{F,W}$ or $c_I>c_{I,W}$	V	$K_{yp}(c_I)$	$K_{BSA}(c_{III})$
II	$c_F<c_{int}$	$c_F=c_{F,W}$ or $c_I=c_{I,W}$	W	$K_{yp}(c_I)$	$m_{3,int}$
II	$c_F<c_{int}$	$c_{F,W}<c_F<c_{F,Y}$ or $c_{I,W}>c_I>c_{I,Y}$	Z	from (1)	$m_{3,int}$
II	$c_F<c_{int}$	$c_F=c_{F,Y}$ or $c_I=c_{I,Y}$	Y	$K_{BSA}(c_I)$	$m_{3,int}$
II	$c_F<c_{int}$	$c_F>c_{F,Y}$ or $c_I<c_{I,Y}$	X	$K_{BSA}(c_I)$	$K_{yp}(c_{III})$
II	$c_F>c_{int}$		X	$K_{BSA}(c_I)$	$K_{yp}(c_{III})$

On the optimization of desorbent and salt consumption

Optimization of isocratic SMB systems only requires optimization of the throughput and the consumption of desorbent. In the gradient SMB, an additional optimization function is the consumption of the gradient forming agent, which is salt in our case. The salt may have large implications on the process economy, possibly via environmental regulations. Obviously, there is an economic optimum between desorbent consumption (i.e. the volume of desorbent used per feed volume, irrespective of the salt concentration) and the salt consumption (i.e. the absolute amount of salt used per feed volume, irrespective of the volume it is dissolved in). At low salt costs, the optimum is at minimum desorbent use. This is favored by a high inlet concentration, which reduces the flow rate ratio in the lower sections at a (slightly) increased salt concentration. At high salt costs, salt consumption should be minimal. This is favored by a lower inlet concentration, which decreases the salt need at the expense of a slightly higher desorbent flow rate.

The magnitudes of the desorbent and salt consumption are strongly influenced by the presence or absence of a recycle of the liquid leaving section IV to section I. In pharmaceutical applications, an "open loop" mode is preferred. The liquid leaving section IV is discarded, which prevents the accumulation of undesired contaminants. In other applications, a "closed loop" mode may be used. The complete m_4 is then recycled, and only a small volume of desorbent is added. By this recycle, the consumption of desorbent and salt may be reduced substantially.

In the following, we will consider a partially closed loop system. The recycle of m_4 is then maximal, but not necessarily complete. A desorbent (of high salt concentration) is used to adjust the flow rate and salt concentration of the recycled stream. Two cases can be distinguished:

- when both salt concentration and flow rate need to be increased, i.e. $m_1 > m_4$ and $c_I > c_{III}$, a desorbent stream of magnitude $m_1 - m_4$ can be used. The required desorbent salt concentration c_D is computed from the mass balance over the position of desorbent addition, as is shown in Figure 1:

$$c_D = \frac{m_1 c_I - m_4 c_{III}}{m_1 - m_4} \tag{3}$$

- when only the salt concentration needs to be adjusted, or when the salt concentration calculated by (3) is unrealistic, part of the liquid leaving section IV is replenished by a concentrated salt solution, of a chosen maximum concentration. In this paper, an arbitrary value of c_D=1M has been used. The magnitude of the desorbent stream is then obtained from the desorbent mass balance:

$$des = m_1 \frac{c_I - c_{III}}{c_D - c_{III}}$$

The desorbent consumption (*DC*) and salt consumption (*SC*) are calculated from:

$$DC = \frac{des}{m_3 - m_2}$$

$$SC = \frac{c_D \, des}{m_3 - m_2}$$

Methods

The numerical optimization of salt concentrations and flow rates was done in Matlab version 5.2 (The Mathworks inc., Boston, USA). The inverse of throughput, the desorbent consumption and the salt consumption were minimized using Matlab's "constr" optimization function.

Results and discussion

Three situations are described in this paragraph:

1. restricted optimization of an SMB operating at a known inlet salt concentration;
2. optimization of an SMB operating at a known salt concentration of the feed;
3. overall optimization of both inlet and feed salt concentration.

SMB at known inlet salt concentration

Optimization of the throughput by changing the feed salt concentration

The optimal feed salt concentration with respect to throughput P in an SMB with known inlet salt concentration can be found analytically. Whenever the optimal point is at X or Y, the throughput is determined by the difference in affinity of the more retained component in section III and the less retained component in section II. We illustrate this using Figure 2. For example in region I, m_2 is on the K_{yp}-line at concentration c_I, whereas m_3 is on the K_{BSA}-line at concentration c_{III}. The throughput is determined by the "affinity difference", the vertical distance between the m_2 and m_3 points. This affinity difference is maximal when the difference in salt concentration in section II and III is maximal; hence in region I, the minimal feed salt concentration is optimal.

In principle, the same holds in region II, unless the optimal point is at *Z, V or W*. Then, m_2 is elevated relative to its lower boundary in order to maintain the correct salt concentration. Throughput is then maximal when the optimal point is at Y; any decrease of the feed concentration would lead to an increase of m_2 at constant m_3 and to lower throughput. The corresponding feed concentration is computed using equation (2).

The results of these calculations are plotted in Figure 4. An unexpected finding is that salt should be added to the feed solution in region II in order to improve throughput. Even, more salt is added than is strictly necessary to overcome the

azeotrope. This is counterintuitive, since the throughput of fixed bed separations always increases upon reduction of the salt concentration of the feed.
Figure 4 also indicates that the optimal feed salt concentration increases with increasing inlet salt concentration. This can mathematically be proofed by taking the derivative of $c_{F,Y}$ (equation (2)) to c_I. This derivative is always positive whenever $zBSA>1$, which explains the observed. However, whenever $zBSA<1$, the derivative is negative and the optimal feed salt concentration decreases with increasing inlet concentration. This situation is not likely, since BSA is the stronger binding component.

The throughput is high in region I when the minimum salt concentration is low (a minimal concentration $c_{F,min}$ of 0.01 M NaCl has been used in Figure 4). As will be shown shortly, the minimum salt concentration strongly influences the magnitude of the throughput. The maximum throughput is obtained in the isocratic situation. The convergence of the isotherms suggests that m_3 profits more than m_2 of a decrease in c_I, which would imply operation at low c_I favors a high throughput. However, by a complete mathematical derivation of the derivative of throughput to c_I, it is found that there can be other optima in c_I in region I, independent of zy, when $zBSA>1$. The occurrence of such optima strongly depends on the values of K and z. The derivative in the isocratic situation is always of negative sign, which implies the isocratic situation is always a local optimum.

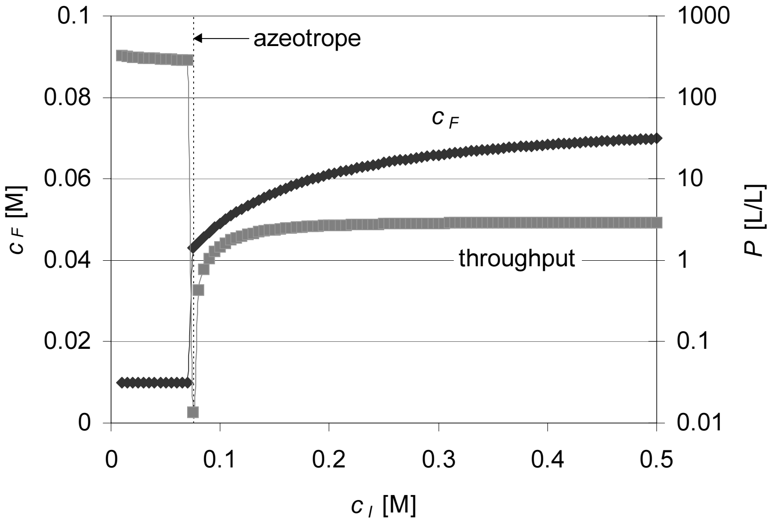

Figure 4. Optimal feed salt concentration and throughput as a function of the inlet salt concentration.

The throughput at the optimal feed concentration in region II is a weakly increasing function of the inlet concentration, since m_3 is fixed at $m_{3,int}$ and m_2 decreases slowly with increasing c_I. This is due to the small effect of charge on the distribution coefficients at high salt concentrations. The throughput in region II is much lower than in region I, since the maximal m_3 is bound by $m_{3,int}$.

SMB at known feed salt concentration

This section deals with a practical question: "what is the most optimal inlet salt concentration starting from a feed of salt concentration c_F?" The isocratic operation is evaluated as an alternative.

Optimization of the throughput by changing the inlet salt concentration

In an isocratic SMB operated in region I, the throughput P is high and decreases with increasing salt concentration (Figure 5), because of the convergent lines of the distribution coefficients as a function of the salt concentration (cf. Figure 2). This means the affinity difference is maximal at low salt concentration and decreases with increasing c_s. Throughput is zero when both c_I and c_F equal c_{int}, because all distribution coefficients are then equal. When the salt concentration is further increased (i.e. operation in region II), the throughput initially increases, because the affinity difference increases with c_s as a result of the divergent lines of the distribution coefficients. After a certain optimum, the throughput decreases, because the lines of the distribution coefficients converge when plotted at a linear scale. Note that the lines still diverge at a logarithmic c_s-scale.

The optimum throughput of the gradient SMB operated in region I is obtained in the isocratic situation (c_I=c_F) as has already been explained at Figure 4. The gradient SMB operated in region II has its maximal affinity difference at the maximum allowed inlet salt concentration. The divergent isotherms suggest that m_2 is more decreased than m_3 at increasing inlet salt concentration, which implies a high inlet salt concentration favors throughput. However, a detailed mathematical analysis of the effect of c_I on throughput in terms of the derivative $\partial(m_3\text{-}m_2)/\partial c_I$ shows that this will not always be the case. At feed salt concentrations below c_{int}, the system is operated at *Y or Z*. In that case, m_3 and c_3 are constant and the derivative is always positive, which means a high c_I is favorable for the throughput. The same result is obtained when the feed salt concentration exceeds c_{int} and $zy<1$. However, whenever $zy>1$ and $c_F>c_{int}$, other optima may exist.

Obviously, there is a limit to the maximum concentration in practical systems. In further calculations, the maximal c_I has been set at an arbitrary value of c_{max} =1M NaCl. The throughput in region II is not very sensitive to the chosen value; at a maximum concentration of 0.5M NaCl the throughput is maximally 3% decreased compared to a 1M inlet salt concentration.

When operating in a gradient in region II at increasing feed salt concentration, the throughput first increases, passes an optimum and then decreases. The explanation lies in the location of the optimal point. At low salt concentration, the optimal point is at *Z*. Upon an increase of the feed salt concentration, this point *Z* moves towards the $K_{BSA}(c_I)$ boundary. Hence, m_2 is decreased at constant m_3, so throughput increases. At a feed salt concentration of 0.073 M NaCl, i.e. the $c_{F,Y}$ corresponding to the 1M inlet salt concentration, the system is operated at point Y; at this point throughput is maximal. At further increasing feed salt concentration, the optimal point is at *X*, at a decreasing m_3 and a constant m_2, which results in a decrease of the throughput with increasing feed salt concentration.

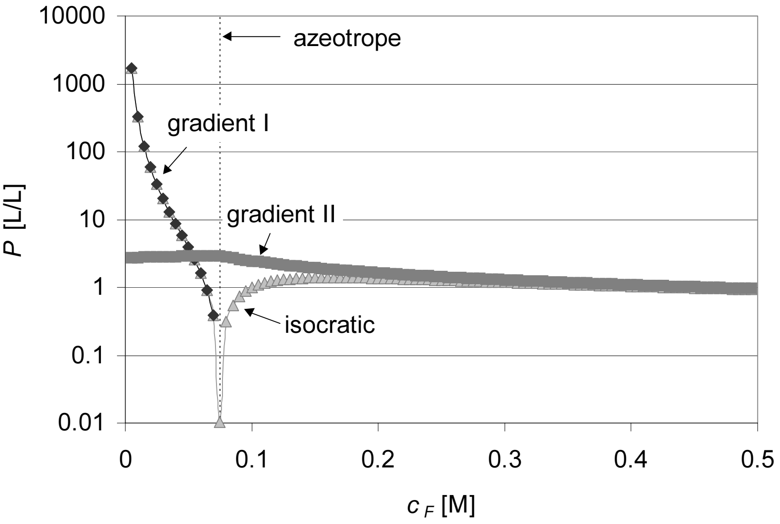

Figure 5. Throughput in isocratic and optimized gradient SMB at a maximum inlet concentration of 1 M NaCl.

It can be concluded that the isocratic SMB operation leads to a (local) maximum in throughput during separation of a feed of low salt concentration. In the considered example of BSA and the yeast protein, the performance of the isocratic SMB is 1 to 3 orders of magnitude better than the gradient SMB operated in region II. At low feed concentrations, the throughput in region II is always lower than in region I, since the maximum m_3 is limited. An important finding is that separation of a feed of salt concentration c_{int} is only possible when using a gradient in region II. The gradient introduces the affinity difference required for separation, which is absent in the isocratic situation. At high feed salt concentrations, the gradient is not very powerful. The introduced affinity difference is low and so the performances of the gradient and isocratic SMB will be similar.

Optimization of the desorbent consumption by changing the inlet salt concentration

In the isocratic SMB, the desorbent consumption DC is close to unity at most salt concentrations, because the desorbent flow rate ratio m_1-m_4 almost equals the feed flow rate ratio m_3-m_2. An asymptote in desorbent consumption is found at (feed) salt concentration c_{int} (cf. Figure 6). At this salt concentration, throughput is zero (see Figure 5), so the volume of desorbent used per feed volume is infinite.

When the gradient SMB is operated at low feed salt concentration in region I, the optimal inlet concentration is close to c_{int} (Figure 6). This “high” inlet concentration favors a low m_1. Also, the recycle of m_4 is most efficient, and hence a low flow rate of a desorbent of 1M NaCl is sufficient. At a feed salt concentration of 0.03 M NaCl, m_1 starts to exceed m_4 and hence the recycled m_4 no longer suffices to supply the necessary flow rate. An increased flow rate of desorbent of decreased salt concentration is then required. This explains why the desorbent consumption abruptly increases at the feed salt concentration of 0.03 M NaCl.

Also when the gradient SMB is operated in region II, a complete recycle of m_4 in combination with a desorbent of maximal salt concentration (1M NaCl) is optimal. This maximal desorbent concentration is maintained at all feed salt concentrations; never, a more diluted desorbent needs to be used. Thus, the recycle of salt is used to the maximum.

At very low feed salt concentration, the system is operated at optimal point *Z*. By substitution of the known c_3, $m_{3,int}$ and c_D=1M NaCl in equation (3), an optimal inlet salt concentration of 0.0794M NaCl is found. At increasing feed salt concentration, operation is still at *Z*, so the optimal inlet salt concentration and m_1 do not change. Throughput increases, since point Z shifts to lower m_2 at increasing feed salt concentration. Thus, the desorbent consumption decreases. At a feed salt concentration of 0.045 M, the system is operated at optimal point *Y*. From that feed concentration on, an increase in inlet concentration leads to:

- an increased throughput (as explained at “throughput”), which decreases the desorbent consumption;
- an increased m_1, which increases the desorbent consumption.

This trade-off results in a gradual increase of the optimal inlet salt concentration. Only by optimization, it can be found that the optimum is at an inlet concentration of 0.05 M.

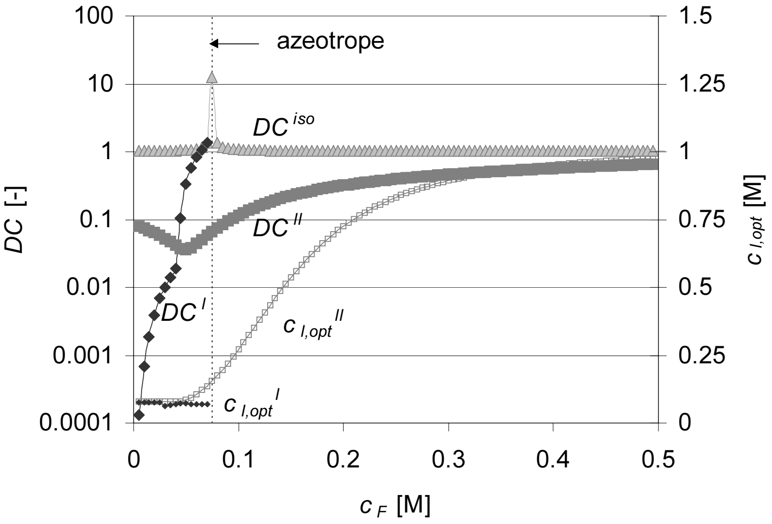

Figure 6. Desorbent consumption and optimal inlet concentration in isocratic and optimized gradient SMB at a maximum inlet concentration of 1 M NaCl.

It can be concluded that the desorbent consumption in closed loop mode is always lower in gradient operation than in isocratic operation. In gradient operation, m_1 is reduced as a result of the low affinity in section I. Furthermore, most of m_1 can be obtained from the recycle of m_4, since in a gradient it is more likely that the flow rate ratio m_4 exceeds m_1. The combination of these two factors results in a very low desorbent flow rate ratio of a desorbent of the maximal salt concentration. This finding seems general and independent of the values of K and z. In the specific case of the separation of BSA and the yeast protein, a gradient in region I may lead to a 8000 fold decrease of the desorbent consumption at very low c_F; a gradient in region II may lead to a thirty fold decrease of the desorbent consumption at c_F =0.05M NaCl (all in comparison to the isocratic situation).

Optimization of the salt consumption by changing the inlet salt concentration

The optimization of the salt consumption in a gradient SMB is not as straightforward as the optimization of throughput or desorbent consumption, since it may require rigorous numerical optimization (see Appendix I). However, in all optimizations carried out, the optimal flow rate ratios in fact equaled the analytical solution. This could not be explained.

In an isocratic SMB, the salt consumption *SC* is proportional to the feed salt concentration c_F, as is shown in Figure 7. The proportionality occurs, because the desorbent salt concentration equals c_F and the desorbent consumption is independent of c_F (cf. Figure 6). The salt consumption has an asymptote at c_{int}, because the desorbent consumption has an asymptote at that concentration.

In a gradient operated in region I at low feed salt concentrations, the salt consumption is minimal when the inlet salt concentration is near c_{int}. At this inlet concentration, m_1 is small and m_4 exceeds m_1, which allows a maximal recycle of m_4. The salt concentration of the recycled liquid can then be increased by the addition of a small volume of desorbent of high concentration. The salt consumption increases upon increasing c_F, because the affinity difference and throughput are reduced as the gradient approaches the isocratic situation (cf. Figure 5). The high inlet salt concentration near c_I remains favorable. Also, m_4 is reduced, which leads to a situation where an increased desorbent flow of decreased c_D is required to adjust both flow rate and salt concentration at c_F=0.04M NaCl. When the feed salt concentration approaches c_{int}, the system can only be operated isocratically.

When the SMB is operated in region II at low feed salt concentration, the conditions of optimal salt consumption coincide with the conditions of optimal desorbent consumption. Again, the maximization of the recycle and the addition of a very small volume of a concentrated desorbent is possible at these low feed salt concentrations. As the throughput increases with increasing c_F and constant c_I and m_1 is also constant, the salt consumption decreases with increasing c_F. Again, as c_F exceeds 0.045M NaCl, an increased inlet salt concentration can be used, since this increases throughput, whereas the recycle is still maximal and little salt needs to be added. The optimal salt concentration of 0.05M NaCl can only be found by optimization.

As c_F further increases, m_4 strongly decreases, because m_4 is related to the salt concentration in section III via *zBSA*; a large *zBSA* introduces a strong dependence. This reduces the percentage of m_1 that can be obtained from the recycle and hence a larger desorbent flow rate is required. Starting at a certain feed salt concentration of 0.07M NaCl, which cannot be deduced analytically, the optimal inlet salt concentration is “fixed”; it cannot decrease, because that would further increase m_1, but it cannot increase either, since this would increase c_3, reduce m_4 and reduce the possibility for salt recycle. From this concentration on, the optimal conditions for desorbent and salt consumption are no longer the same. This clearly demonstrates the trade-off mentioned in the theory section: a smaller m_I at higher inlet salt concentration may impose a larger salt need and hence be less beneficial than a (somewhat) larger m_I at lower inlet salt concentration.

At high feed salt concentration, the isocratic situation is optimal to reduce the salt usage. Throughput then hardly profits from the gradient, as shown in Figure 5. Gradient operation would only result in an increased demand for salt in the desorbent, because the recycle is very small.

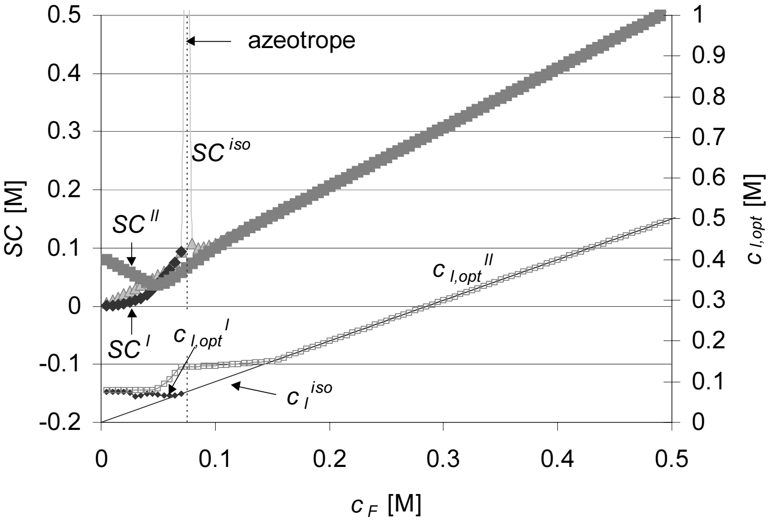

Figure 7. Salt consumption and optimized inlet concentration in isocratic and optimized gradient SMB at a maximum inlet concentration of 1 M NaCl.

It can be concluded that the salt consumption in closed loop mode can be lower in gradient operation than in isocratic operation. The reuse of the liquid leaving section IV to supply a flow rate and a starting salt concentration for the liquid in section I is very important. Thus, the addition of a very small amount of salt is possible. This finding seems general and does not depend on the values of K and z. In the specific separation of BSA and the yeast protein separation used as an example, the gradient in region I results in a reduction of the salt consumption of up till a factor 40 compared to the isocratic situation. The gradient SMB operated in region II at feed concentrations near c_{int} is better than isocratic operation, because the isocratic separation has an asymptote at that concentration. However, when the feed salt concentration is about twice c_{int}, isocratic operation is most favorable for reduction of salt consumption.

Overall comparison of isocratic and gradient SMB

Thus far, we have only regarded one optimization function at the time. However, the optimization of one function may lead to a poor result with respect to the other function. In Table IV, for all optimized functions, the other output functions are listed as well. The table clearly indicates the dilemma. For example, a high inlet salt concentration is beneficial to maximize the throughput in region II, but this also means the desorbent and salt consumption are far beyond the optimal values.

Unexpectedly, the conditions for optimal desorbent and salt consumption are equal, both in region I and in region II. This is a result of the high extent of recycling at the low salt concentrations, which decreases both desorbent and salt consumption.

From the table it can be concluded that the “overall optimum” is most likely a gradient SMB operated in region I at the minimal feed salt concentration and an inlet salt concentration near c_{int}. These conditions lead to a near-optimum throughput and minimal desorbent consumption and salt consumption. With respect to desorbent consumption, it is very advantageous to operate under gradient conditions; the gradient is able to reduce the desorbent consumption by almost a factor 8000 for the underlying example.

Table IV. Optimized and calculated process parameters.

optimized function	c_F [M]	c_I [M]	*P* [L/L]	*DC* [-]	*SC* [mol/L]
P (region I)	0.005	0.005	1700	1.020	0.005
P (region II)	0.073	1.000	2.953	0.222	0.222
DC (region I)	0.005	0.075	1610	$1.32\cdot10^{-4}$	$1.32\cdot10^{-4}$
DC (region II)	0.049	0.083	0.644	0.036	0.036
SC (region I)	0.005	0.075	1610	$1.32\cdot10^{-4}$	$1.32\cdot10^{-4}$
SC (region II)	0.049	0.083	0.644	0.036	0.036

Conclusions

A procedure was developed for the optimization of the SMB separation of dilute mixtures of proteins that obey mass action isotherms. The procedure was illustrated using the separation of BSA and a yeast protein on Q-Sepharose FF as an example. The following general conclusions could be drawn:

- a gradient is useful to improve throughput, desorbent consumption and/or salt consumption when the feed is at a salt concentration below two times the concentration of reversal of selectivity (c_{int});
- a feed of salt concentration (near) c_{int} can only be separated with a reasonable throughput in a gradient operated at salt concentrations exceeding c_{int} (i.e. region II);
- when operating in region II and when $zBSA>1$, the addition of salt to the feed improves throughput. In effect, the addition of more salt than strictly necessary for avoiding azeotropic phenomena is preferable. This is truly counterintuitive!
- isocratic operation leads to a (local) maximum of throughput in region I;
- operation of a gradient in region I reduces desorbent and salt consumption compared to isocratic SMB;
- desorbent and salt use benefit most from the maximization of the recycle of the liquid from section IV to section I. A very small desorbent flow of a concentrated solution is then sufficient to adjust flow rate and salt concentration;
- under maximal recycle, the conditions of minimal desorbent and minimal salt consumption coincide;
- the preferred way of operating the SMB for separation of dilute mixtures of proteins is at minimal feed salt concentration, at an inlet salt concentration near c_{int}.

Acknowledgements

This research was sponsored by the Dutch ministry of Economic affairs through Senter in the framework of IOP-milieu preventie.

Notation

c	concentration in the liquid phase	[M]
DC	desorbent consumption	[-]
des	flow rate ratio of desorbent	[-]

K	distribution coefficient	[-]
m	flow rate ratio	[-]
P	throughput	[L feed/L sorbent]
q	concentration in the sorbent phase	[M]
S	selectivity constant	[-]
SC	salt consumption	[M]
V,W,X,Y,Z	optimal point	[-]
z	ionic charge	[C/mole]

greek

α	discrepancy factor	[-]

super- and subscripts

D	desorbent
F	feed
i	component index (BSA, yp)
I	in section I, inlet
int	at the intersection
iso	in the isocratic situation
max	maximal
min	minimal
opt	at the optimal point
p	protein
s	salt
W,Y	at the optimal point W or Y

Literature

Ballanec, B. and G. Hotier, “From batch to simulated countercurrent chromatography,” In: *Preparative and production scale chromatography,* G. Ganetsos and P.E. Barker (eds.), Marcel Dekker, New York (1993).

Ching, C.B. and D.M. Ruthven, “Experimental study of a simulated countercurrent adsorption system IV Non-isothermal operation,” *Chem. Enging. Sci.* **41**, 3063 (1986).

Freitag, R. and S. Vogt, “Comparison of particulate and continuous-bed columns for protein displacement chromatography,” *J. Biotechnol.* **78**, 69 (2000).

Houwing, J., H.A.H. Billiet, J.A. Wesselingh and L.A.M. van der Wielen, "Azeotropic phenomena during separation of dilute mixtures of proteins by simulated moving bed chromatography," *J. Chem. Technol. Biotechnol.,* **74**, 213 (1999), chapter 3 of this thesis.

Houwing, J., T.B. Jensen, S.H. van Hateren, H.A.H. Billiet and L.A.M. van der Wielen, "Positioning of salt gradients in ion exchange SMB," *A.I.Ch.E. J.*, **49**, 665 (2003), chapter 5 of this thesis.

Jensen, T.B., T.G.P. Reijns, H.A.H. Billiet and L.A.M. van der Wielen, "Novel simulated moving bed method for reduced solvent consumption," *J. Chromatogr.*, **873**, 149 (2000).

Juza, M., M. Mazzotti and M. Morbidelli, "Simulated moving-bed chromatography and its application to chirotechnology," *Tibtech.*, **18**, 108 (2000).

Mazzotti, M., G. Storti and M. Morbidelli, "Supercritical fluid simulated moving bed chromatography," *J. Chromatogr.*, **786**, 309 (1997a).

Mazzotti, M., G. Storti and M. Morbidelli, "Robust design of countercurrent adsorption separation processes: 4. Desorbent in the feed," *A.I.Ch.E. J.*, **43**, 64 (1997b).

Natarajan, V., B.W. Bequette and S.M. Cramer, "Optimization of ion-exchange displacement separations. I. Validation of an iterative scheme and its use as a methods development tool," *J. Chromatogr.*, **876**, 51 (2000).

Ruthven, D.M. and C.B. Ching, "Countercurrent and simulated countercurrent adsorption separation processes," *Chem. Eng. Sci.,* **44,** 1011 (1989).

Schulte, M. and J. Strube, "Preparative enantioseparation by simulated moving bed chromatography," *J. Chromatogr.,* **906**, 399 (2001).

Storti, G., M. Masi, S. Carrà and M. Morbidelli, "Optimal design of multicomponent countercurrent adsorption separation processes involving non-linear equilibria," *Chem. Eng. Sci.*, **44**, 1329 (1989).

Appendix I: optimum flow rates

This appendix proves that the flow rate ratios at the optimal point of the region of complete separation (point *V, W*, *X, Y, Z*), and the maximal m_4 and minimal m_1 at given salt concentrations c_I and c_F generally lead to the optimal concentration factors, eluent and salt consumption.

The optimal flow rate ratio at maximum/minimum process variable is found by equating the derivative of the variable on the flow rate ratio to zero. In this differentiation, the flow rate ratios are independent variables, as they can be chosen independent of one another (as long as they are chosen within the constraints). When there is no zero in the constrained interval, the optimal flow rate ratio is found at the limits of the interval.

In Table V, all derivatives of the optimization functions to m_1 through m_4 are shown. In most cases, no zero occurs in the respective interval; maximal or minimal indicates which extreme of the flow rate ratio is optimal.

Table V. Derivatives of optimization functions.

f	$\frac{df}{dm_1}$	$\frac{df}{dm_2}$	$\frac{df}{dm_3}$	$\frac{df}{dm_4}$
DC $(c_D < c_{D,max})$	$\frac{1}{m_3 - m_2}$ minimal m_1	$\frac{m_1 - m_4}{(m_3 - m_2)^2}$ minimal m_2	$-\frac{m_1 - m_4}{(m_3 - m_2)^2}$ maximal m_3	$-\frac{1}{m_3 - m_2}$ maximal m_4
DC $(c_D > c_{D,max})$	$-\frac{x}{xm_2 - ym_3}$ minimal m_1	$\frac{x^2}{(xm_2 - ym_3)^2}$ minimal m_2	$\frac{-xy}{(xm_2 - ym_3)^2}$ maximal m_3	0 -
SC $(c_D < c_{D,max})$	$\frac{c_I}{m_3 - m_2}$ minimal m_1	$\frac{c_I(m_1 - m_4)}{(m_3 - m_2)^2}$ minimal m_2	see below	$\frac{-xm_2 - c_F m_4}{m_3(m_3 - m_2)}$ maximal m_4
SC $(c_D > c_{D,max})$	$-\frac{xc_D}{xm_2 - ym_3}$ minimal m_1	$\frac{x^2 c_D}{(xm_2 - ym_3)^2}$ minimal m_2	$\frac{-xyc_D}{(xm_2 - ym_3)^2}$ maximal m_3	0 -

where $x = c_I - c_F$ and $y = c_D - c_F$.

The missing equation in the table is:

$$\frac{dSC}{dm_3} = \frac{-m_1 c_I m_3^2 + m_4 c_F m_3^2 + 2 m_2 m_3 m_4 x - m_4 x m_2^2}{(m_3 - m_2)^2 m_3^2}$$

This equation cannot be solved analytically.

From this table we conclude that it is generally favorable to use the minimal m_1 and m_2, and the maximal m_3 and m_4. However, this does not hold true in case of the salt consumption when the required desorbent concentration exceeds the maximal allowed one. In that case, a complete optimization of both m_1, m_2, m_3, and m_4 is necessary. Note that the equations in Table V are independent of the equilibrium constants and hence are applicable to any separation.

Appendix II: general applicability

In this appendix, it will be shown that the approach is not limited to the specific example used as illustration, but is general.

First, we'll proof that the curves are of similar shape, independent of the isotherm parameters K_i and zi. The optimal point is determined by at least one limit on m_3. Rewriting in terms of m_2 makes the equations explicit:

$$m_2 = m_3 \frac{\left(\frac{K_i}{m_3}\right)^{\frac{1}{z_i}} - c_F}{c_I - c_F}$$

The maximum or minimum of this equation is found by setting the derivative of m_2 to m_3 to zero:

$$\frac{dm_2}{dm_3} = \frac{\left(\frac{K_i}{m_3}\right)^{\frac{1}{zi}}\left(1 - \frac{1}{z_i}\right) - c_F}{c_I - c_F} = 0 \qquad \mathbf{(4)}$$

Irrespective of the values of K_i and zi, there is only one solution to this equation, which is:

$$m_3 = K_i \left(\frac{1 - \frac{1}{zi}}{c_F}\right)^{zi}$$

It follows that each limit on m_3 only has one maximum when plotted as a function of m_3. When each of the two limits on m_3 has one maximum, the lines can intersect at two points at maximum, irrespective of the values of K_i and zi. These points of intersection are found by equating the m_3 values.

Complete separation dictates that the SMB can only be operated at combinations of m_2 and m_3 that are inside the curve of the more retained component and outside the curve of the less retained component. Hence, when there is one point of intersection of the limits on m_3, the shape of the region of complete separation is similar to the region described in the main text. The conditions for the optimal point listed in Table III can then be used: the approach is general. When there is no point of intersection, the optimal point is at *X*, although it should be kept in mind that part of the region of complete separation can be accessible. When there are two points of intersection, the region of complete separation is split in two. The optimal point is again at *X*, but a large part of the region of complete separation is not accessible.

5

Positioning of salt gradients in ion exchange SMB

Abstract

Salt gradients can be used to improve the efficiency of ion exchange separations in Simulated Moving Bed (SMB) systems. The gradient, formed by the use of feed and desorbent solutions of different salt concentrations, introduces regions of increased and decreased affinity of (e.g.) proteins for the matrix.

Several shapes of the gradient can be formed, depending on the flow rate ratios and salt concentrations used. Only some of these effectively increase throughput or decrease desorbent consumption. Correct gradient positioning is essential, but not trivial, because salt adsorbs to the resin. A procedure has been developed to select the flow rate ratios that allow correct positioning of gradients. It is based on wave theory and incorporates the non-linear Donnan isotherm of salt on ion exchange resins. Predictions are verified by experiments combined with a mathematical equilibrium stage (true moving bed) model. A comparison of upward and downward gradients with respect to the use of desorbent and salt is included.

This paper has been published in: *A.I.Ch.E. J.* **49**, 1158 (2003).

Introduction

More and more, Simulated Moving Bed (SMB) systems are used for separation of fine chemicals and pharmaceuticals. The countercurrent chromatographic process has successfully been applied for more efficient separation of similar molecules, reduction of resin inventory and reduction of solvent consumption relative to conventional chromatographic processes (Juza *et al*., 2000; Van Walsem and Thomson, 1997; Ballanec and Hotier, 1993).

In earlier work, we have introduced the salt gradient SMB. The gradient, a situation of high affinity above the feed and a low affinity below the feed, improves the separation of diluted protein mixtures by ion exchange chromatography (Houwing *et al.*, 1997, 1999). In protein separations, salt is often used to manipulate the affinity of proteins for the ion exchange resin (Kopaciewitz *et al.*, 1989). The affinity is reduced at increased salt concentration. Thus, different salt concentrations in the feed and desorbent of an SMB can introduce regions of high and low affinity (Figure 1). The high affinity situation above the point of feed introduction enables loading of a large volume of feed. The low affinity below the feed point facilitates elution of the protein. Thus, compared to the isocratic situation, throughput is increased whereas solvent consumption is decreased. Only few references on gradients in SMB systems have been found in literature.

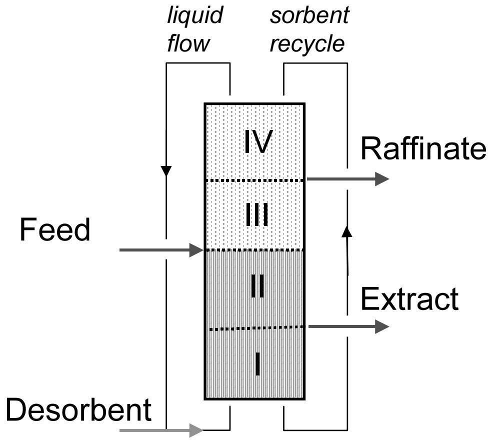

Figure 1. Schematic representation of a gradient in an SMB system. An increased intensity of shadings indicates an increased salt concentration, i.e. a decreased affinity.

These include the use of temperature gradients for separation of amino-acids (Ruthven and Ching, 1989) and enantiomeric amino-acid derivatives (Migliorini *et al.*, 2001), pressure gradients in supercritical fluid SMB (Mazzotti *et al.,* 1997) and gradients in solvent strength in reversed phase chromatography (Jensen *et al.*, 2000).

In previous work (Houwing *et al.*, 1997, 1999), we have assumed that the sorbent is saturated with salt, independent of the location in the SMB. However, salt may adsorb unto the resin in a concentration dependent manner (Jansen *et al.*, 1996). Then, the positioning of the gradient is no longer straightforward. The distribution of salt over the two phases, which depends on the location in the system, needs to be computed similar to that of any adsorbing component. The movement of salt should thus be considered for correct flow rate selection. Several procedures have been described for the selection of the relative liquid to sorbent flow rates in SMB systems. These rely on the True Moving Bed (TMB) analogy of the simulated moving bed, i.e. where both sorbent and solvent move. The most important procedures are based on wave theory. “Triangle theory”, is based on the net flow of components and uses a mathematical transformation (omega-transform) (Storti *et al.*, 1993). A similar approach, without transformation, is suggested by Ma and Wang (1997). Also, McCabe Thiele analysis is used for flow selection (Ruthven and Ching, 1989).

This paper starts with the description of a typical isotherm of salt on an ion exchange resin. This isotherm is used in the procedure for positioning of the salt gradient in the SMB, based on wave theory. Experimental results are shown that confirm the theory. The paper concludes with a comparison of upward and downward gradients with respect to solvent and salt use.

Theory

Salt isotherm

For the description of the behavior of salt solutions on ion exchange resins, we would like to draw a parallel to membrane science. In nanofiltration, a charged membrane is used to separate charged ionic species. At low salt concentrations, the co-ions, i.e. ions of like charge as the membrane do not enter the membrane, due to ionic repulsion. This is also known as “Donnan exclusion”. At increased salt concentrations, the co-ion also passes the membrane, as the electrical shielding extends over a shorter range at increased ionic strength. (Mulder, 1991).

A similar phenomenon has been observed in ion exchange chromatography (Jansen *et al.* 1996). At low salt concentration, only the counterions enter the resin and are exchanged, whereas the co-ions are excluded. However, at increased concentration, the integral salt molecule is taken up as a result of the reduced charge effects.

Consider an ion exchange resin of capacity *Q,* that is contacted with a solution of sodium chloride at molarity *c*. The concentration of ions in the sorbent and liquid at equilibrium can be calculated by equating the chemical potentials of ion *i* in the two phases:

$$\Delta\mu_i^{\ 0} + RT\ln\frac{x_i}{y_i} + z_i F\Delta\Psi = 0 \qquad \textbf{(1)}$$

Where $x_i = c_i/Q$, $y_i = q_i/Q$, z_i is the charge of ion *i*, $\Delta\mu^0$ denotes the difference in standard chemical potential of the liquid to the sorbent phase and $\Delta\Psi$ is the electrical potential difference of liquid to sorbent phase. In the derivation, it has been assumed that the solutions behave thermodynamically ideal and that swelling effects can be neglected. Since both sodium and chloride experience the same potential difference, $\Delta\Psi$ is eliminated by addition of the two component balances. The result is:

$$\frac{y_{Cl}}{x_{Cl}} = S\frac{x_{Na}}{y_{Na}} \qquad \text{where} \qquad S = \exp\left(\frac{\Delta\mu_{Na}^0 + \Delta\mu_{Cl}^0}{RT}\right) \qquad \textbf{(2)}$$

The quantity *S* is a selectivity coefficient, which is similar to the selectivity coefficient during uptake of two counterionic species.

The concentrations of sodium and chloride are related by the electroneutrality equations for liquid and sorbent phase:

$$\begin{aligned} &\text{liquid:} & x_{Na} &= x_{Cl} \\ &\text{sorbent:} & 1 + y_{Na} &= y_{Cl} \end{aligned} \qquad \textbf{(3)}$$

Substitution of (3) in (2) leads to:

$$y_{Na} = -\frac{1}{2} + \frac{1}{2}\sqrt{1 + 4S\,x_{Na}^{\ 2}} \qquad \textbf{(4)}$$

At low concentrations, salt is predicted to be excluded from the resin, whereas at high concentrations, it is taken up proportionally to the salt concentration, with a proportionality constant that equals the square root of the selectivity (Figure 2). This shape of isotherm results in diffuse breakthrough fronts during loading of a column with increasing concentrations as well as sharpening breakthrough fronts during elution with decreasing concentrations (Helfferich and Klein, 1970).

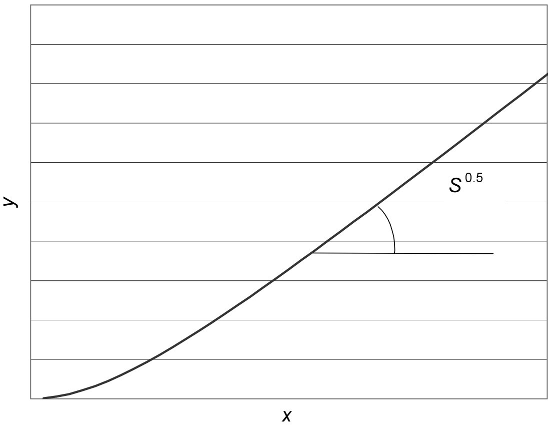

Figure 2. Donnan-based isotherm of salt on an ion exchange resin.

Upward and downward movement

Any component present in the SMB is moved in a certain direction relative to the fixed in- and outlets. In fact, it is not the component that is moved, but the fronts between the loaded and unloaded portions of the column. The direction and rate of movement can be determined from wave theory; the front velocity *(w)* in the countercurrent separation system is calculated from (Rhee *et al.*, 1971):

$$w = \frac{v_s \beta \left(m - \frac{\partial q}{\partial c} \right)}{\left(1 - \beta \frac{\partial q}{\partial c} \right)} \qquad \textbf{(5)}$$

Where v_s is the interstitial solids velocity, β is the column phase ratio (=$(1-\varepsilon)/\varepsilon$), where ε is the column porosity, $m=\Phi_L/\Phi_S$ indicates the flow rate ratio of liquid to resin phase and $\partial q/\partial c$ is the slope of the isotherm. In case of shock waves, all $\partial q/\partial c$ are replaced by $\Delta q/\Delta c$, the chord of the isotherm.

A positive wave velocity indicates upward movement (cf. Figure 1). Hence, upward movement will only occur when the numerator is of positive sign, i.e. when the value of m exceeds the local slope $\partial q/\partial c$ (in case of diffuse wave) or chord $\Delta q/\Delta c$ (in case of sharpening wave) of the isotherm.

Gradient shapes

Salt is an adsorbing component. Hence, the fronts that determine the gradient can move both upward and downward. Thus, gradients can occur in different shapes and can be formed from different starting conditions. For reasons of clarity, let us define the gradient shapes:

- a "top gradient" is the situation of high affinity above the feed and low affinity below the feed.
- a "bottom gradient" is the situation of low affinity above the feed and high affinity below the feed.
- an "upward gradient" is the situation where the salt is predominantly transported by the liquid phase.
- a "downward gradient" is the situation where the salt is predominantly transported by the sorbent phase.

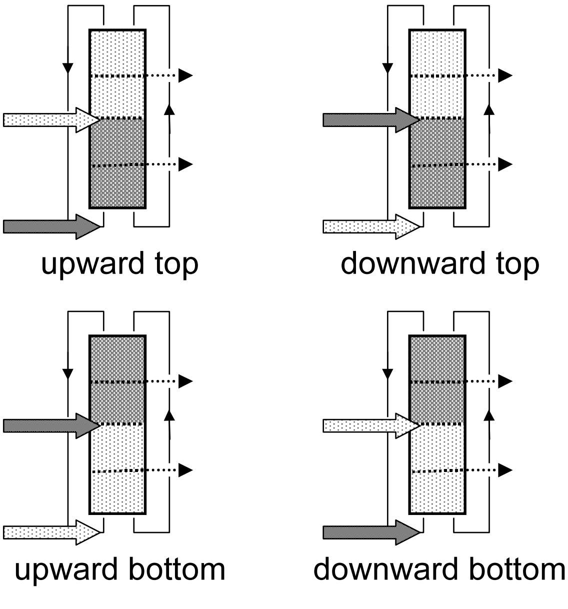

Figure 3. Schematic drawing of gradient shapes. A high intensity of shading indicates a high concentration of salt, i.e. a low affinity of proteins for the matrix.

In the previous work (Houwing *et al.*, 1997, 1999), we have discussed the most obvious form of the gradient, the “upward top” gradient (Figure 3). A desorbent of high salt concentration and a feed solution of lower salt concentration are used. This situation is only possible at low affinity of the salt or at high flow rate ratios, i.e. where salt is transported predominantly by the liquid.

A less obvious form of the gradient, the “downward top” gradient, occurs when there is a strong interaction of salt and the ion exchange resin and flow rate ratios are relatively low. Salt is then predominantly transported by the sorbent. The top gradient is formed by the use of a low salt concentration in the desorbent and a high salt concentration in the feed.

Similarly, “bottom” gradients can be formed. An “upward bottom” gradient is formed using concentrated feed and less concentrated desorbent at flow rate ratios that allow upward motion. The “downward bottom” gradient is formed using concentrated desorbent and less concentrated feed at flow rate ratios that allow downward transport. However, only the “top” gradients have the desired effect of improvement of the loading capacity and reduction of solvent consumption. The “bottom” gradient is very unfavorable, since the low affinity in the top sections reduces the loading capacity of the adsorbent and the high affinity in the bottom sections increases solvent consumption. In the following, we will only consider the “top” gradients.

Positioning of gradient

In order to correctly position the gradient, the relative liquid to sorbent flow rates ratios need to be chosen carefully. The procedure to estimate these flow ratios is based on wave theory (Helfferich and Klein, 1970; Rhee *et al.,* 1971) and is similar to the procedures suggested by Storti *et al.* (1993) and Ma and Wang (1997). The basis is the wave velocity equation (5), where the flow rate ratios are adjusted to assure upward or downward movement.

The procedure can be summarized as follows:

1. Define the concentrations at the lower (L) and upper (U) side of the fronts. The lower side of the front is the side nearest to the lower section number (cf. Figure 1).
2. Realize the shape of the front: shock fronts or spreading fronts may occur as a result of the non-linear isotherm.
3. Calculate the front velocity from wave theory and adjust the flow rate ratios such that upward or downward movement is assured.

Step 1: defining concentrations.

The concentrations occurring in the SMB are governed by the flow rates used. On beforehand, the profiles in the SMB can be drawn qualitatively. In the following, we will only consider an “open-loop system”, where the liquid leaving section IV is not recycled to section I.

In case of an upward gradient, the lower sections (I and II) of the simulated moving bed are saturated with the desorbent. At the point of feed introduction, the feed solution and the stream leaving section II are mixed, leading to a lower concentration, which will extend all over sections III and IV.

The change in concentration at the feed point cannot be abrupt, as a result of dispersion as well as of local non-equilibrium at the feed position. Thus, there is a gradual decrease in concentration just below the feed inlet. The gradual decrease cannot occur above the feed, since it would then immediately be transported through the column, as any front. A similar situation occurs at the desorbent inlet. An indicative drawing is shown in Figure 4.

In case of a downward gradient, sections III and IV are at the higher concentration. The gradual transitions in concentrations are located just above the feed and desorbent point as indicated in Figure 4. No change in concentration is seen just below these points, since any change in concentration is immediately transported downward as a new front.

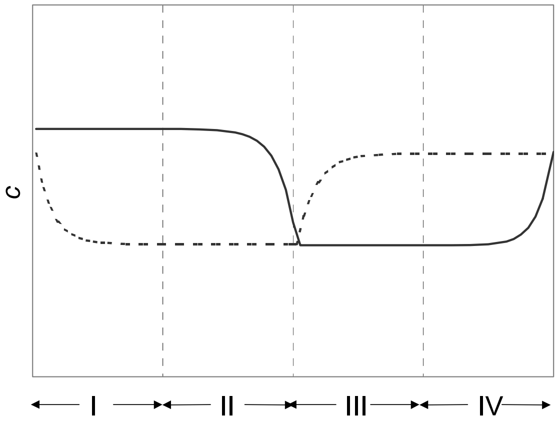

Figure 4. Schematic drawing of the profile in an equivalent TMB at an upward (drawn line) and downward (dashed line) gradient. Roman numbers indicate section numbers.

For quantitative description of the concentrations, mass balances need to be solved.

In case of the upward gradient, there is one unknown concentration, namely the concentration in sections III and IV. It can be calculated as a function of m_3 from a mass balance over the feed position:

$$m_2\, c_D + (m_3 - m_2)c_F - m_3\, c_{III} + q_{III} - q_D = 0 \qquad \textbf{(6)}$$

Where c_F and c_D are the feed and desorbent concentrations, respectively, and q_D is the resin phase concentration in equilibrium with the desorbent. Equilibrium is assumed to be reached in all sections (cf. Storti *et al.*, 1993); hence the solid phase concentration in section *j* can be calculated from the corresponding liquid phase concentration from the isotherm. This equation differs from the one used in previous work (Houwing *et al.*, 1999), where the terms q_{III} and q_D cancel because of the assumed constant saturation of the resin.

In case of a downward gradient, there are two unknown concentrations, namely the concentrations at saturation in the major part of section I and section II (c_{II}) and the major part of section III and section IV (c_{IV}). They can be obtained from the mass balance over the feed point, combined to the mass balance over the desorbent point.

The mass balance over the feed point reads:

$$m_2 c_{II} + (m_3 - m_2)c_F - m_3 c_{IV} + q_{IV} - q_{II} = 0 \qquad \textbf{(7)}$$

Where q_{II} and q_{IV} are the sorbent concentrations in equilibrium with c_{II} and c_{IV}, respectively.

The mass balance over the desorbent point reads:

$$m_3 c_{IV} - (m_4 - m_3)c_R - m_4\, c_W + m_1\, c_D - m_2\, c_{II} - (m_1 - m_2)c_E + q_{II} - q_{IV} = 0 \qquad \textbf{(8)}$$

The quantities c_E, c_R and c_W are the concentrations at the extract, raffinate and waste stream, respectively. Between section II and the extract outlet exists no front. Neither exists a front between section IV and the waste outlet, nor between section IV and the raffinate outlet (cf. Figure 4) so:

$$\begin{aligned} c_E &= c_{II} \\ c_R &= c_W = c_{IV} \end{aligned} \qquad \textbf{(9)}$$

Then, the mass balance over the desorbent point can be rewritten to:

$$m_1\left(c_D - c_{II}\right) + q_{II} - q_{IV} = 0 \tag{10}$$

By this procedure, all important concentrations are defined as a function of *m*.

Step 2: Identification of waves

The wave velocity, equation (5), depends on the shape of the wave. In case of the Donnan isotherm, the loading of a fixed bed column with increasing salt concentrations results in diffuse waves, whereas the elution of a column with decreasing concentration results in shock waves (Helfferich and Klein, 1970), as has already been indicated. The same occurs in case of SMB systems (Rhee *et al*., 1971; Storti *et al*., 1989). A wave is a shock wave when a lower concentration displaces a higher concentration relative to the direction of liquid flow, whereas a diffuse wave will occur in the reverse situation.

Step 3: Calculation of front velocity and determination of flow rate ratio

Once the concentrations and shapes of the fronts are identified, the flow rate ratios required for upward or downward movement can easily be calculated using equation (5).

The results of step 1 through 3 are given in Table I. In case of the upward gradient, both fronts are bound by c_D and c_{III}. The entire spreading wave must have a positive velocity in sections I and II. Hence, the flow rate ratios m_1 and m_2 have to exceed the maximal slope of the isotherm in the concentration interval, i.e. at concentration, i.e. c_D. The shock wave in section III and IV must also have a positive velocity, so the flow rate ratios m_3 and m_4 need to exceed the chord of the isotherm. Similarly, in case of the downward gradient, the shock wave bound by c_{II} and c_D in section I and II must move downward, so m_1 and m_2 need to be smaller than the chord of the isotherm. The maximum *m* in section III and IV is determined by the minimal slope in the concentration interval c_{II} to c_{IV}, that is the slope at the maximum concentration c_{IV}.

So far, the maximum or minimum flow rate ratios are obtained as a function of the concentrations in the system, as summarized in the far right column of Table I. The boundaries of an "operating region" (Storti *et al.,* 1993) can be calculated by equating *m* to the limiting value and simultaneously solving this equation and the mass balance equations over the feed and desorbent position (equations

(6), (7) and (10)). The result is a restricted area, which defines the flow rates that can be used for correct positioning of the gradient.

Table I. Constraints on flow rate ratios for the desired gradients (after Storti et al., 1993).

	Front	c_L	c_U	Front shape	m
Upward Gradient	I	c_D	c_{III}	Spreading	$m_1, m_2 > \left(\partial q / \partial c\right)_{c_D}$
	II	c_{III}	c_D	Shock	$m_3, m_4 > \left(\Delta q / \Delta c\right)_{c_D - c_{III}}$
Downward Gradient	I	c_D	c_{II}	Shock	$m_1, m_2 < \left(\Delta q / \Delta c\right)_{c_{II} - c_D}$
	II	c_{II}	c_{IV}	Spreading	$m_3, m_4 < \left(\partial q / \partial c\right)_{c_{IV}}$

Experimental

Materials

All salts were of analytical grade and were obtained from Merck. The sorbent, Q-Sepharose FF, was obtained from Amersham Pharmacia Biotech. This strong anion exchanger, based on highly cross-linked agarose has an average particle size of 90 µm and has a capacity for small ions of 0.2 mol/L packed bed (Pharmacia Biotech, 1996). All solutions used were based on a 0.01 M Tris buffer, pH 8.0.

Columns

Columns were prepared by packing the sorbent in empty columns according to the procedure described by the sorbent manufacturer. The sorbent was packed in 0.01 m diameter Omnifit glass columns, yielding a volume of 7.1 mL per column. The reproducibility of the packing procedure was checked by determination of the breakthrough volume of a 1.0 M NaCl solution on each column equilibrated with 0.2 M NaCl and vice versa. The resulting breakthrough volume was 7.16 ± 0.08 mL. The porosity of the packed bed ε was assumed to 0.4,which is near ideal packing of spherical particles.

SMB system

The 12 column simulated moving bed was assembled by the workshop of the Kluyver Laboratory for Biotechnology, analogous to the system described by Priegnitz (1996). Streams were connected to the correct columns by four twelve-port valves (Valco). An additional, twenty-four-port valve (Valco) served as a central valve in order to establish unidirectional flow (Priegnitz, 1996). All valves were controlled by software developed in the Kluyver Laboratory for Biotechnology. Liquid was supplied to the system by two Shimadzu LC8a pumps; the extract and raffinate streams were withdrawn by two Pharmacia P-600 pumps. The actual flow rates were measured by weighing of effluent amounts that were collected during a known time interval. The concentration of salt was monitored by a Pharmacia flow through conductivity electrode (Pharmacia Conductivity monitor CM-P). The dead volume of the assembled system was determined by breakthrough experiments of salt on the system without columns and was approximately 0.38 mL per column. Flow rate ratios were corrected for the dead volume as described by Migliorini *et al.* (1999).

Determination of isotherm

The distribution coefficient of salt was determined from the time of breakthrough of a stepwise change in salt concentration on individual columns, as well as on twelve columns connected in the SMB fashion. The steps in salt concentration used were 1.0 to 0.2 M as well as 0.30 to 0.22 M NaCl and vice versa. The time of breakthrough was identified as the time needed for reaching half of the concentration difference.

SMB experiments

During operation of the system, the recycle stream was wasted. Before the experiment, columns were regenerated using 1.0 M NaCl and preferably reequilibrated with 0.22 M NaCl. All experiments were carried out at room temperature, without temperature control.

Numerical procedures

Breakthrough profiles were simulated using mathematical column model programmed in Matlab. Mass transfer was included in the form of a linear driving force approximation, with an overall mass transfer coefficient determined from relations between Stanton, Reynolds and Schmidt dimensionless numbers (Houwing *et al.*, 2003). The system of partial differential equations was solved by spatial discretization using a fourth order Runge Kutta method. The steady state TMB profiles were computed using an equilibrium stage model as described in Ruthven and Ching (1989). In this model, the mass balances of all equilibrium stages were solved simultaneously using the Optimization Toolbox of Matlab. The number of equilibrium stages was adjusted to match mass transfer and dispersive effects.

Results and discussion

Distribution coefficients

The breakthrough experiments of NaCl on a single column and 12 columns in series were fitted by a mathematical model, based on the assumption of local equilibrium. A satisfactory fit was obtained at S=1.09 and Q=0.22 M (cf. Figure 5). The experimental time of breakthrough at the 0.22 M to 0.30 M NaCl step was smaller than at the time of breakthrough at the 0.2 M to 1.0 M NaCl step. This is in agreement with the equilibrium model, which predicts a low affinity at concentrations below Q and a higher affinity at higher concentrations (cf. Figure 2).

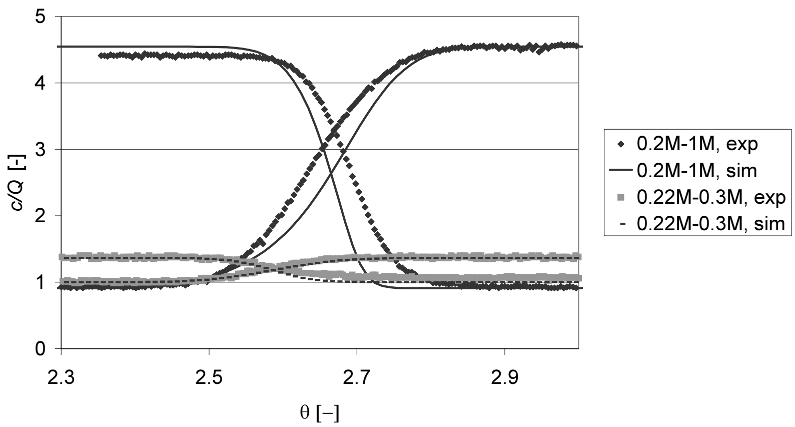

Figure 5. Experimental and simulated breakthrough of sodium chloride on 12 columns that form the laboratory-scale SMB system in series. Predicted line: S =1.09, Q =0.22 M.

Operating region

Using the experimental equilibrium isotherm, an operating region has been constructed in the case of an upward and downward gradient, following the procedure outlined in the theory section (Figure 6). In case of an upward gradient, the diffuse wave in section II sets the minimum flow rate ratio m_2 equal to the slope of the salt isotherm at the "slowest" desorbent concentration. The boundary on m_3 is not relevant, as the shock wave in section III always has a higher velocity than the velocity at the desorbent concentration. Hence, upward movement of this wave is already obtained at the limiting flow rate ratio m_2. At any point above the positive feed line, the salt wave in section III will move upward. As long as m_1 is chosen well above the critical value (Table I), its value does not influence the shape of the triangle. The concentration in section II invariably equals c_D and the concentration in section III is determined by m_2 and the feed flow rate only. The flow rate in section IV does not influence the concentration as long as it is chosen larger than the minimal value (see Table I). The minimal m_4 is actually smaller than the minimal m_2, because the shock wave in section IV is faster than the limiting concentration of the spreading wave in section II.

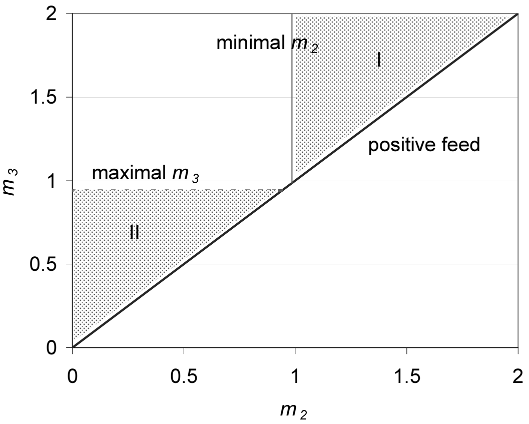

Figure 6. Operating region in case of an upward (I) and downward (II) gradient. In the latter case, m_1 has been set at its maximum.

Unlike for the upward gradient, m_1 does influence the shape of the region in case of a downward gradient, as is shown in Figure 7. Via the mass balance over the desorbent entry, equation (10), its value determines the concentrations in the simulated moving bed. At increasing m_1, more of the less concentrated stream is introduced and consequently, the concentrations in the SMB decrease (Figure 8). Thus, the slope and chord of the salt isotherm decrease and the region shifts to decreased *m*-values. Meanwhile, the maximal m_2 is reduced at decreasing m_1. This is necessary, since the extract stream is removed per definition, so m_2 cannot exceed m_1. This situation will frequently occur in practical situations, because eluent consumption is minimal at minimal m_1.

Obviously, m_1 has more influence on the salt concentration in bed III than it has on the concentration in bed II (Figure 8). This is expected, because the desorbent concentration is predominantly transported into section III and IV when the gradient moves downward. At increasing m_1, more of the desorbent of lower concentration is added, so the concentration in beds III and IV decreases.

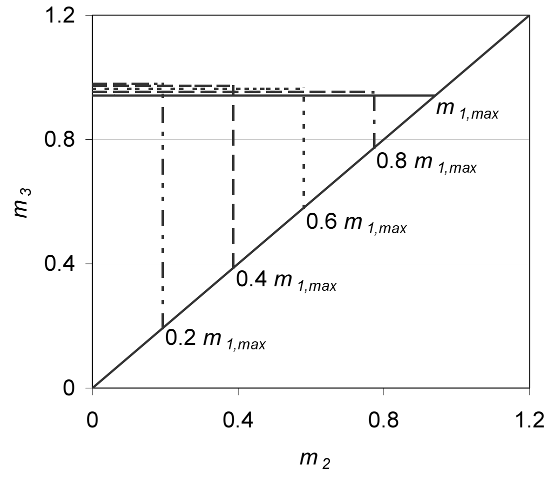

Figure 7. Influence of m_1 on the region of separation in case of a downward gradient.

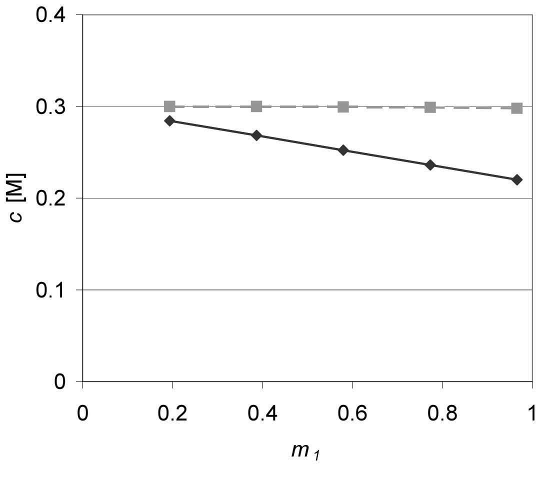

Figure 8. Influence of m_1 on the salt concentrations in section I and II (■) and III and IV (♦) in case of a downward gradient at m_2 =0.06 and at maximal m_3 assuming TMB operation. Conditions: c_D =0.22M, c_F =0.3M.

In case of a downward gradient, the boundary on m_2 as described in Table I is of little importance. When m_1 is chosen at its maximum value, it can be calculated using equation (10) that the concentration in the top sections is close to c_D, whereas the concentration in the lower sections is close to c_F. The flow rate ratio in section II (m_2) is then limited by the shock wave from c_F to c_D, whereas m_3 is bound by the wave velocity at c_D (Table I). Since c_D is the lowest concentration possible, this represents the maximal velocity that can occur at this set of concentrations. The shock in section II wave will per definition have a lower velocity. The criterion in bed II is always met, because the necessary positive feed prohibits that m_2 ever exceeds m_3. When m_1 is chosen below the maximum value, the criterion of m_2 is already met since the bounds on m_1 and m_2 are the same.

Experimental verification

Several SMB experiments have been carried out to confirm that only at flow rate ratios inside the triangular regions, the correct salt profile is obtained. The location of the experiments inside the operating region has been indicated in Figure 9, where the numbers correspond to the experiment numbers as given in Table II. During the experiments, the concentrations in the desorbent and feed as well as the values of m_1 have been changed slightly. Hence, the operating region is slightly different for each experiment. In the figure, shaded boundaries indicate the region between the maximal and minimal value during all experiments. Experiment 8 is not indicated in the figure, because fairly different salt concentrations have been used in that experiment.

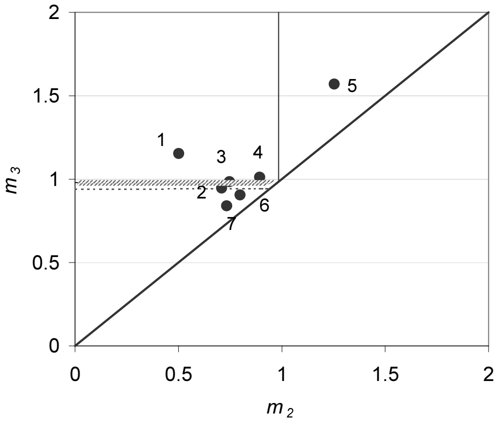

Figure 9. Position of experimental points in operating region. Hatched boundaries indicate the range; the boundaries slightly vary per experiment due to changing m_1 and salt concentrations (see Table II).

The experimental conditions and observed directions of movement are shown in Table II. Negative flow rate ratios are a result of the dead volume in the system, which has been accounted for using the approach of Migliorini (1999). The dead volume effect is quite important, because the dead volume is large compared to the column volume in a laboratory-scale system. The dead volume effect is enhanced further by the low distribution coefficient (about unity), which allows only low flow rate ratios, certainly in case of a downward gradient.

For prediction of direction of movement, the salt concentrations in the top and bottom sections have been calculated from the variables m, c_D and c_F using the mass balance equations, followed by determination of the direction of movement using the equations shown in Table I. In most experiments, the observed direction of movement of the salt agreed well with the predictions as is shown by the bold typeface used in Table II. In some experiments (e.g. experiment 1), the concentrations in the sections could not be calculated, since the experimental profile was not one of the gradient types assumed.

Table II. Experimental conditions and observed direction of movement. Bold indication of the direction of movement means that the observed direction of movement agrees with the direction of movement predicted from theory.

Exp.	1	2	3	4	5	6	7	8
c_D	0.22	0.22	0.22	0.22	0.3	0.22	0.22	0.27
c_F	0.3	0.3	0.3	0.3	0.22	0.31	0.31	0.15
m_1	1.12	0.95	0.93	0.98	1.56	0.95	0.88	2.11
m_2	0.50	0.71	0.75	0.89	1.25	0.80	0.73	1.12
m_3	1.15	0.95	0.98	1.01	1.57	0.91	0.84	3.07
m_4	-0.11	-0.34	-0.28	0.11	1.25	0.00	-0.05	1.09
Movement of salt in section								
I	**up**	up	**down**	**up**	**up**	up	**down**	**up**
II	**down**	**down**	**down**	**down**	**up**	**down**	**down**	**up**
III	up	**down**[1]	up	**up**	**up**	**down**[1]	**down**	**up**
IV	down	**down**	**down**	**down**	**up**	**down**	**down**	**up**

[1] no movement is predicted based on the calculated concentrations.

The experimental profiles at steady state were well predicted by an equilibrium stage TMB model, as is shown in Figure 10, where the experimental points represent the values at the mid-point of the switch interval (cf. Ruthven and Ching, 1989). In case of the upward gradient (experiment 8, Figure 10A), the fronts are positioned just before the outlet of the bed. This is the result of the front moving in upward direction all over the system; so the front "bounces" against the feed and desorbent inlet. A similar situation is seen in case of a downward gradient (experiment 7, Figure 10B), except that the fronts are now just after the feed and desorbent position.

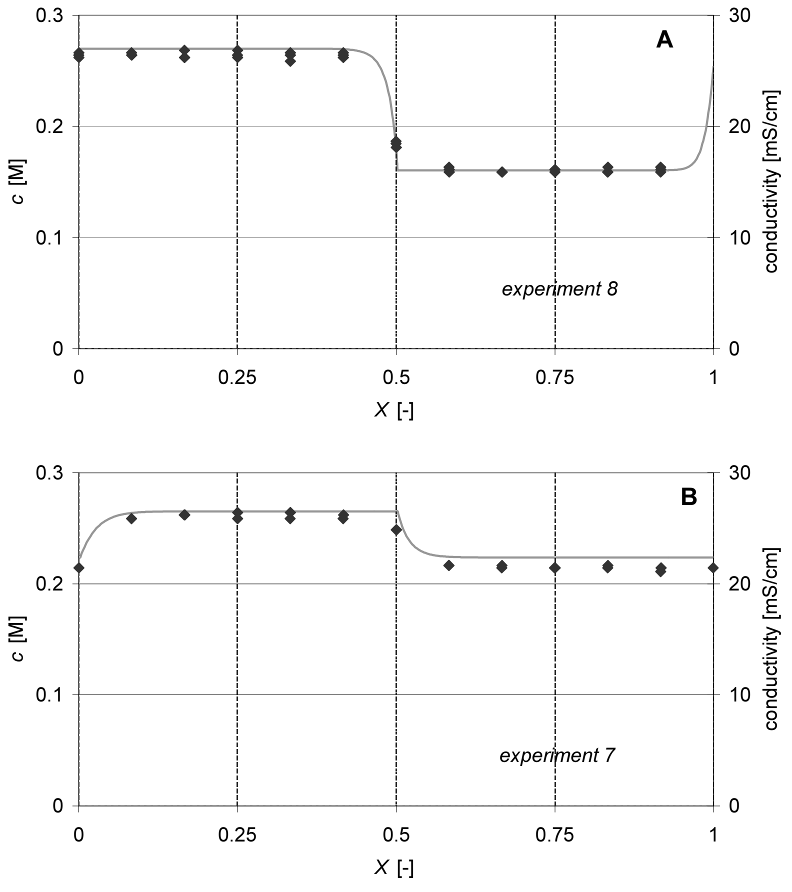

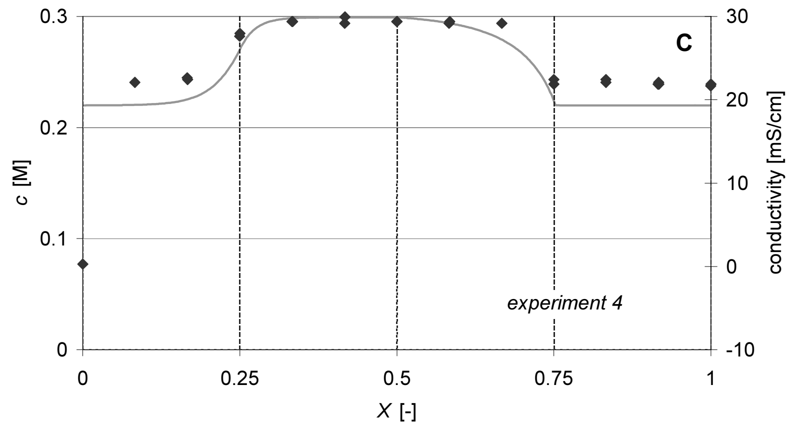

Figure 10. Simulated concentration profiles (lines) and experimental conductivity profiles (points) and at steady state.

Experiment 4 was positioned besides the operating region. In this experiment, both m_1 and m_3 exceeded the maximal allowed flow rate ratio. Upward movement in section I and downward movement in section II resulted in positioning of the first front between these sections. Similarly, the front between section III and IV is a result of upward movement in section III and downward movement in section IV (Figure 10C). The obtained gradient is neither a "top" nor a "bottom" gradient, but could be called a "center" gradient. It is of low practical value, since the high concentration of salt in the middle sections (II and III) induce a low affinity and hence a low throughput. Meanwhile, a high desorbent consumption is induced by the high affinity in section I.

Upward or downward gradient?

This paper shows that both upward and downward gradients can be achieved. Which of the two is to be used primarily depends on the characteristics of the proteins to be separated, as will be shown in a following paper. Here, we will only give some general considerations with respect to throughput and desorbent and salt consumption.

Throughput

An upward gradient is generally preferable with respect to throughput, i.e. the volume of feed loaded per volume of sorbent, which is proportional to the feed flow rate (m_3-m_2). In the upward gradient, an upper limit to m_3 is absent, which enables operation at high feed flow rate ratios (seen in Figure 6 as a long distance of the operating point to the “positive feed” line). On the contrary, a maximum m_3 is set in the downward gradient, imposed by downward movement of salt. Hence, productivity is limited, and the use of sorbent may be considerable. It should be noted that the upward gradient SMB may have a technological limit in the (feed) flow rate, since highly asymmetrical SMBs with a low flow rate in the lower sections and an extremely high flow rate in the upper sections can hardly be operated accurately.

Desorbent and salt consumption.

Let us first focus on the absolute amount of desorbent consumed. This quantity is set by the flow rate ratio in section I, m_I. In the downward gradient, m_I is to be smaller than the chord of the isotherm between the high concentration c_{II} and the low concentration c_D (see Table I). In the upward gradient, m_I is to exceed the slope of the isotherm at concentration c_{II}, which is always larger than the mentioned chord (cf. Figure 2). Hence, the downward gradient is always operated at lower m_I, and hence the absolute consumption of desorbent is lower in the downward gradient in comparison to the upward gradient.

For a comparison of the desorbent use relative to the feed volume, we have chosen a number of gradient compositions, characterized by a fixed concentration c_{II} of 0.3 M NaCl, and a fixed concentration c_{III}, between 0 and 0.3 M. For each of these gradients, we have computed the m-values and the required feed and desorbent concentration in both up and downward gradient, using the mass balances and Table I. Some additional chosen variables are given in Table III. The value of m_1 and m_2 have been chosen near the minimal value indicated in Table I, thus minimizing desorbent use and maximizing throughput. Furthermore, the concentration of salt in the feed in case of an upward gradient was chosen near the aimed concentration in the top sections, which allows for a large feed flow rate and maximum throughput. To finalize the analysis, the desorbent use ($=m_1/(m_3-m_2)$) as well as the consumption of salt ($=c_F+c_D{\cdot}m_1/(m_3-m_2)$) relative to the feed volume have been calculated.

Table III. Parameters used in comparison of upward and downward gradient.

parameter	value	meaning
α_1	1.1	ratio $m_1/m_{1,min}$, upward gradient
α_2	1.05	ratio $m_2/m_{2,min}$, upward gradient
α_3	1.05	ratio $m_{3,max}/m_3$, downward gradient
α_4	1.05	ratio c_{III}/c_F, upward gradient
$m_{1,min}$	0.4	minimal m_1,downward gradient
$m_{2,min}$	0.1	minimal m_2, downward gradient

The desorbent as well as the salt use in an upward gradient SMB increase at increasing difference between the bottom and top concentration (cf. Figure 11). This is easily explained: the larger the difference in top- and bottom concentration, the larger the amount of feed that can be added, and the higher throughput. Meanwhile, the desorbent flow is constant at constant c_{II}, which minimizes the ratio of desorbent to feed flow rate ratio.

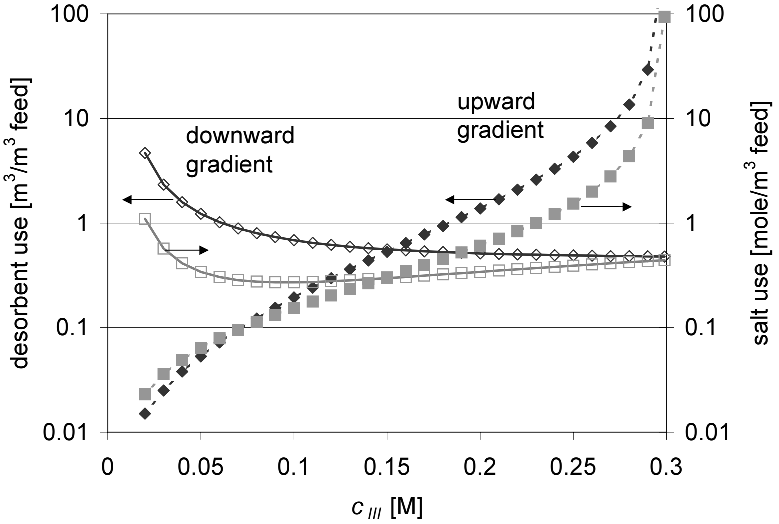

Figure 11. Comparison of desorbent use (♦) and salt use (■) in upward gradient (closed symbols) and downward gradient (open symbols). In all cases, the salt concentration in the lower sections was maintained at 0.3M. Further assumptions as shown in Table III.

Similarly, the desorbent and salt use in the downward gradient are small for small differences in top and bottom concentrations. Then, the salt concentration is predominantly determined by the (high) feed concentration. Hence, only a low desorbent flow rate can be applied, which favors a low desorbent consumption. At increasing difference of the two concentrations, more desorbent is applied relative to the feed, in order to maintain the gradient, thus increasing desorbent use.

Obviously, which of the two gradients is the most favorable with respect to desorbent or salt use strongly depends on the difference in salt concentration between the top and bottom sections. At a small difference between the two, the downward gradient is preferred, whereas the upward gradient is preferred at a large difference in salt concentration. Further optimization requires information on the proteins to be separated and is not carried out in this paper.

Conclusions

Salt gradients may improve the throughput during separation of proteins by ion exchange in simulated moving bed. This paper shows how at least four forms of the gradient can be formed. Variants include “upward” and “downward”, as well as “top” and “bottom” gradients. In the less obvious “downward gradient” form, the gradient forming salt moves towards the bottom of the system, due to its high affinity for the ion exchange matrix, as well as by dead volume effects. “Top” gradients, with a high concentration in the top sections, are more favorable than “bottom” gradients with respect to throughput.

A procedure for the selection of flow rates that lead to correct positioning of both upward and downward gradients has been developed. The procedure is based on wave theory and incorporates the non-linear Donnan isotherm of salt on an ion exchange matrix. An operating region in the m_2-m_3 plane is identified. Only within its boundaries, correct positioning of the gradient is expected. Experiments combined with mathematical modeling confirm the theoretical predictions.

Upward and downward gradients have been compared with respect to the use of desorbent and salt. When the difference in salt concentrations in the top and bottom sections is large, a downward gradient is favorable with respect to minimization of the use of desorbent and salt. At small difference in gradient concentration, the upward gradient is most favorable. Further optimization requires information on the proteins to be separated.

Acknowledgements

The Dutch Ministry of Economic Affairs is gratefully acknowledged for the financial support in the framework of the IOP Milieutechnologie (Preventie) program.

Nomenclature

c	concentration in the liquid phase	[kmole/m^3]
F	Faraday's constant	[C/mole]
m	flow rate ratio ($=\Phi_L/\Phi_S$)	[-]
q	concentration in the sorbed phase	[kmole/m^3]
Q	ion exchange capacity of the resin	[kmole/m^3]
R	gas constant	[J/mole/K]
S	selectivity constant	[-]
t	time	[s]
T	temperature	[K]
v	interstitial velocity	[m/s]
v_s	sorbent interstitial velocity	[m/s]
V	volume of one column	[m^3]
V_d	dead volume per column	[m^3]
x	liquid phase ionic fraction	[-]
X	dimensionless distance	[-]
y	sorbed phase ionic fraction	[-]
z	ionic charge	[C/mole]

greek

α	discrepancy parameter	[-]
β	phase ratio ($=(1-\varepsilon)/\varepsilon$)	[-]
ε	bed porosity	[-]
Φ	flow rate	[m^3/s]
μ	chemical potential	[J]

θ	dimensionless time ($t\cdot v_0/L$))	[-]
τ	switch time	[s]
ψ	electrical potential	[V]

super- and subscripts

0	standard state
i	index
L	liquid
S	sorbent

Literature

Ballanec, B. and G. Hotier, "From batch to simulated countercurrent chromatography," In: *Preparative and production scale chromatography,* G. Ganetsos and P.E. Barker (eds.), Marcel Dekker, New York (1993).

Helfferich, F.G. and G. Klein, "Multicomponent chromatography: theory of interference," Marcel Dekker, New York (1970).

Houwing, J., L.A.M. van der Wielen and K.Ch.A.M. Luyben, "Development of large sale purification process for recombinant HSA using SMB technology," In: *proc. A.I.Ch.E. Annual meeting*, Los Angeles (1997).

Houwing, J., H.A.H. Billiet, J.A. Wesselingh and L.A.M. van der Wielen, "Azeotropic phenomena during separation of dilute mixtures of proteins by simulated moving bed chromatography," *J. Chem. Technol. Biotechnol.,* **74**, 213 (1999), chapter 3 of this thesis.

Houwing, J., H.A.H. Billiet and L.A.M. van der Wielen, "Mass transfer effects during separation of proteins in SMB by size exclusion," *A.I.Ch.E. J.,* **49**, 1158 (2003), chapter 2 of this thesis.

Jansen, M.L., A.J.J. Straathof, L.A.M. van der Wielen, K.Ch.A.M. Luyben and W.J.J. van den Tweel, "A rigorous model for ion exchange equilibria of strong and weak electrolytes," *A.I.Ch.E. J.*, **42**, 1911 (1996).

Jensen, T.B., T.G.P. Reijns, H.A.H. Billiet and L.A.M. van der Wielen, "Novel simulated moving bed method for reduced solvent consumption," *J. Chromatogr.*, **873**, 149 (2000).

Juza, M., M. Mazzotti and M. Morbidelli, "Simulated moving-bed chromatography and its application to chirotechnology," *Tibtech.*, **18**, 108 (2000).

Kopaciewitz, W., M.A. Rounds, J. Fausnaugh and F.E. Regnier, “Retention model for high-performance ion-exchange chromatography,” *J. Chromatogr.*, **226**, 3 (1989).

Ma, Z. and N.-H. L. Wang, “Standing wave analysis of SMB chromatography: linear systems,” *A.I.Ch.E. J.*, **43,** 2488 (1997).

Mazzotti, M., G. Storti and M. Morbidelli, “Supercritical fluid simulated moving bed chromatography,” *J. Chromatogr.*, **786,** 309 (1997).

Migliorini, C., M. Mazzotti and M. Morbidelli, “Simulated moving bed units with extra-column dead volume,” *A.I.Ch.E. J.*, **45**, 1411 (1999).

Migliorini, C,. M. Wendlinger, M. Mazzotti and M. Morbidelli, “Temperature gradient operation of a simulated moving bed unit,” *Ind. Eng. Chem. Res.*, **40**, 2606 (2001).

Mulder, M., “Basic principles of membrane technology”, Kluwer academic press, Dordrecht, the Netherlands (1991).

Pharmacia Biotech, *Ion exchange chromatography: principles and methods.* Västra Aros tryckeri AB9511, Sweden (1996).

Priegnitz. J.W., *Small scale simulated moving bed separation process.* US patent 5,565,104. (1996).

Rhee, H.-K., R. Aris and N.R. Amundson, “Multicomponent adsorption in continuous countercurrent exchangers,” *Phil. Trans. Roy. Soc. Lond. A.*, **269,** 187 (1971).

Ruthven, D.M. and C.B. Ching, “Countercurrent and simulated countercurrent adsorption separation processes,” *Chem. Eng. Sci.*, **44**, 1011 (1989).

Storti, G., M. Masi, S. Carrà and M. Morbidelli, “Optimal design of multicomponent countercurrent adsorption separation processes involving non-linear equilibria,” *Chem. Eng. Sci.*, **44**, 1329 (1989).

Storti, G., M. Mazzotti, M. Morbidelli and S. Carrà, “Robust design of binary countercurrent adsorption separation processes,” *A.I.Ch.E. J.*, **39**, 471 (1993).

Van Walsem, H.J. and M.C. Thompson, “Simulated moving bed in the production of lysine,” *J. Biotechnol.*, **59**, 127 (1997).

6

Effect of salt gradients on the separation of dilute mixtures of proteins by ion exchange in SMB

Abstract

Salt gradients can improve the efficiency during fractionation of proteins by ion exchange in Simulated Moving Beds (SMB). The gradients are formed using feed and desorbent solutions of different salt concentrations. The thus introduced regions of high and low affinity may reduce eluent consumption and resin inventory compared to isocratic SMB systems.

This paper describes a procedure for the selection of the flow rate ratios that enable successful fractionation of a dilute binary mixture of proteins in a salt gradient. The procedure is based on the so-called "triangle theory" and can be used both for upward gradients (where salt is predominantly transported by the liquid) and downward gradients (where salt is predominantly transported by the sorbent). The procedure is verified by experiments.

This paper has been published in: *J. Chromatogr.* **952**, 85 (2002).

Introduction

Simulated Moving Bed (SMB) technology, a countercurrent chromatographic separation technique, is increasingly popular for chromatographic fractionation of various biotechnological and pharmaceutical mixtures. Many studies concern the fractionation of enantiomers for use as chiral drugs (Juza *et al.*, 2000; Schulte and Strube, 2001). Other examples are the separation of amino acids (Van Walsem and Thompson, 1997) and antibiotics Jensen *et al.*, 2000). Advantages of the SMB over fixed bed chromatography are an increased efficiency during separation of like molecules, reduction of the consumption of sorbent, and reduction of the consumption of buffers (Ballanec and Hotier, 1993).

In order to achieve the desired degree of separation in SMB, correct selection of the liquid and solid phase flow rates is crucial. The selection of the liquid to sorbent flow rate ratios has been studied extensively. In most studies, the analogy between true moving bed (TMB) and SMB is exploited. Wave theory is then used to select the flow rate ratios (Ma and Wang, 1997; Storti *et al.*, 1993). The most current method for flow rate ratio selection is “triangle theory”, as developed by the group of Morbidelli (Storti *et al.*, 1993).

A novel development in SMB technology is the use of gradients in solvent strength. The gradient is formed by the use of a desorbent and feed solution of different modulator concentration. It introduces regions of high and low affinity of the solutes towards the resin in the SMB. When the top sections (sections III and IV in Figure 1) have a high affinity, a high feed flow rate can be applied. This is highly beneficial to the throughput, the volume of feed that can be processed per resin volume. When the bottom sections (sections I and II in Figure 1) have a low affinity, a low desorbent flow rate suffices to regenerate the sorbent. Thus, the gradient increases throughput and reduces solvent consumption in comparison to the isocratic situation. Examples of gradients in SMB systems are in the separation of sugars using temperature gradients (Ruthven and Ching, 1989), in supercritical fluid chromatography using pressure gradients (Mazzotti *et al.*, 1997), in reversed phase separation of antibiotics, using methanol gradients (Jensen *et al.*, 2000), and in ion exchange separation of proteins, using salt gradients (Houwing *et al.*, 1999).

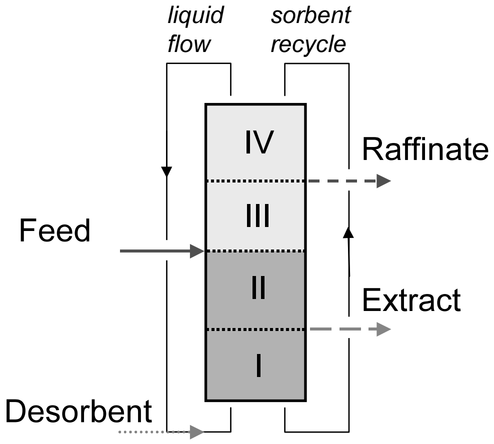

Figure 1. Schematic representation of gradient in SMB and numbering of sections therein. A dark color indicates a low affinity of the protein for the matrix.

In this paper we will further elaborate the protein separations in SMB aided by salt gradients. In general, the affinity of proteins towards the resin is reduced by increasing the salt concentration (Kopaciewitz *et al.*, 1989; Whitley *et al.*, Brooks and Cramer, 1992). In a previous paper (Houwing *et al.*, 2003b), the positioning of the salt gradient in the SMB has been addressed for salts interacting with the sorbent. The gradient can have two forms, namely an "upward gradient", where salt is predominantly transported by the liquid towards the top of the system (section IV) and as an "downward gradient", where salt is predominantly transported by the sorbent towards the bottom (section I).

In the current paper, we have applied the salt gradient SMB for separation of dilute mixtures of two proteins, namely Bovine Serum Albumin (BSA) and myoglobin (myo). The procedure for selection of the flow rates is extended to the presence of proteins. The predictions are verified by experiments.

Theory

The current methods for selection of the relative flow rates in an SMB assume local equilibrium. They rely on the quantitative understanding of the equilibrium distribution coefficient of solutes over the liquid and sorbent phase. When separating dilute binary mixtures of proteins in a gradient SMB, the current method of selection of flow rate ratios needs to be adjusted at some points:

1. Solutes substantially differ in size, which leads to a combination of size exclusion and ion exchange mechanisms;
2. The strong relation between the flow rate ratio, salt concentrations, and protein and salt distribution coefficients in all sections demands an integral approach for flow rate selection.

In the following, we have assumed that the ion exchange of proteins does not influence the distribution of salt on the ion exchange resin, because diluted solutions of proteins were used.

Size exclusion and ion exchange

The three solutes considered, two proteins and a salt, differ in their molecular weight. Due to size exclusion effects, the volume fraction of the sorbent particle that is accessible to the large protein molecules is much smaller than the fraction accessible to the small salt molecule. We treated this situation by assuming that:

- Liquid flow only occurs in the void fraction (ε_b) of the particle bed;
- The pore liquid always contains the same salt concentration as the bulk liquid, as a result of very fast diffusion;
- The average concentration in the particle q^* is determined by the pores, filled with the liquid concentration c and the resin of the concentration q, which is in ion exchange equilibrium with the pore liquid:

$$q^* = \varepsilon_p c + (1 - \varepsilon_p) q \qquad \textbf{(1)}$$

Several models have been developed to describe the ion exchange equilibrium of the proteins and the ion exchange matrix. Examples thereof are the mass action model of Kopaciewitz *et al.*, (1989), a similar model that includes size exclusion (Whitley *et al.*, 1989), the Steric Mass Action (SMA) model (Brooks and Cramer, 1992), which includes the steric blocking of ion exchange sites by the bulky protein molecule, and the extension to the SMA model that incorporates the pH-dependence of the ion exchange equilibrium (Bosma and Wesselingh, 1998). At the low protein concentrations used in this study, the models lead to very similar results. Hence, we used the simplest mass action description of the ion exchange equilibrium (Kopaciewitz *et al.*, 1989). Ion exchange is then regarded as an reaction of a characteristic number of charges, z_p, of a protein (P) with as many salt ions bound to the ion exchanger (RX), where the protein is bound ($R_{zp}P$) and the salt ions (X^-) are released into solution:

$$P^{z_p-} + z_p RX^- \quad \Leftrightarrow \quad R_{z_p}P + z_p X^-$$

Hence, the equilibrium distribution coefficient of protein over sorbent and liquid depends on the concentration of salt. In case of dilute solutions, where competition between proteins for exchange sites is absent, the distribution coefficient K_{IEX} ($=q_p/c_p$) can be written as:

$$K_{IEX} = K_0 \, c_s^{-z_p} \qquad \textbf{(2)}$$

Where K_0 is a reference distribution coefficient in a 1 molar salt solution and c_s is the concentration of salt.

The values of K_0 and z_p are determined experimentally from the residence times of pulses of protein at varying salt concentrations. The exact procedure is described by Kopaciewitz *et al.* (1989).

The overall equilibrium constant is defined as:

$$K_i = \varepsilon_p + \left(1 - \varepsilon_p\right) \cdot K_{0,i} \, c_s^{-z_i} \qquad \textbf{(3)}$$

where *i* denotes either of the two proteins.

The distribution of salt over the ion exchange resin and the liquid is assumed to be governed by a mechanism based on Donnan interaction, as has been described elsewhere (Houwing *et al.*, 2003b). At low concentration, co-ions are excluded from the resin as a result of Donnan repulsion, but at high concentration, charges are shielded and the entire salt “molecule” can enter the resin. In case of a salt consisting of two single-valent ions, such as sodium chloride, the resulting isotherm equation is:

$$\frac{q_s}{Q} = -0.5 + 0.5\sqrt{1 + 4S\left(\frac{c_s}{Q}\right)^2} \qquad \textbf{(4)}$$

A similar equation can be derived for multivalent ions, such as calcium chloride or sodium sulfate, as well as for reactive buffer systems, such as acetic acid buffers (Jansen *et al.*, 1996).

The previously reported parameters for sodium chloride in a 10 mM Tris buffer at pH 8.0 on a Q-Sepharose FF ion exchange matrix are S=1.09, Q=0.22. Tris and salt have been regarded as one species, since the salt concentration (200-500 mM) largely exceeded the Tris concentration (10 mM).

Region of complete separation

In order to select the liquid to sorbent flow rate ratios that lead to complete separation of the feed, an extended version of the “triangle theory” as developed by Morbidelli and co-workers (Storti *et al*., 1993) has been developed. Key parameters are the liquid to sorbent flow rate ratios m, which can be calculated from the SMB flow rates Φ^{SMB}, switch time τ, column volume V and dead volume per column V_d by (Migliorini *et al*.,1999):

$$m = \frac{\Phi^{SMB} \cdot \tau - V\varepsilon - V_d}{V(1-\varepsilon)} \tag{5}$$

The flow rate ratios are constrained by $m_j = K(c_{s,j})$, where m_j is the flow rate ratio in section j and $K(c_{s,j})$ is the “distribution coefficient” of salt or protein as a function of the salt concentration c_s in section j (Houwing *et al*., 1999; Houwing *et al*., 2003b). The constraints thus are implicit relations of the salt concentrations in all sections. In dilute systems, where ion exchange of proteins does not influence the salt distribution, the salt concentrations can be calculated from the mass balances over the points of feed and desorbent entry. In the following, we assume there is no recycle of the liquid leaving section IV to the desorbent, a so-called “open loop system”. Also, we impose that the gradient is properly established, hence the concentrations in the lower sections I and II are equal and denoted as c_{II}, and the concentrations in the upper sections III and IV are also equal and denoted as c_{III}. Imposing the correct gradient is similar to imposing complete separation to calculate the region of complete separation. A mass balance over the part of the SMB between the middle of section II and the middle of section III then reads:

$$m_2 c_{II} + (m_3 - m_2)c_F - m_3 c_{III} + q_{III} - q_{II} = 0 \tag{6}$$

We will further refer to this equation as the feed balance. The first three terms represent the salt entering via the liquid in section II, entering via the feed at concentration c_F, and leaving via the liquid from section III. The last two terms represent salt entering via the sorbent in section III and leaving via the sorbent in section II. In all sections, equilibrium between the liquid and sorbed phases is assumed.

At this point, the choice between an upward or downward gradient needs to be made. In case of an upward gradient, the salt concentration in the lower sections

c_{II} equals the desorbent concentration c_D. The concentration in the upper sections c_{III} is computed from equation (6).

In case of a downward gradient, none of the concentrations c_{II} and c_{III} is known. To find all salt concentrations, an additional mass balance is required. This balance is over the top of the SMB, over the part limited by the middle of section IV and the middle of section I (Houwing *et al.*, 2003b):

$$m_1\left(c_D - c_{II}\right) + q_{II} - q_{III} = 0 \qquad \textbf{(7)}$$

Where the first term represents the salt entering section I via the liquid as desorbent and leaving via the liquid; the latter terms represent the salt entering via the sorbent from section II and leaving to section IV. The consequence of equation (7) is, that m_I needs to be specified before the constraints to the operating region can be found.

With the obtained salt concentrations, the boundaries of the operating region are identified. As correct movement of all components needs to be assured, three boundaries $m_j = K(c_{s,j})$ are found per section; one for each component. Sometimes, a limiting boundary has to be identified from two minimum or maximum boundaries. This is dealt with in the following manner:

- The limiting maximum flow rate equals the smallest distribution coefficient at the local salt concentration of the components moving downward. Once this component of smallest retention moves downward, all other components with higher retention will surely move downward.
- The limiting minimum flow rate equals the largest distribution coefficient at the local salt concentration. Whenever the most retained component moves upward, all components of lower retention will surely move upward.

Salt has a convex curved isotherm, so salt fronts can either be diffuse (during loading of a column with a solution of increased salt concentration) or a shock (during elution with a solution of decreased salt concentration) (Helfferich and Klein, 1970). It is important to take the correct front shape into account, since shock and diffuse waves move at different velocities. Further details on salt positioning are described elsewhere (Houwing *et al.*, 2003b).

The completed results of the procedure for flow rate ratio selection are shown in Table I. There, $(\partial q/\partial c)_c$ denotes a diffuse front at the concentration c, $(\Delta q/\Delta c)_{c1\text{-}c2}$ denotes a shock front between concentrations $c1$ and $c2$, and c_j is the salt concentration in section j. By simultaneous solution of the mass balance equations (6) and (7) and the equations of limiting flow rate ratios in Table I, the constraints to the flow rate ratios are found.

Using the criteria on m_2 and m_3, a region of complete separation in the m_2-m_3 plane is constructed, analogous to “triangle theory”. When operating points are chosen within the defined region, separation of the two protein components in section II and III is guaranteed.

Table I. Flow rate ratio constraints in upward and downward gradients. A: less retained protein, B: more retained protein. The salt concentration in section II, cII and section III, cIII, are calculated from the mass balance equations (1) and (2).

	Upward gradient		downward gradient	
	Lower boundary	Upper boundary	Lower boundary	Upper boundary
m_1	Maximum of $\left(\partial q / \partial c\right)_{c_D}$, $K_A(c_D)$	-	$K_A(c_{II})$	$\left(\Delta q / \Delta c\right)_{c_D - c_{II}}$
m_2	Maximum of $\left(\partial q / \partial c\right)_{c_D}$, $K_A(c_D)$	$K_B(c_D)$	$K_A(c_{II})$	Minimum of $\left(\Delta q / \Delta c\right)_{c_D - c_{II}}$, $K_B(c_{II})$
m_3	Maximum of $\left(\Delta q / \Delta c\right)_{c_D - c_{III}}$, $K_A(c_{III})$	$K_B(c_{III})$	$K_A(c_{III})$	Minimum of $\left(\partial q / \partial c\right)_{c_{III}}$, $K_B(c_{III})$
m_4	$\left(\Delta q / \Delta c\right)_{c_D - c_{III}}$	$K_A(c_{III})$	-	Minimum of $\left(\partial q / \partial c\right)_{c_{III}}$, $K_A(c_{III})$

Regeneration of desorbent and sorbent

Optimal operation of the SMB in terms of desorbent use, and purity and recovery of the extract and raffinate products requires regeneration of the sorbent in section I and of the desorbent in section IV. The purpose is to remove the proteins, while not disturbing the salt gradient. This is established by careful selection of the flow rate ratios m_1 and m_4. That is not a trivial task, since conflicting situations may occur in section IV in an upward gradient and in section I in a downward gradient.

The regeneration of the desorbent in section IV in an upward gradient requires that salt moves upward and the two proteins move downward in section IV. A conflicting situation occurs when the plots of the distribution coefficients of salt and protein as a function of the salt concentration intersect. A typical example of this azeotropic situation (Houwing *et al.*, 1999) is shown in Figure 2. Components A and B are two arbitrary proteins, of which the distribution coefficients $K_A(c_s)$ and $K_B(c_s)$ have been plotted as a function of the salt concentration. According to Table II, the salt distribution coefficient in section IV is represented by $(\Delta q/\Delta c)_{cD\text{-}cIII}$. In the figure, c_D is constant and c_{III} is variable. The lines of the distribution coefficient of the less retained protein A and salt intersect at $c_{crit,IV}$. Only at concentrations below $c_{crit,IV}$, it is possible to find a flow rate ratio that results in downward movement of the less retained protein (i.e. $m<K_A(c_s)$) and simultaneous upward movement of the salt (i.e. $m>(\Delta q/\Delta c)_{cD\text{-}cIII}$).

Table II. Distribution coefficients of BSA and myoglobin on Q Sepharose FF, in 10 mM Tris buffer, pH 8.

component	isotherm	parameters			
protein	$K=\varepsilon_p+(1-\varepsilon_p)K_0\,c_s^{-z_p}$	*component*	ε_p	K_0	z_p
		BSA	0.49	$1.61\cdot10^{-3}$	5.61
		myoglobin	0.64	$0.76\cdot10^{-3}$	1.31
salt	$\frac{q_s}{Q}=-\frac{1}{2}+\frac{1}{2}\sqrt{1+4S\left(\frac{c_s}{Q}\right)^2}$	*component*	Q	S	
		NaCl	0.22	1.09	

Obviously, regeneration of the desorbent will only occur when c_{III} exceeds $c_{crit,IV}$. This implies the feed concentration has to be below that critical concentration. As the flow rate ratios, m_2 and m_3 also determine the concentration c_{III}, these are also restricted. An additional boundary to the region of complete separation is found by imposing the critical concentration in section IV. This concentration is found by equating the distribution coefficient of salt and protein A, at the chosen desorbent concentration. The supporting flow rate ratios are calculated from the feed mass balance (6). Thus, a straight line is obtained:

$$m_3 = \frac{m_2(c_D - c_F) + q_{crit,IV} - q_D}{c_{crit,IV} - c_F} \tag{8}$$

In order to regenerate the sorbent in section I in a downward gradient, upward movement of all proteins and downward movement of salt is required in that section. A conflicting situation occurs when the lines of the salt and protein distribution coefficients intersect as a function of the salt concentration. According to Table II, the distribution coefficient of salt is then given by $(\Delta q/\Delta c)_{cD\text{-}cII'}$. In Figure 2, the salt distribution coefficient is plotted at constant c_D and variable c_{II}. At $c_{crit,I}$, the distribution coefficients of the more retained protein A and salt are equal. Only if the salt concentration c_{II} exceeds this critical salt concentration of section I, $c_{crit,I}$, salt can move downward (by choosing $m<(\Delta q/\Delta c)_{cD\text{-}cII'}$) and proteins move upward (by choosing $m>K_B(c_s)$). Else, both B and salt move downward.

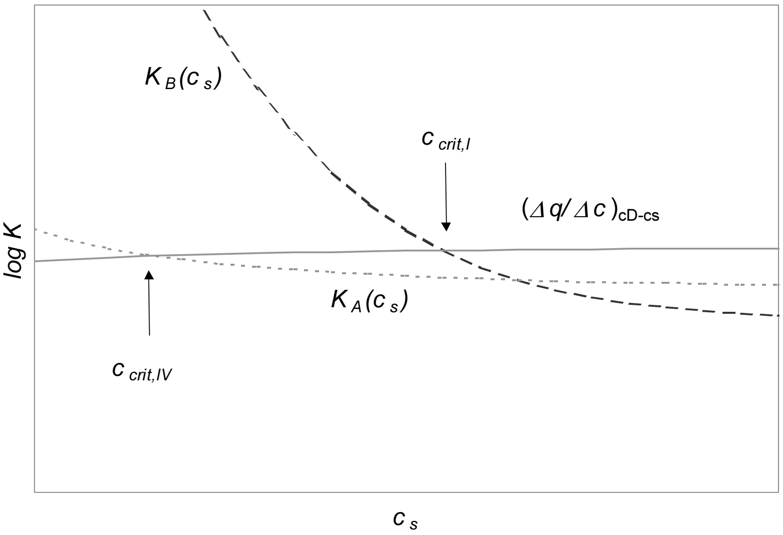

Figure 2. Typical example of distribution coefficients of proteins as a function of salt concentration and definition of critical concentrations.

The requirement to achieve the critical concentration in section I imposes that the feed concentration has to exceed $c_{crit,I}$ and that the flow rate ratios m_2 and m_3

support that concentration. An additional boundary to the region of complete separation is found by imposing the critical concentration in section I, and then calculating the supporting flow rate ratios from the mass balances (6) and (7). By imposing a constant c_{II}, c_{III} is also fixed. Thus, a straight line of m_3 as a function of m_2 is obtained:

$$m_3 = \frac{m_2(c_{crit,I} - c_F) + q_{III} - q_{crit,I}}{c_F - c_{III}} \tag{9}$$

Experimental

Materials

In this study, a synthetic mixture of myoglobin from horse heart (Sigma cat no. M1882, >90% pure, Sigma Aldrich chemie, Zwijndrecht, the Netherlands) and Bovine Serum Albumin (Sigma cat no. A7906, Sigma Aldrich chemie, Zwijndrecht, the Netherlands) was used as a feed solution. All solutions were based on a 10 mM Tris buffer, pH 8.0, to which sodium chloride was added for controlling the salt concentration. All salts were obtained from Merck (Darmstadt, Germany). The sorbent, Q-Sepharose FF, was obtained from Amersham Pharmacia biotech (Upsala, Sweden). This strong ion exchange matrix, based on highly cross-linked agarose has an average particle size of 90 µm and a capacity for small ions of 200 mM (Pharmacia Biotech, 1996).

Columns

Columns were packed according to the procedure described by the manufacturer (Pharmacia Biotech, 1996). One Pharmacia XK16 column of 14.5 mL volume was used for isotherm determination on a Pharmacia FPLC system. In the lab-scale simulated moving bed, the sorbent was packed in 1 cm diameter Omnifit glass columns to a column volume of 7.1 mL. The packing quality of these columns was checked by determination of the breakthrough of a salt solution.

SMB system

The simulated moving bed system used for experiments has been described elsewhere (Houwing *et al*., 2003a). The concentrations of the two proteins in the system were calculated from the adsorbance at 280 and 405 nm, as determined by an in-line Shimadzu SPD-M10Avp Photo-diode array detector, operated under Class-VP-software (version 4.2, Shimadzu). The dead volume of the assembled system was determined by breakthrough experiments of salt on the system without columns attached at 0.38 mL per column.

Determination of isotherm

The proteins' characteristic charges and reference equilibrium constants were determined from retention times of pulses at varying concentrations of salt, analogous to the method described by Kopaciewitz *et al.* (1989). The injected pulses of 100 μL contained solutions of 10 g/L BSA or 1.0 g/L myoglobin, with a salt concentration adjusted to the eluent concentration. Experiments were carried out at a flow rate of 2 mL/min.

The data obtained by pulse experiments were verified by breakthrough experiments. A solution of either 0.5 g/L BSA or 0.1 g/L myoglobin was applied at 3 mL/min onto the column equilibrated during 5 column volumes. The equilibration buffer and the sample contained the same salt concentration in the range of 200 to 300 mM NaCl. After loading, the column was regenerated using a 1M NaCl solution.

The isotherm of sodium chloride on Q-Sepharose FF has been described elsewhere (Houwing *et al*., 2003b).

SMB experiments

During operation of the system, the recycle stream was wasted, instead of being reused for further reduction of consumption of eluent.

Before the experiment, columns were regenerated using 1M NaCl and preferably re-equilibrated with 0.22M NaCl. The best results were obtained by first running the SMB using a feed solution only containing salt. After about four cycles, when the salt gradient was formed, the feed was switched to the protein containing solution. By this procedure, long lasting start-up effects were avoided.

Numerical procedures

Breakthrough profiles were simulated by numerical integration of the mass balance equations of liquid and sorbent phase, wherein mass transfer is approximated using a linear driving force approximation:

$$\begin{aligned}\frac{\partial c}{\partial t} &= -v\frac{\partial c}{\partial x} + E\frac{\partial^2 c}{\partial x^2} - \beta \cdot k_o a \cdot (q_{eq} - q)\\ \frac{\partial q}{\partial t} &= k_o a \cdot (q_{eq} - q)\end{aligned} \qquad \textbf{(10)}$$

Where q_{eq} is the solid phase concentration in equilibrium with liquid concentration c, v is the interstitial velocity, β is the phase ratio ($(1-\varepsilon)/\varepsilon$) and a is the specific interfacial area ($=6/d_p$, where d_p is the particle diameter). The mass transfer coefficient k_o was calculated from dimensionless relations, as described before (Houwing *et al.*, 2003a). The used diffusion coefficients in free liquid were $D_{BSA}=6\cdot10^{-11}$ m^2/s and $D_{myo}=10.8\cdot10^{-11}$ m^2/s. The solids diffusion coefficients were $D_{p,BSA}=0.73\cdot D_{BSA}$ and $D_{s,myo}=0.84\cdot D_{myo}$, as cited in that paper.

The model, programmed in Matlab, uses spatial discretization and a fourth order Runge Kutta algorithm for numerical integration. Axial dispersion was approximated by numerical dispersion.

The operating region was constructed by repeatedly simultaneous solving of the mass balance equations (1) and (2) and the flow rate criteria (Table I), at chosen values of m_1 (only at downward gradient), and m_2 or m_3, using the Optimization Toolbox of Matlab.

Steady state TMB profiles were calculated using an equilibrium stage model as described before (Houwing *et al.*, 2003b; Ruthven and Ching, 1989). Profiles were obtained by simultaneously solving the mass balances of all equilibrium stages, using the Optimization Toolbox of Matlab.

Results and discussion

Distribution coefficients

Pulse experiments revealed that the ion exchange equilibrium coefficient of BSA on Q-Sepharose FF at pH 8.0 strongly depends on the salt concentration (see Figure 3). The slope of the line, i.e the characteristic charge z_{BSA} is 5.61.

This value is slightly higher than the value of 3.5 reported by Bosma and Wesselingh (1998) and 3.1 reported by Whitley *et al.* (1989). The correlated negative charge of myoglobin was 0.92. This value is in the range of 0.6-1.3 as reported for adsorption of myoglobin unto various ion exchangers at pH 4-5 by Whitley *et al.* (1989). These observations support the conclusion drawn by Bosma and Wesselingh (1998), that the protein has a constant binding charge, which is predominantly determined by steric factors instead of pH effects.

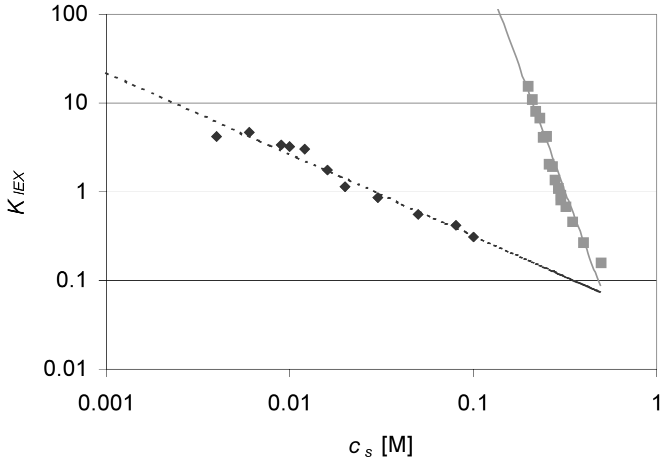

Figure 3. Measured (points) and correlated (lines) ion exchange isotherms of BSA (■) and myoglobin (♦) in 10 mM Tris buffer pH 8.0 on Q Sepharose FF.

From the retention times under non-retaining conditions, i.e. in 1M NaCl, the fraction of the pores accessible to the protein molecules was calculated, assuming a bed porosity ε_b of 0.4. For the larger BSA molecule (68 kD), only 49% of the particle volume is accessible. The fraction of the total bed accessible to BSA is 69%, which is close to the 70% reported by Bosma and Wesselingh (1998). The smaller myoglobin molecule (18 kD) can penetrate into 64% of the particle volume (Table II). The small NaCl molecule was assumed to be able to penetrate in the entire particle; possible exclusion effects were included in the ion exchange equilibrium coefficient.

Breakthrough experiments were used to verify the pulse equilibrium data and to estimate mass transfer parameters. A good agreement between the experimental and simulated breakthrough curves of BSA was found when the equilibrium

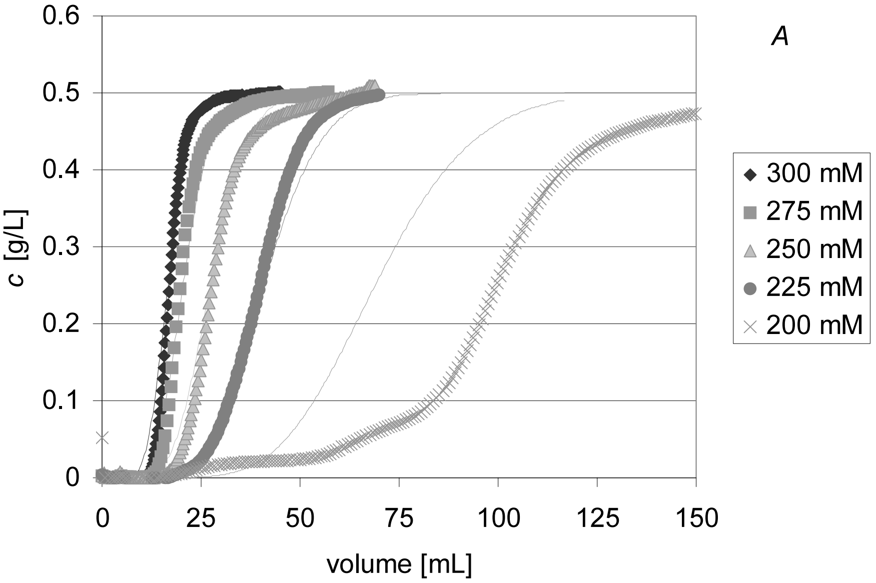

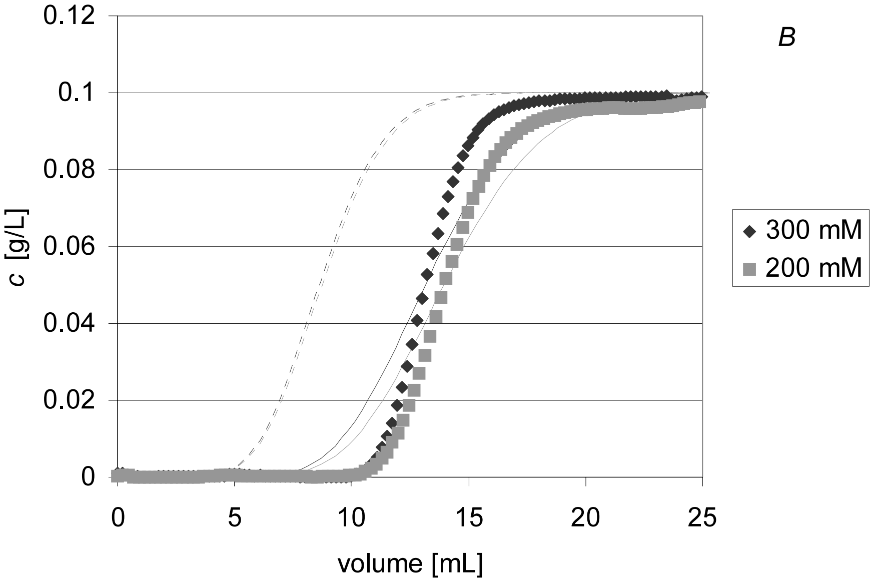

Figure 4: Measured and simulated breakthrough curves of BSA (A) and myoglobin (B). In the latter figure, dotted lines indicate simulations using equilibrium data obtained from pulse experiments, drawn lines indicate simulations using the equilibrium data given in Table II.

data from pulse experiments and 20 discretization steps were used (see Figure 4A). The agreement of the experimental and simulated breakthrough curves of myoglobin was bad (see Figure 4B). A possible explanation is that the breakthrough curves were determined in much higher salt concentrations (200 – 300 mM) than used during pulse experiments (4 – 100 mM). We decided to use the equilibrium coefficients fitted from the breakthrough curves, because the SMB experiments were also done at high salt concentrations. The equilibrium data used in further processing are given in Table II.

Upward gradient

Region of complete separation

The boundaries to the region of complete separation of an upward gradient using c_D=0.27M and c_F=0.15M were determined using the experimental distribution coefficients given in Table II. The resulting lines are shown in Figure 5. Their origin and their implications are:

- positive feed: only above this line, feed can be added
- $m_2$min NaCl: on this line, m_2 equals the slope of the salt isotherm at concentration $c_{II}=c_D$. The line is straight, since c_D is constant. Only at m_2 exceeding this value, NaCl moves upward in section II.
- $m_2$max BSA: on this line, m_2 equals the distribution coefficient of BSA at concentration c_D. Only at m_2 smaller than this value, BSA moves downward in section II.
- $m_2$min myo: on this line, m_2 equals the distribution coefficient of myoglobin at concentration c_D. Only at m_2 exceeding this value, myoglobin moves upward in section II.
- $m_3$max BSA: on this line, m_3 equals the distribution coefficient of BSA at concentration c_{III}, which is calculated from the feed mass balance (1). The line is curved, since c_{III} varies over the line. Only at m_3 smaller than this value, i.e. inside the curve, BSA moves downward in section III.
- $m_3$min myo: on this line, m_3 equals the distribution coefficient of myoglobin at concentration c_{III}, calculated from the feed mass balance (1). Only at m_3 larger than this value, i.e. outside the curve, myoglobin moves upward in section III.
- m_4 crit: on this line, defined by (3), c_{III} equals the concentration at intersection of the myoglobin and NaCl isotherm ($c_{crit,IV}$)

which equals 0.16M at the chosen desorbent concentration. Only at combinations of m_2 and m_3 to the left of this line, regeneration of the desorbent in section IV is established since the c_{III} is then below this critical concentration.

From these observations it is concluded that complete separation is only possible in the shaded area depicted in Figure 5. Due to the lower concentration of salt in section III compared to section II, a high feed flow rate can be applied and a high throughput can be achieved. The shape of the region closely resembles the previously reported one (Houwing *et al.*, 1999). However, instead of the less retained protein, salt now governs the minimal m_2, as a result of interaction of the salt with the sorbent.

Note that this region of complete separation does not provide complete guidelines for correct choice of m_1 or m_4. The flow rate ratio m_1 should exceed the maximum equilibrium coefficient in section I (cf. Table I) to enable regeneration of the sorbent. The flow rate ratio m_4 should be between the distribution coefficient of salt and myoglobin at salt concentration c_{III} to enable regeneration of the desorbent.

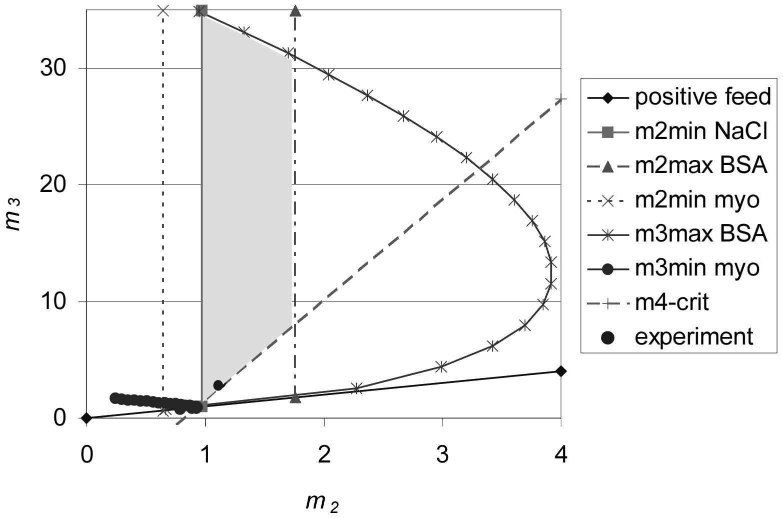

Figure 5. Region of complete separation in case of an upward gradient, using c_F=0.15M and c_D=0.27M NaCl. Complete separation is possible in the shaded area. The symbol indicates the experiment (cf. Table III).

Verification by experiment

Figure 6 and Table III show that the upward salt gradient was well positioned at the experimental point indicated in Figure 5. Note that Figure 6 does **not** show a profile over the SMB. Instead, the experimental points at half switch time are plotted at equal distance, thus assuming a constant species velocity in all section. Hence, the figure can only be interpreted as "the front enters a section, not knowing how far". This figure allows an easy determination of the achievement of steady state from the detector signal.

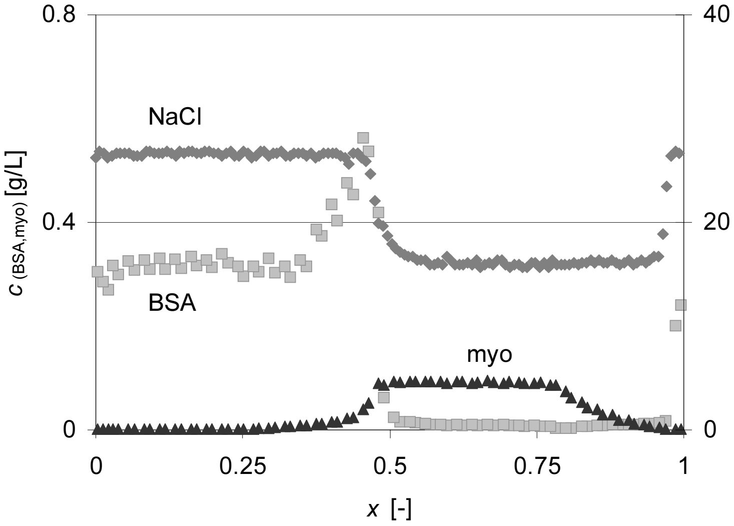

Figure 6. "Profile" at half switch time during a downward gradient experiment (conditions in Table III).

In all sections, downward movement of BSA was observed. In sections II through IV, this agreed well to the theoretical prediction, because the experimental point was well below the $m_2$max BSA and the $m_3$max BSA lines and m_4 was chosen well below the calculated distribution coefficient at the predicted salt concentration. The experimental behavior of BSA in section I could not be understood on the basis of equilibrium theory. On basis of the flow rates and distribution coefficients, the anticipated movement of BSA in section I was upward, whereas downward movement was observed. No explanation for this behavior could be verified. However, we think pH effects may have contributed, since the ion exchange of proteins is a strong function of pH and the pH on the ion exchanger varies in a salt gradient (Jansen *et al.*,1996). In the experimental SMB system, the pH could not be monitored.

The experimental upward movement of myoglobin in sections I through IV agreed very well to the theoretical predictions (cf. Table III). The experimental flow rate ratios in sections II and III were chosen well above $m_2$min myo and $m_3$min myo respectively. The salt concentration c_{III}=0.16M was slightly below $c_{crit,IV}$, which agreed to the position relative to the $m_4$crit line in Figure 5. In principle regeneration of the desorbent would have been possible. However, the value of m_4 (1.09) was chosen above the distribution coefficient of myoglobin at that concentration (0.94), resulting in upward movement. Also, m_1 exceeded the distribution coefficient at the calculated concentration.

The results indicate that a situation of complete separation can well be established after selection of the flow rates using the developed method.

Table III. Conditions and observed directions of movement of components during upward gradient experiment, with c_D=0.27M, c_F=0.15M and τ=250.9 s.

section	*m*	movement of components[1]		
		NaCl	BSA	myo
I	2.11	**up**	down	**up**
II	1.12	**up**	**down**	**up**
III	3.07	**up**	**down**	**up**
IV	1.09	**up**	**down**	**up**

[1] Directions of movement in **bold** typeface indicate agreement between experiment and prediction.

Downward gradient

Region of complete separation

The boundaries to a region of complete separation of a downward gradient were calculated at c_D=0.22M, c_F=0.31M and m_1=0.88, using the equations given in Table II. The choice of salt concentration was only determined by the possibility to achieve complete separation of the two components in section II and III, whereas the choice of m_I was only determined by the salt movement in section I. The resulting boundaries are shown in Figure 7. In each of these, the salt concentrations c_{II} and c_{III} were computed from the feed and desorbent mass balances (1) and (2). The meaning and the implications of the boundaries are (similar to those in Figure 5):

- positive feed: only above this line, feed can be added
- $m_2$max BSA: on this line, m_2 equals the distribution coefficient of BSA at concentration c_{II}. The line is curved, since c_{II} is a function of m_2 and m_3 chosen. Only below this line, BSA moves downward in section II.
- $m_2$min myo: on this line, m_2 equals the distribution coefficient of myoglobin at concentration c_{II}. Only above this line, myoglobin moves upward in section II.
- $m_3$max NaCl: on this line, m_3 equals the chord of the salt isotherm between concentrations c_{II} and c_D. Only below this line, salt moves downward in section III and IV.
- $m_3$max BSA: on this line, m_3 equals the distribution coefficient of BSA at concentration c_{III}. The line is curved, since c_{III} varies over the line. Only below this line, BSA moves downward in section III. The curve is not shown in Figure 6, since it is found at high m_3.
- $m_3$min myo: on this line, m_3 equals the distribution coefficient of myoglobin at concentration c_{III}. Only above the curve, myoglobin moves upward in section III.
- $m_2$max(m_1): only to the left of this line, an extract stream can be withdrawn ($m_I > m_2$).

This latter line could be regarded as an artifact, that results of an incorrect choice of m_I. At correct choice of m_I, the minimum allowed m_I equals the maximum allowed $m_2 = K_{BSA}(c_{II})$, so $m_I > m_2$ per definition. Whenever m_I is chosen too low, its value restricts m_2.

Complete separation in section II and III is only possible in the shaded area in Figure 7. The chosen salt concentrations do not support regeneration of the sorbent in section I, because the critical salt concentration $c_{crit,I}$=0.32M cannot be reached using c_F=0.31M. The critical salt concentration was obtained by equating the slope of the salt isotherm between c_D=0.22M and $c_{crit,I}$ to the BSA distribution coefficient at $c_{crit,I}$. Correct functioning of section I will be elaborated in a later paragraph.

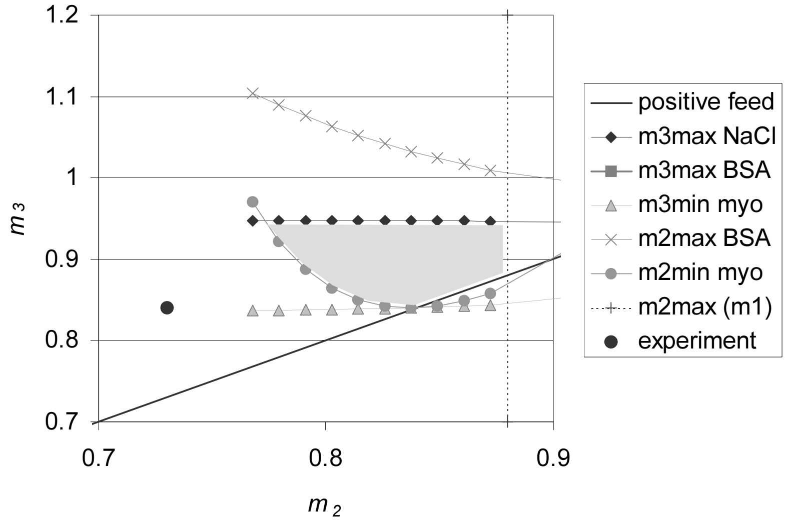

Figure 7. Region of complete separation (lines and small markers) and experiment (large o) in case of a downward gradient, using c_F=0.22M, c_D=0.31M NaCl and m_I=0.88. Complete separation in section II and III is obtained in the shaded area, however regeneration of the sorbent in section I is not established.

Verification by experiment

Figure 8 shows that the downward salt gradient was very well positioned using the experimental conditions of Table IV, represented by the experimental point in Figure 7. This is expected, because the point is well below the $m_3$max NaCl line indicated in Figure 7.

Complete separation of BSA and myoglobin did not occur; myoglobin contaminated the extract. This can be explained by the position of the experimental point relative to the $m_2$min myo line; m_2 was chosen at a too low value, and consequently myoglobin moved downward in section II. In section III, the movement of myoglobin was predominantly downward. The point is above the $m_3$min line, so theory predicts upward movement (Table IV). However, only by a slight experimental error in flow rates or salt concentrations, the direction of movement is likely to be reverted, because the experimental point is very close tot the $m_3$min myo line.

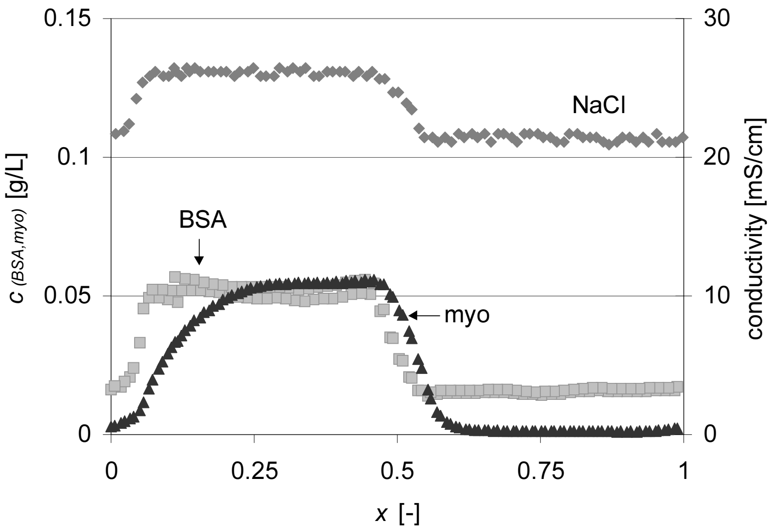

Figure 8. "Profile" at half switch time during a downward gradient experiment (conditions in Table IV).

BSA moved downward in both section II and III. This is well understood from the position of the experimental point, which is well below the $m_2$max BSA and $m_3$max BSA lines.

In section IV, all components moved downward, which is well explained from the very low value of m_4 chosen. In section I, BSA moved downward, which is also predicted at the experimental salt concentrations and flow rate ratios. The downward movement of BSA in section I had the result that the sorbent was not properly regenerated. Hence, BSA was transported along with the sorbent to section IV. This explains the high concentrations of BSA seen in section III and IV in Figure 8.

Table IV. Conditions and observed directions of movement of components during downward gradient experiment, with c_D=0.22M, c_F=0.31M and τ=150.9 s.

section	m	movement of components[1]		
		NaCl	BSA	myo
I	0.88	**down**	**down**	**up**
II	0.73	**down**	**down**	**down**
III	0.84	**down**	**down**	down
IV	-0.05	**down**	**down**	**down**

[1] Directions of movement in **bold** typeface indicate agreement between experiment and prediction.

Regeneration of sorbent

A second region of complete separation was constructed for a downward gradient operated under conditions that support regeneration of the sorbent in section I. Figure 9 shows the result at c_F=0.45M, c_D=0.22M, and m_I=0.94. At this combination of salt concentrations and m_I, the salt concentration $c_{crit,I}$ necessary for sorbent regeneration can in principle be reached. The actual realization of that concentration depends on m_2 and m_3; hence an additional constraint is found, which implies:

- m_1 crit: on this line, given by (4), c_{II} equals the concentration at intersection of the BSA and NaCl isotherm, $c_{crit,I}$=0.32M at the corresponding c_D. Only at combinations of m_2 and m_3 to the left of this line, c_{II} exceeds this critical concentration, and downward movement of NaCl as well as upward movement of the proteins is established.

This additional criterion strongly reduces the region of complete separation.

In Figure 9, the $m_2$max(m_1) line no longer imposes a constraint to the region, as it did in Figure 7. This is the result of correct selection of m_I (cf. explanation at Figure 7).

Figure 9 does not provide guidelines for selection of m_4. The flow rate ratio m_4 can have any value below the minimal distribution coefficient at c_{III}, in order to move all components downward and regenerate the desorbent.

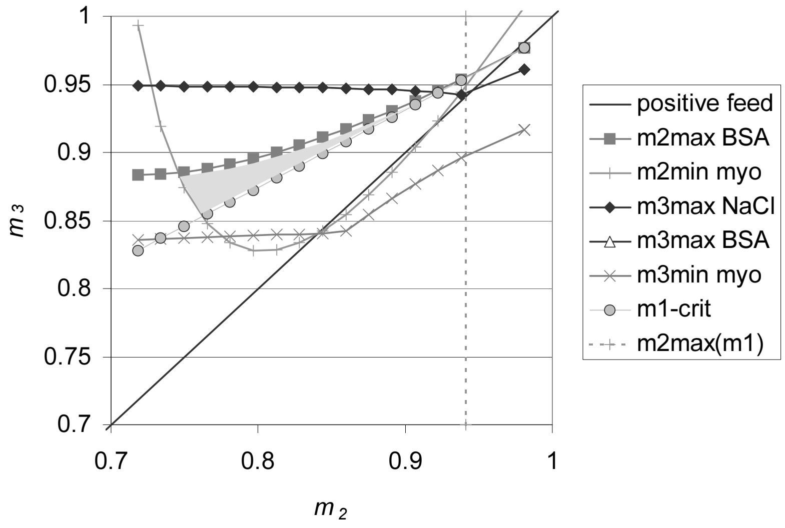

Figure 9. Region of complete separation in case of a downward gradient, using c_F=0.45M, c_D=0.22M, and m_1=0.94. Complete separation is only possible in the shaded area.

Center gradient

Correct positioning of the salt gradient is essential to be able to separate the proteins. However, even experiments with wrongly positioned salt gradients should support the theory for movement of the proteins. In the three experiments listed in Table V, the salt gradient was not correctly positioned. Figure 10 shows the “center” gradient obtained during experiment 3 as an example.

Complete separation can no longer be predicted on the basis of Table II, as the salt concentrations are incorrectly predicted by the mass balance equations (1) and (2), that assume a correct (downward) gradient. In order to verify the movement of components, we used a steady state TMB model to calculate the salt concentrations.

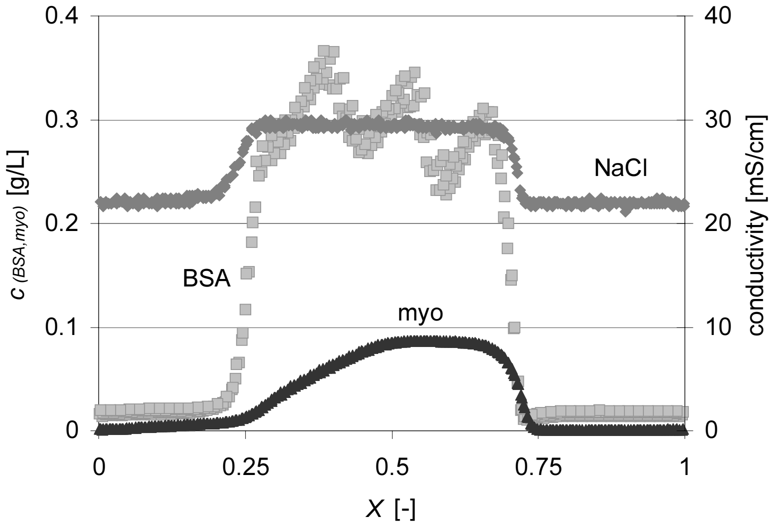

Figure 10. "Profile" at half switch time during center gradient experiment 3 (conditions in Table V).

Using the calculated salt concentrations, the upward movement of myoglobin in sections I to III, as well as the downward movement of BSA in section II and the downward movement of both components in section IV in experiment 3 were well predicted (cf. Table V). The upward movement of BSA in section III could not be understood. Neither were the oscillations in the BSA signal.

Also in the other "center gradient" experiments, the observed directions of movement of the proteins agreed well to those predicted at the calculated concentrations of salt (cf. Table V). This supports the developed method for flow selection.

Table V. Conditions and observed directions of movement of components during center gradient experiments, with c_D=0.22M, c_F=0.31M and τ=150.9 s.

exp.	section	m	c_s	movement of components[1]		
			[M]	NaCl	BSA	myo
1	I	0.95	0.22-0.29	up	*down*	*up*
	II	0.71	0.29	*down*	*down*	*down*
	III	0.95	0.29-0.22	*down*	*down*	*up*
	IV	-0.34	0.22	*down*	*down*	*down*
2	I	0.93	0.22-0.2	*down*	*down*	*up*
	II	0.75	0.29	*down*	*down*	*down*
	III	0.98	0.29-0.22	up	up	*up*
	IV	-0.28	0.22	*down*	*down*	*down*
3	I	0.98	0.22	*up*	up	*up*
	II	0.89	0.30	*down*	*down*	*up*
	III	1.01	0.30-0.22	*up*	up	*up*
	IV	0.11	0.22	*down*	*down*	*down*

[1] Directions of movement in *italics* indicate agreement between the experiment and the direction of movement predicted at the salt concentrations calculated by a TMB equilibrium stage model.

Conclusions

This paper describes the fractionation of a dilute binary mixture of proteins using salt gradient SMB. A method for flow rate selection is developed based on "triangle theory" (Storti *et al.*, 1993). The procedure ensures complete separation of the proteins as well as regeneration of the sorbent in section I and regeneration of the desorbent in section IV. Therefore, it includes the correct positioning of the salt gradient as described in Houwing *et al.*, (2003b). The separation of the proteins is ensured by adjusting the flow rate to the distribution coefficient of the protein at the concentration of salt that is calculated at those flow settings. The regeneration of the sorbent and desorbent is ensured by realization of a critical salt concentration in section I and IV. Due to the intersection of the salt- and protein distribution coefficients as a function of the salt concentration, the salt concentration in section I has to exceed a critical salt concentration $c_{crit,I}$ in case of a downward gradient, whereas the salt concentration in section IV needs to be lower than the critical salt concentration $c_{crit,IV}$ in case of an upward gradient. These critical concentrations impose additional demands on both the desorbent- and feed concentration, as well as the flow rate ratios in all sections.

The equilibrium and mass parameters of BSA and myoglobin on Q-Sepharose FF at pH 8.0 were obtained from pulse and breakthrough experiments. The operating regions calculated using these parameters could be verified by experiments. In both upward, downward and center gradients, the experimental movement of components agreed fairly well to the movement predicted on the basis of the location relative to the region of complete separation.

Acknowledgements

The Dutch ministry of Economic Affairs (through Senter) has financially supported this research in the framework of IOP-milieu preventie. The authors thank Thomas Jensen for many stimulating discussions and Bart van Beek and Dirk Geerts for the experimental isotherm determination.

Notation

a	specific interfacial area	[1/m]
c	concentration in the liquid phase	[mole/L]
D	diffusion coefficient	[m^2/s]
d_p	particle diameter	[m]
K	distribution coefficient	[-]
k_o	mass transfer coefficient	[m/s]
m	flow rate ratio	[-]
q	concentration in the sorbed phase	[mole/L]
Q	ion exchange capacity of the resin	[mole/L]
t	time [s]	
V	volume of one column	[L]
V_d	dead volume per column	[L]
x	distance	[m]
z	ionic charge	[C/mole]

greek

β	phase ratio, $(1-\varepsilon_b)/\varepsilon_b$	[-]
ε_b	bed porosity	[-]

ε_p	accessible pore fraction	[-]
Φ	flow rate	[L/s]
τ	switch time	[s]

super- and subscripts

D	desorbent
eq	at equilibrium
F	feed
j	section number (*I, II, III, IV*)
p	protein
s	salt

Literature

Ballanec, B. and G. Hotier, "From batch to simulated countercurrent chromatography," In: *Preparative and production scale chromatography,* G. Ganetsos and P.E. Barker (eds.), Marcel Dekker, New York (1993).

Bosma, J.C. and J.A. Wesselingh, "pH dependence of ion-exchange equilibrium of proteins," *A.I.Ch.E. J.,* **44**, 2399 (1998).

Brooks, C.A. and S.M. Cramer, "Steric mass-action ion exchange: displacement profiles and induced salt gradients," *A.I.Ch.E. J.,* **38,** 1969 (1992).

Helfferich, F.G. and G. Klein, "Multicomponent chromatography: theory of interference," Marcel Dekker, New York (1970).

Houwing, J., H.A.H. Billiet, J.A. Wesselingh and L.A.M. van der Wielen, "Azeotropic phenomena during separation of dilute mixtures of proteins by simulated moving bed chromatography," *J. Chem. Technol. Biotechnol.,* **74**, 213 (1999), chapter 3 of this thesis.

Houwing, J., H.A.H. Billiet and L.A.M. van der Wielen, "Mass transfer effects during separation of proteins in SMB by size exclusion," *A.I.Ch.E. J.*, **49**, 1158 (2003a), chapter 2 of this thesis.

Houwing, J., T.B. Jensen, S.H. van Hateren, H.A.H. Billiet and L.A.M. van der Wielen, "Positioning of salt gradients in ion exchange SMB," *A.I.Ch.E. J.*, **49**, 665 (2003b), chapter 5 of this thesis.

Jansen, M.L., A.J.J. Straathof, L.A.M. van der Wielen, K.Ch.A.M. Luyben and W.J.J. van den Tweel, "A rigorous model for ion exchange equilibria of strong and weak electrolytes," *A.I.Ch.E. J.*, **42**, 1911 (1996).

Jensen, T.B., T.G.P. Reijns, H.A.H. Billiet and L.A.M. van der Wielen, "Novel simulated moving bed method for reduced solvent consumption," *J. Chromatogr.*, **873**, 149 (2000).

Juza, M., M. Mazzotti and M. Morbidelli, "Simulated moving-bed chromatography and its application to chirotechnology," *Tibtech.*, **18**, 108 (2000).

Kopaciewitz, W., M.A. Rounds, J. Fausnaugh and F.E. Regnier, "Retention model for high-performance ion-exchange chromatography," *J. Chromatogr.*, **226**, 3 (1989).

Ma, Z. and N.-H. L. Wang, "Standing wave analysis of SMB chromatography: linear systems," *A.I.Ch.E. J.*, **43,** 2488 (1997).

Mazzotti, M. G. Storti and M. Morbidelli, "Supercritical fluid simulated moving bed chromatography," *J. Chromatogr.*, **786**, 309 (1997).

Migliorini, C., M. Mazzotti and M. Morbidelli, "Simulated moving bed units with extra-column dead volume," *A.I.Ch.E. J.*, **45**, 1411 (1999).

Pharmacia Biotech (1996), *Ion exchange chromatography: principles and methods.* Västra Aros tryckeri AB9511, Sweden.

Ruthven, D.M. and C.B. Ching, "Countercurrent and simulated countercurrent adsorption separation processes," *Chem. Eng. Sci.,* **44,** 1011 (1989).

Schulte, M. and J. Strube, "Preparative enantioseparation by simulated moving bed chromatography," *J. Chromatogr.,* **906**, 399 (2001).

Storti, G., M. Masi, S. Carrà and M. Morbidelli, "Optimal design of multicomponent countercurrent adsorption separation processes involving non-linear equilibria," *Chem. Eng. Sci.*, **44**, 1329 (1989).

Van Walsem, H.J. and M.C. Thompson, "Simulated moving bed in the production of lysine," *J. Biotechnol.*, **59**, 127 (1997).

Whitley, R.D., R. Wachter, F. Liu and N.-H. L. Wang, "Ion exchange equilibria of lysozyme, myoglobin and bovine serum albumin. Effective valence and exchanger capacity," *J. Chromatogr.*, **465**, 137 (1989).

7

A generalized approach for flow selection in SMB: separation of concentrated protein mixtures by gelfiltration

Abstract

Gelfiltration isotherms are curved at the high protein concentrations preferably used in simulated moving beds (SMB). In this paper, the method for flow selection in such systems is developed, starting from the latest version of "triangle theory" (Migliorini *et al.*, 2000). The thermodynamic model of Wills *et al.* (1995), which is based on an osmotic virial expansion, is used to describe the isotherm. The flow selection method is able to handle both the attractive and repulsive interactions as well as the azeotropic phenomena that are predicted by this isotherm model. The effect of the binary interaction coefficient on the shape of the region of complete separation is shown in case of a fictive model system.

Introduction

Gelfiltration or size exclusion chromatography is traditionally performed in fixed bed in a pulse-wise manner. This leads to the undesired dilution of products, and the concomitant consumption of a large volume of sorbent and liquid. In a previous publication (Houwing *et al.*, 2001), we have shown that separation of mixtures of proteins can be achieved by gelfiltration in simulated moving beds (SMB). The advantages of the countercurrent simulated moving bed technology are the reductions of the resin and solvent flows for a particular separation (Bosma, 2001). As a result of the lower extent of dilution of the products, the components' concentrations in the SMB are much higher than in the fixed bed columns.

In gelfiltration, a linear isotherm is generally assumed. However, some experiments and theoretical studies published in literature indicate that deviations from linearity occur at high concentration (Fanti and Glandt, 1990; Shearwin and Winzor, 1990; Wills *et al.,* 1995; Bosma and Wesselingh, 2000; Lazzarra *et al.*, 2000). Shearwin and Winzor (1990) showed an increase of partition coefficient of Bovine Serum Albumin (BSA) in the concentration range from 0 to 10 g/L. Their single-component measurements were correlated by a thermodynamic model, which will be described in the theory section. The modeling study of Lazzarra *et al.* (2000) indicates that both an increase as well as a decrease of partition coefficient may occur when the concentrations of (multiple) solutes are increased.

The partition coefficient is the crucial parameter during the selection of the flow rates of the liquid and sorbent phase in the Simulated Moving Bed. Several methods have been described for design of the SMB (Storti *et al.*, 1993; Ma and Wang, 1997). All are based on wave theory (Helfferich and Klein, 1970; Rhee *et al.*, 1971) and exploit the analogy between simulated and true moving beds. "Triangle theory", the methodology developed by the group of Morbidelli (Storti *et al.*, 1993) is currently the most used procedure for SMB design. In triangle theory, a triangular region of complete separation is defined. Only when the liquid to sorbent flow rate ratios in the separating sections of the SMB are chosen inside this region, both a pure extract and a pure raffinate product can be harvested. The current version of "triangle theory" (Migliorini *et al.*, 2000) is restricted to purely competitive isotherms, and is not able to incorporate the non-linear isotherm during gelfiltration at increased protein concentrations.

This paper starts with a theoretical comparison of two of the available isotherms describing equilibrium in gelfiltration in concentrated systems. A thermodynamic model, which can account for both (entropic) repulsion and attraction, is elaborated. In a second theoretical paragraph, "triangle theory" is extended in order to be able to incorporate the gelfiltration isotherm, irrespective of the convex or concave shape of the isotherm. By simulation using a fictive model system, the effect of attractive and repulsive interactions on the region of complete separation is demonstrated.

Theory

Modeling size exclusion of concentrated protein solutions

For the description of the thermodynamical equilibrium involved in size exclusion, we use the model proposed by Wills *et al.,* (1995). The model assumes two phases, the liquid phase L and the sorbent phase S, in which the chemical potential of the species *i* is given by a virial expansion including two body interaction, truncated after the second term:

$$\begin{aligned}\mu_{i,L} &= \mu_{i,L}^{0} + RT\left(\ln c_i + 2B_{ii}c_i + 2B_{ij}c_j\right)\\ \mu_{i,S} &= \mu_{i,S}^{0} + RT\left(\ln q_i + 2B_{ii}q_i + 2B_{ij}q_j\right)\end{aligned} \qquad \textbf{(1)}$$

Where $\mu_{i,L}{}^{0}$ is the chemical potential of species *i* in the reference state, which is an infinitely dilute solution of the solute in gelfiltration buffer, and $\mu_{i,S}{}^{0}$ is the reference state of an infinitely dilute sorbed state. This includes solute-fiber interactions, which are assumed to be independent of solute concentration. The parameter c_i is the molar liquid concentration, and q_i is the molar solid phase concentration relative to the sorbent bead inclusive the impenetrable sorbent fibers. B_{ii} and B_{ij} are the second osmotic virial coefficient for two body interaction of equal and dissimilar species, respectively, in L/mol. In B_{ij}, excluded volume effects and other (charge) interactions are combined. From statistical mechanics it is concluded that the excluded volume contribution $B_{ij}{}^{ex}$ is related to the radius of the spherical solute *r,* via:

$$2B_{ij}^{ex} = \frac{4\pi}{3}\cdot 1000 Nav\left(r_i + r_j\right)^3 \qquad \textbf{(2)}$$

The excluded volume contribution of spheroids has been elaborated by Neal and Lenhoff (1995).

Note that this truncated virial model is a strong simplification, as it includes the effects of (buffering) salts in the solution in the standard state, and does not include three-body interactions. It has been shown that charge, pH, and three body interactions have a large effect on the activity coefficients of proteins (e.g. Vilker *et al.*, 1981, Haynes, *et al.*, 1993). However, for the purpose of this paper, the simplification is adequate, since it elegantly shows the effect of increased concentration on gelfiltration isotherms and SMB-flow rate selection.

At equilibrium, the chemical potentials in the two phases are equal:

$$\mu_{i,L} = \mu_{i,S}$$

Which leads to:

$$\frac{\mu_{i,L}^0 - \mu_{i,S}^0}{RT} = \ln\frac{q_i}{c_i} + 2B_{ii}(q_i - c_i) + 2B_{ij}(q_j - c_j) \qquad \textbf{(3)}$$

The first term is obtained from the dilute solution distribution coefficient:

$$\frac{\mu_{i,L}^0 - \mu_{i,S}^0}{RT} = \ln\frac{q_i}{c_i} = \ln K_i^{og}$$

Where K_i^{og} is the dilute solution distribution coefficient determined by size effects only, as described by Ogston (1958):

$$\ln K^{og} = -\phi_f\left(1 + \frac{r_i}{r_f}\right)^2$$

Where ϕ_f is the volume fraction of fibers and r_i and r_f are the radii of solute and fiber, respectively.

After substitution of the Ogston distribution coefficient and $K_i = q_i/c_i$, the isotherm in gelfiltration of concentrated solutions reads:

$$\ln\frac{K_i}{K_i^{og}} = 2B_{ii}c_i(1 - K_i) + 2B_{ij}c_j(1 - K_j) \qquad \textbf{(4)}$$

A second approach, by Blankschtein and coworkers (Lazzarra *et al.*, 2000) is more mechanistic in nature. It calculates the probability of a protein being at a certain place, by summing all the volumes excluded to a solute by (the finite size of) other solutes and fibers. The following expression is derived for the distribution of two spherical solutes in a system containing one fibrous species:

$$\ln\frac{K_i}{K_i^{og}} = \varphi_i\alpha_{ii(s,s)}\left(1-K_i\right)+\phi_j\alpha_{ij(s,s)}\left(1-K_j\right) \qquad \textbf{(5)}$$

where ϕ_i, the volume fraction of solute i and $\alpha_{ij(s,s)}$, the geometric parameter of two spherical solutes are given by:

$$\phi_i = \frac{4}{3}\pi c_i r_i^3 N_{av}\cdot 1000$$

$$\alpha_{ij(s,s)} = \left(1+\frac{r_i}{r_j}\right)^3 \qquad \textbf{(6)}$$

By substitution of (6) in (5), and by substitution of (2) in (4) the same result is obtained. Thus, the mechanistic model of Blankschtein is a limiting case of the thermodynamic model of Wills. However, the latter is more widely applicable, since it can also include forces other than the entropic repulsion, and it may also extend to systems where attractive forces between the solutes are encountered, as is indicated by negative values of B_{ij}.

General procedure for flow rate selection in SMB.

In this section we describe how “triangle theory” is adapted to the isotherm described in the previous section. The latest paper in the “robust design” series of the group of Morbidelli (Migliorini *et al.*, 2000) serves as the starting point. As in the previous papers in the “robust design” series, the SMB is designed on the basis of the analogy of TMB and SMB, by the use of wave theory. In this latest paper, the design criteria are given terms of the actual concentrations, instead of transformed composition variable Ω, as used in the previous papers of the series. This extends the use of triangle theory to systems obeying non-stoichiometric isotherms. As yet, the described procedure is restricted to purely competitive systems. In the current work, the existing theory is adapted to be able to include both competitive and non-competitive isotherms, which can occur during gelfiltration of concentrated solutions. The additional criteria that are a result of this extension will be highlighted during the following description of the general procedure.

Crucial to the design of the TMB are the four waves that exist in the TMB when separating a binary mixture (Figure 1). These waves originate at the feed position, and have a specific velocity, which depends on the flow rates and concentrations, as will be shown shortly. Complete separation requires that these four waves are fixed at the positions depicted in Figure 1 at steady state. Only then, the extract product contains the more retained component (A) in a pure form and the raffinate product contains the less retained component (B) in a pure form.

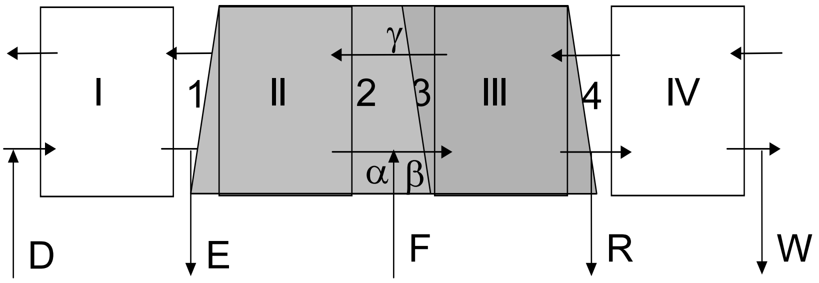

Figure 1. Nomenclature of the TMB: sections in roman numbers, waves in Arabic numbers, ports in capital letters, and the positions near the feed point in Greek letters. Shading indicates the presence of the feed constituents; light shading: more retained component, dark shading: less retained component.

A wave is fixed at a given position when its velocity is zero at that position. Wave theory (Helfferich and Klein, 1970, Rhee *et al.*, 1971) allows the calculation of the velocities of the waves starting from a differential mass balance over a cross section of the TMB, which is at local equilibrium:

$$\varepsilon v \frac{d\mathbf{c}}{dz} + \varepsilon \frac{d\mathbf{c}}{dt} - (1-\varepsilon) v_s \frac{d\mathbf{q}}{dz} + (1-\varepsilon)\frac{d\mathbf{q}}{dt} = 0$$

where ε is the column porosity, v and v_s are the liquid and solids interstitial velocity, respectively, **c** and **q** are the vectors representing the liquid and solid phase composition, z is distance and t is time. After some rearrangement of this equation, the following equation is found to calculate w, the velocity of a composition **c** (cf. Hwang, 1995):

$$w = (\mathbf{I} + \beta\mathbf{M})^{-1} \cdot (\beta v_s (m\mathbf{I} - \mathbf{M})) \tag{7}$$

where $\beta=(1-\varepsilon)/\varepsilon$ is the phase ratio, $m=v/\beta v_s$ is the ratio of the liquid to the solids flow rates, and **M** is the matrix of partial derivatives of the solid to the liquid phase concentrations, $\mathbf{M}_{i,j}=\partial q_i/\partial c_j$. A positive composition velocity indicates movement in the direction of liquid flow. The composition is fixed when the flow rate ratio m equals λ, the eigenvalue of the matrix **M** (Helfferich and Klein, 1970). This is a consequence of "coherence", which is described in the

Appendix. In a binary mixture, there are always two waves originating from a given composition, and hence there are two possible values of λ. The maximum relates to the gradient of the isotherm of the more retained component. In a dilute gelfiltration system, the two eigenvalues equal the Ogston distribution coefficients of the two species.

All compositions in a wave have their own composition velocity. A wave is said to be diffuse when the composition velocity increases in the direction of liquid flow. For instance, when the composition velocity at the right end of wave 3 exceeds the composition velocity at its left end, wave 3 is a diffuse wave. A wave is said to be a shock wave in the inverse case. In shock waves, there is only one velocity, which is an average of all velocities. The shock velocity is given by:

$$w = \frac{\beta v_s (m - \Lambda)}{1 + \beta \Lambda} \qquad \textbf{(8)}$$

where $\Lambda = \Delta q_i / \Delta c_i$, corresponding to the concentration changes over the entire wave. In the following, we will refer to both Λ and λ as the “eigenvalue”.

The wave is fixed when the flow rate ratio *m* equals the eigenvalue (cf. eq. (7) and (8)). Of all velocities present in the (diffuse) wave, a characteristic velocity is taken. This velocity is related to the limiting compositions, namely the composition that is required to pass through the bed or be arrested “before” the bed. For instance consider section II. The entire wave 1 needs to pass through this section, including the “slow” composition (c_A^{II},0). The maximum eigenvalue in (c_A^{II},0) is then taken for calculation of the characteristic velocity. Similar reasoning for the other waves leads to the scheme presented in Table I. Note that this table does not impose a certain “wave pattern”, a specific form of waves one through four. This is in extension to the approach of Migliorini *et al.*, (2000), which is restricted to purely competitive isotherms, which implies waves 1 and 2 are diffuse waves and waves 3 and 4 are shock waves.

Table I. Limiting compositions, eigenvalues and boundaries.

wave	limiting compositions	which λ,Λ ?	limiting λ (diffuse wave)	limiting Λ (shock wave)	boundary
1	$(0,0)$, $(c_A^{II},0)$	maximum	$\lambda(c_A^{II},0)$	$\Lambda = \frac{q_A^{II}}{c_A^{II}}$	$m_2 < \lambda,\Lambda$
2	$(c_A^{II},0)$, $(c_A^{\alpha},c_B^{\alpha})$	minimum	$\lambda(c_A^{II},0)$	$\Lambda = \frac{q_B^{\alpha}}{c_B^{\alpha}}$	$m_2 > \lambda,\Lambda$
3	$(c_A^{\beta},c_B^{\beta})$,$(0,c_B^{III})$	maximum	$\lambda(0,c_B^{III})$	$\Lambda = \frac{q_A^{\beta}}{c_A^{\beta}}$	$m_3 < \lambda,\Lambda$
4	$(0,c_B^{III})$, $(0,0)$	minimum	$\lambda(0,c_B^{III})$	$\Lambda = \frac{q_B^{III}}{c_B^{III}}$	$m_3 > \lambda,\Lambda$

The yet unknown concentrations are calculated from mass balances. At complete separation, all A entering the system via the feed is transported to section II, and all B leaves via section III. Hence the overall mass balances on component A and B at complete separation are:

$$(m_3 - m_2)c_A^F = q_A^{II} - m_2 c_A^{II} \tag{9}$$

$$(m_3 - m_2)c_B^F = m_3 c_B^{III} - q_B^{III} \tag{10}$$

The liquid and solid phase concentrations in the bed are assumed to be in equilibrium, as is inherent to the local equilibrium assumption.

The concentrations at position α are obtained from the mass balances at the top of section II:

$$m_2\left(c_A^{II} - c_A^{\alpha}\right) + q_A^{\gamma} - q_A^{II} = 0 \tag{11}$$

$$-m_2 c_B^{\alpha} + q_B^{\gamma} = 0 \tag{12}$$

And similarly, the concentrations at position β are obtained from the mass balances at the bottom of section III:

$$m_3 c_A^{\beta} - q_A^{\gamma} = 0 \tag{13}$$

$$m_3\left(c_B^{\beta} - c_B^{III}\right) + q_B^{III} - q_B^{\gamma} = 0 \tag{14}$$

By substitution of the flow rate constraints (Table I) in these mass balance equations, it can be shown that $c^{\alpha} = c^{\gamma}$, when wave 2 is a shock wave and $m_2 = m_{2,min}$, and $c^{\beta} = c^{\gamma}$ when wave 3 is a shock wave and $m_3 = m_{3,max}$.

The relation between the compositions at location γ and $(c_A^{II},0)$ or $(0,c_B^{III})$ is given by the "coherence criterion". The coherent compositions in a diffuse wave are calculated from the composition path grid, as shown in the Appendix.

By combination of the flow rate criteria (Table I), mass balance equations (equations (9) through (14)) and coherence criteria, the region of complete separation can be constructed; the details will be shown below. The developed approach can in principle be applied to any isotherm. However, there are some exceptional situations that cannot be treated (yet).

A single wave must connect the compositions $(c_A^{II},0)$ and $(c_B^{III},0)$ to the composition α,β or γ. In complex isotherms, which are not purely competitive, this may not be the case, and complete separation is not possible.
Azeotropic phenomena may occur. Azeotropy is known from distillation processes, where components cannot be separated because of a reversal of the selectivity. The above described thermodynamic equilibrium model suggests a similar azeotropic processes may also occur in the gelfiltration of concentrated protein solutions. At some combinations of the interaction coefficients B_{ij}, the affinity of one species increases, whereas the affinity of the other species decreases at increasing concentration, and at some composition, the affinities are equal and components can no longer be separated. As far as we know, azeotropy in gelfiltration processes has never been described in literature. Note that azeotropic phenomena are more often observed in chromatographic processes (Houwing *et al.*, 1999).

In chromatography, the "selectivity", defined $S_{A,B} = q_A/c_A \cdot c_B/q_B$, is not a sufficient criterion to define azeotropy. Azeotropy occurs in chromatography when the wave velocities, i.e. the eigenvalues, of two waves are equal. As both waves can be shock and diffuse waves, there are four criteria for the occurrence of azeotropy in the middle sections of the TMB. The criterion to be used depends on the shapes of the waves 2 and 3, as is shown in Table II. As is easily seen, the conventional definition of "selectivity" only applies to the case waves 2 and 3 are shock waves.

The criteria listed in Table II can be plotted as a line in composition space (cf. the Appendix). Complete separation will only occur if none of the compositions in the TMB exceeds this line.

Table II. Azeotropy criteria dependent on wave pattern.

wave pattern of waves 2 and 3	azeotropy criterion
diffuse-diffuse	$\lambda^{\min}(\mathbf{c}) = \lambda^{\max}(\mathbf{c})$
diffuse-shock	$\lambda^{\min}(\mathbf{c}) = \Lambda = \frac{q_B^{\gamma}}{c_B^{\gamma}}$
shock-diffuse	$\lambda^{\max}(\mathbf{c}) = \Lambda = \frac{q_A^{\gamma}}{c_A^{\gamma}}$
shock-shock	$\frac{q_A^{\gamma}}{c_A^{\gamma}} = \frac{q_B^{\gamma}}{c_B^{\gamma}}$

Composite waves, where part of the wave is a shock and part of the wave is a diffuse wave may occur (Migliorini *et al.*, 2000). The selection of the characteristic concentration is then not trivial, and has not been developed yet.

Construction of the region of complete separation

Above, we have given the general guidelines for determining the complete separation region. In this section, matters considering implementation of the criteria and four independent boundaries are discussed.

Prior to the construction of a “region of complete separation” or “triangle”, it should be checked whether complete separation is possible at all. In order to check the ability to reach the compositions (c_A^{II},0) and (0,c_B^{III}) by a single wave and to determine whether composite waves occur, no explicit methods have been developed yet. Instead, we construct some of the composition paths, starting at the feed composition. When all these paths cut the axes and no maximum or minimum eigenvalue is seen, it is assumed that separation is possible. However, careful checks are required.

Secondly, the wave pattern is determined. The spreading behavior of waves 2 and 3 is obtained by inspecting the change in eigenvalues at the paths originating at the feed composition; for waves 1 and 4, the desorbent composition (0,0) is used as a starting point. Using the wave pattern and the equations in Table II, the azeotropy line is constructed in the composition path grid. In order to operate the TMB in the complete triangle at a given feed concentration, the feed concentration is taken below this line. We have not yet considered the situation of feed concentrations at which part of the triangle is accessible (near the positive feed line).

Based on the calculated wave pattern, the four boundaries of the region of complete separation as indicated in Figure 2 can be constructed. In the following description of these, we will refrain from denoting that equilibrium between the solid and liquid phase is assumed in section II, III and at location γ. The locations of characteristic points on the curves are denoted as coordinates in a plot (m_2, m_3).

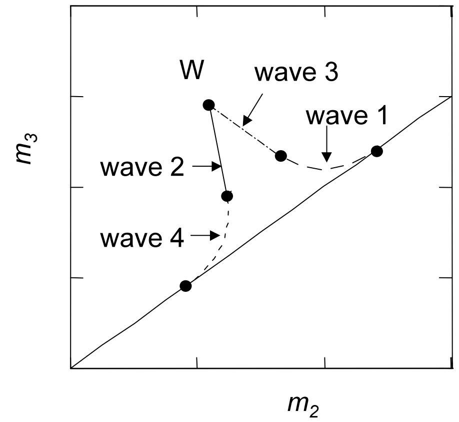

Figure 2. Waves and corresponding boundaries.

Wave 1: When wave 1 is a diffuse wave, its boundary is constructed starting from the dilute solution starting point, (K_A^{og}, K_A^{og}). The concentration c_A^{II} is taken as the running variable, and the corresponding m_2 and m_3 are calculated from the flow rate criterion and the mass balance on component A. When wave 1 is a shock wave, the combination of the flow rate criterion and the mass balance yields the positive feed line.

Wave 2: When wave 2 is a diffuse wave, its boundary is found by simultaneous solving of the flow rate criterion and the mass balance on component A. Once more, c_A^{II} is used as a running variable. The construction of the wave is started at the point (K_B^{og}, K_B^{og}). When wave 2 is a shock wave, the concentration at location γ determines the wave velocity. This concentration is obtained from the coherence of wave 3, which implies the numerical integration of the composition path whenever wave 3 is a diffuse wave. The boundary on wave 2 is constructed starting at the optimal point W, taking c_B^{III} as the running variable, and solving the overall mass balance on component B, the coherence of wave 3, and the flow constraint on wave 2.

Wave 3: Calculation of the boundaries on wave 3 is similar to the calculation of the boundaries on wave 2. When wave 3 is a diffuse wave, the boundary is constructed starting at the point (K_A^{og}, K_A^{og}), taking c_B^{III} as a running variable and solving the flow rate constraint and the overall mass balance on component B. When wave 3 is a shock wave, the boundary is again constructed starting at the optimal point, taking c_A^{II} as a running variable, and solving the shock wave criterion, the overall mass balance on component A and the coherence condition on wave 2 (for calculation of c^γ).

Wave 4: When wave 4 is a diffuse wave, it is constructed starting at the dilute system limit (K_B^{og}, K_B^{og}), by solving of the flow rate criterion and the overall mass balance on component B. The concentration c_B^{III} is taken as a running variable. When wave 4 is a shock wave, the positive feed criterion is found.

Optimal point: The point of maximum throughput, the left-hand top corner of the region of complete separation is frequently used as a starting point for construction of the region of complete separation. At this point W (Figure 2), the constraints on both m_2 and m_3 are fulfilled. Hence, the optimal point is found by simultaneously solving the appropriate equations on waves 2 and 3, as described above at the respective waves.

As an initial estimate, the composition at location γ is taken equal to the feed composition, since this represents the maximal concentrations possible. The starting points of shock waves are then: $m_2 = q_B^F/c_B^F$ and $m_3 = q_A^F/c_A^F$. The starting points of diffuse waves are: $m_2 = \lambda^{\min}(c_A^{II},0)$ and $m_3 = \lambda^{\max}(0,c_B^{III})$, where $(c_A^{II},0)$ and $(0,c_B^{III})$ are the compositions that are coherent with the feed composition.

Methods

The sets of equations governing each boundary were solved in Matlab, version 5.2, using the programmed *fsolve* routine (The Mathworks, USA). A Levenberg-Marquardt iteration schedule was used for its reduced time to convergence in comparison to the standard iteration scheme.

In order to show the effect of the interaction coefficients on the region of complete separation, a fictive model system has been used, of which the parameters are shown in Table III. The reason for the use of a fictive model system is the scarcity of binary interaction coefficients (of unlike species) in literature. The available data (e.g. Haynes *et al.*, 1993) do not allow a straightforward demonstration of the effect of repulsion or attraction on the triangle, not in the least because these effects are overshadowed by non-trivial competition effects, composite waves et cetera.
The fictive model system is chosen such, that the effect of small and large molecules can be shown, and by variation of the binary interaction coefficient, both repulsive and attractive interaction between components can be demonstrated.

Table III. Properties of fictive model system.

component	r_p [nm]	r_f [nm]	ϕ_f [-]	ρ [kg/m^3]	MW [g/mol]
A	0.5	-	-	1350$^{2)}$	250
B	4.0	-	-	1350$^{2)}$	$130 \cdot 10^3$
fiber	-	1.29	0.022$^{1)}$	-	-

1) chosen based on: Vonk, 1994.
2) chosen based on: Wills *et al.*, 1995.

Results

In this section, the effect of the binary interaction coefficients on the "triangular region" are shown. We will start with the simple case, where components only show interaction with like molecules. In second instance, the interaction between unlike molecules is described.

No interaction with other species: B_{AB}=0.

The effect of the self-interaction coefficient B_{ii} on the single component isotherm is shown in Figure 3. When B_{ii} is zero, a linear isotherm with slope K^{og} is obtained. When B_{ii} is positive, the isotherm is convex, and the distribution coefficient (i.e. the chord of the curve) increases with increasing protein concentration. This is explained by the smaller protein density inside the sorbent particle, which is a result of the exclusion. As the repulsion is proportional to the particle density, the repulsion between two protein molecules is smaller inside the sorbent particle than in the bulk liquid. It is energetically more favorable for a protein to enter the sorbent than to remain in the bulk at increasing concentration.

When B_{ii} is negative, the isotherm is concave and the distribution coefficient decreases with protein concentration, which is explained by similar reasoning.

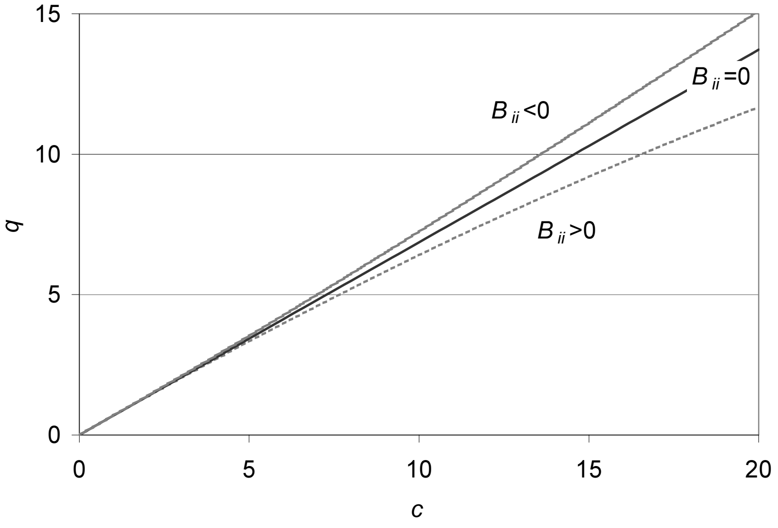

Figure 3. Effect of binary self-interaction coefficient B_{ii} on a single component isotherm.

The sign and magnitude of B_{ii} determines the pattern of the waves in the TMB. In a single component system, a wave is diffuse whenever the eigenvalue, i.e. the slope of the isotherm, decreases in the direction of liquid flow. At negative B_{AA}, wave 1 is diffuse, as is wave 2 at negative B_{BB}. This is in agreement with the common behavior during elution in case of a concave isotherm. At negative

B_{AA}, wave 3 is a shock wave, as is wave 4 at negative B_{BB}. This is in agreement with the behavior observed during loading in case of a concave isotherm. At positive B_{ii}, the situation is inverted. The dilute system limit is found when B_{ii}=0; all waves are then ‘indifferent”.

We will continue by discussing the effect of the self-interaction coefficients B_{ii} on the region of complete separation. Each of the two has been given three values: (a) the entropic two-body repulsion term calculated from (eq. (2)), (b) a value of zero, and (c) an attractive interaction term, which we have set equal to the negative of (a). When there is no cross interaction between the solutes (B_{ij}=0), the triangle is just a superposition of the single-component waves. Each wave has three possibilities: diffuse, indifferent, or shock, depending on the signs of B_{ij}, as explained above. All possible boundaries are depicted in Figure 4.

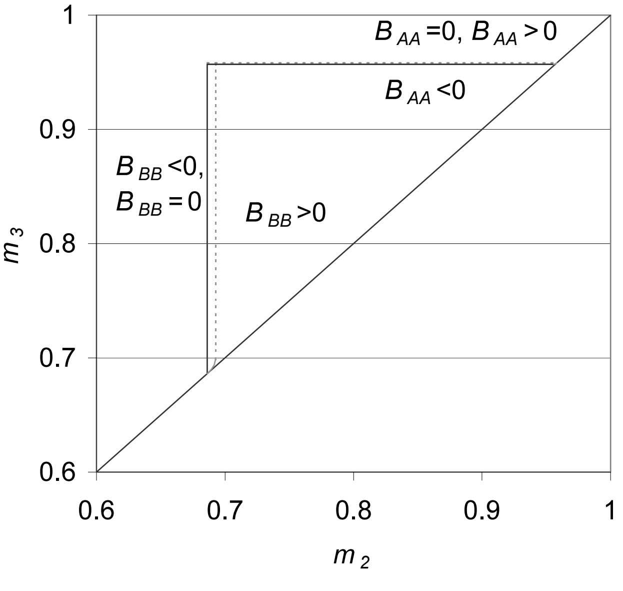

Figure 4. Effect of binary self-interaction coefficient B_{ii} on the region of complete separation.

The boundaries corresponding to the diffuse waves, i.e. wave 2 when B_{BB}>0, and wave 3 when B_{AA} <0, always coincide with the boundaries corresponding to indifferent waves (B_{AA}=0, or B_{BB}=0) and also coincide with the dilute system boundaries. This is easily explained when regarding Table I. For instance, m_2 is determined by the minimal eigenvalue at $(c_A^{II},0)$. In this particular case, it equals K^{og}_B, because the concentration of B is zero by definition and as B_{AB}=0, the concentration of A has no effect on K_B. Hence, the boundary on m_2 is invariably at K^{og}_B, irrespective of the concentrations of the two species in the feed and the values of B_{ii}. Similar reasoning holds for component A in section III.

The boundaries of the shock waves differ from the dilute system boundaries. When B_{AB}=0, the concentration of only one component changes over a wave, since the concentration changes are not coupled. In other words, c_A^{II} equals c_A^{α} and c_B^{III} equals c_B^{γ}. Combination of the overall mass balance equation on B (eq. (10)) and the flow rate constraint $m_2 = q_B^{\gamma}/c_B^{\gamma}$ leads to the conclusion that there is only a solution when $c_B^{III} = c_B^{\gamma} = c_B^{F}$. Hence, the boundary on m_2 corresponding to wave 2 is invariably found at $m_2 = q_B^{F}/c_B^{F}$. Similar reasoning on the overall mass balance on component A and the flow rate criterion in section III leads to the conclusion that the boundary on m_3 corresponding to wave 3 is invariably found at $m_3 = q_A^{F}/c_A^{F}$. It is obvious that both the feed concentration and the exact values of B_{ii} influence the position of those lines. When wave 2 or 3 is a shock wave, the boundaries to the region of complete separation near the positive feed line are formed by wave 1 and 4. Consequently, the limits are at the K^{og} values near the positive feed line, which is expected at the corresponding low concentration.

Including interaction with other species, $B_{AB} \neq 0$

At the end of this section, we will discuss changes in the regions of complete separation as a function of the interaction coefficients. For the explanation of the occurring effects, information from the isotherm, the composition path grid and the reversal of selectivity is required. These topics will first be addressed.

The interaction of the two species via the binary interaction coefficient B_{AB} has a large impact on the isotherm of the species. Some examples of contour plots of the isotherms are shown in Figure 5. It is seen that the behavior of the larger molecule B is rather sensitive to the concentration of the smaller molecule A. When all interaction coefficients are positive, the many repulsive forces in the liquid at increased concentration increasingly force the large molecule into the resin, where the particle density is lower and repulsive forces are less. The effect of the small molecule is large, since it has a high particle density.

The small component A hardly experiences any effect of the repulsive forces; its thermodynamical behavior is rather ideal at the small B_{AA}. When all forces are attractive, i.e. at negative B_{ij}, the larger molecule more and more remains in the liquid at increasing concentration of both A and B. Migration into the resin is less favorable, since this reduces the number of energetically favorable attractive forces. Again, the effect of the small ion is rather large. The smaller molecule A also shows a faint tendency to stay in the bulk liquid. The effect is again much smaller than in case of the large molecule B.

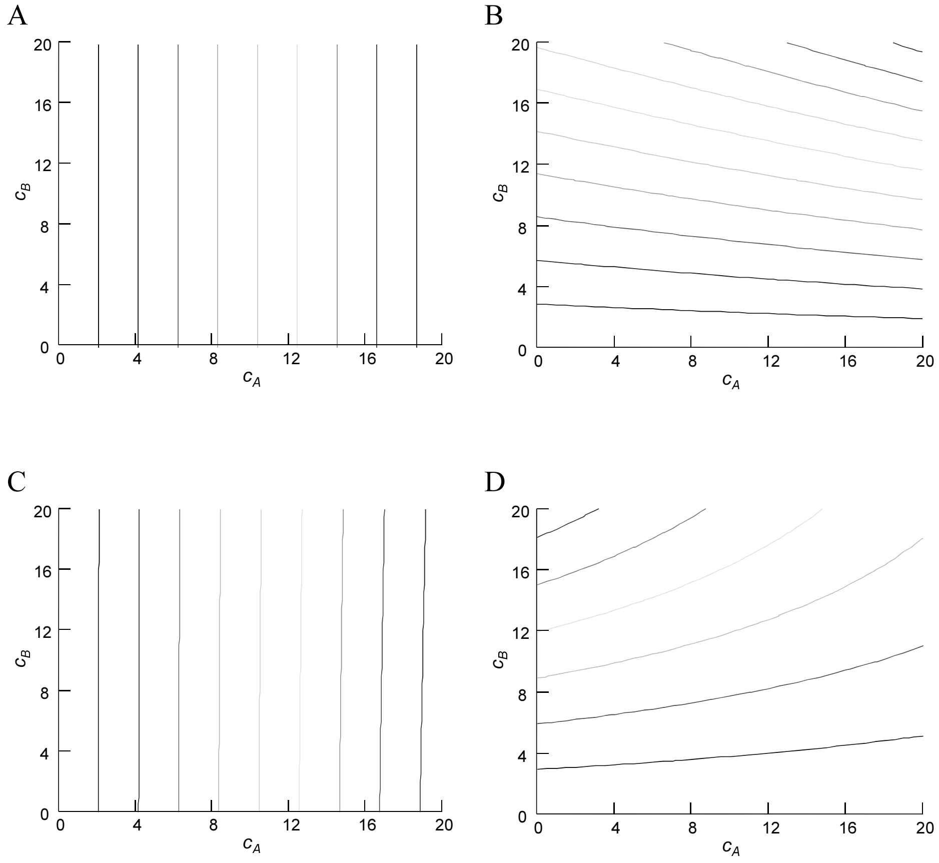

Figure 5. Examples of contour plots of isotherms. A and B: positive B_{AA}, B_{AB}, and B_{BB}; C and D: negative B_{AA}, B_{AB}, and B_{BB}; A and C: contours of q_A; B and D: contours of q_B. Contours are shown at intervals of 2 g/L.

Under these interacting conditions, the distribution coefficients of the components may even reach values that exceed unity at high concentrations. This is an important observation, since usually, the distribution coefficient in gelfiltration is thought to range between zero and one.

The composition path grid (see Appendix) provides us with important information on the changes of concentrations over waves. Any cross-interaction between the species leads to deviation of the composition paths from horizontal or vertical lines. A large angle between the composition paths and the axes is favorable for separation performance, because it defines the extent of concentration or dilution of the product as governed by equilibrium. The same effect is seen as a roll-up effect, which is generally known to occur in Langmuir-type systems. In case of the model system, the sign of the cross-interaction coefficient determines which component is concentrated in the SMB. To illustrate this, the composition paths starting at 5 g/L have been drawn for positive B_{AA} and B_{BB}, at positive and negative B_{AB} in Figure 6. The line crossing the c_A-axis corresponds to wave 2, the line crossing the c_B-axis corresponds to wave 3. First consider wave 2. Independent of the sign of B_{AB}, this line is almost vertical. This is a result of the almost constant distribution coefficient of A; as in linear isotherms, the concentration of A hardly changes over the wave. At positive B_{AB}, the concentration of A at the axis exceeds the starting concentration, which implies that A can (a little) be concentrated in this wave. At negative B_{AB}, the situation is inverted.

When we look at wave 3, similar phenomena are seen, but the effects are much larger. This is due to the larger changes in the “distribution coefficient” of B at changing concentration.

Please note that Figure 6 only shows the paths corresponding to diffuse waves. It is known from literature that paths corresponding to shock waves may not coincide with these (Helfferich and Whitley, 1996). The shock paths that have been computed show the same tendencies in changes in concentration.

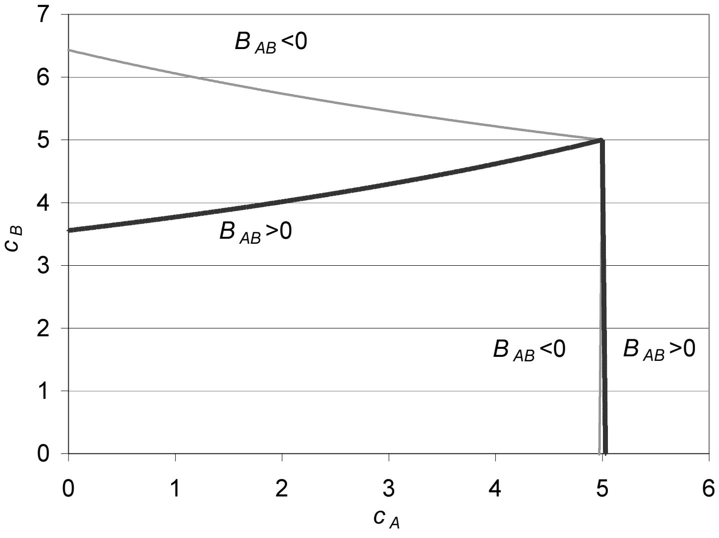

Figure 6. Effect of B_{AB} on composition paths when B_{AA},B_{BB} >0.

In the fictive model system used, azeotropic phenomena occur when the cross-interaction coefficient B_{AB} is positive. This is easily explained looking at the change in "distribution coefficient", which is currently the slope or the chord of the isotherm, depending on de wave shape. A positive B_{AB} results in a positive contribution to the "distribution coefficient" of both species, as a result of the increased repulsion between the species. However, the effect on the large, less retained component is much larger than on the small component. At a certain composition, the "distribution coefficients" equal, and azeotropy occurs. Obviously, this only occurs when the relative effect of the cross-interaction coefficient is large, and is not overshadowed by the self-interaction effects. The calculated concentration of A at which azeotropy occurs in the current model system are approximately 19 g/L (when all Bij positive), 17 g/L (when B_{AA},B_{AB} positive, B_{BB} negative) and 14 g/L (when B_{AA} negative, B_{AB}, B_{BB} positive), independent of the concentration of B.

When B_{AB} is negative, no azeotropic phenomena are seen, provided that the cross-interaction determines the increase or decrease of the "distribution coefficient". At negative B_{AB}, both "distribution coefficients" then decrease. As the effect on the large, less retained molecule is larger than the effect on the small, more retained molecule, it is excluded that the two "distribution coefficients" will ever be equal.

When the two species do influence the distribution behavior of both, the construction of the region of complete separation is no longer a matter of superposition of the single component waves. The feed concentration is getting more and more important. In the following, we will show the effect of the binary interaction coefficients B_{ij} on the region of complete separation. The regions of complete separation have been constructed in case of all eight possible combinations of attractive and repulsive interaction between two species. These have been grouped in four pictures (Figure 7A through D). In each picture, the self interaction coefficients B_{AA} and B_{BB} are kept constant and the cross interaction coefficient is varied. A feed concentration of 5 g/L has been chosen, as the concentration where no azeotropy occurs for all combinations of B_{ij} used.

Firstly, notice that the wave pattern (indicated in Figure 7 by a four letter code) does not depend on the sign of B_{AB}. In case of wave 1 and 4, this is easily explained, as these waves are determined by one component only (i.e. component A in wave 1 and component B in wave 4), hence the interaction coefficient does not influence wave shape. The invariance of the wave shape of waves 2 and 3 with B_{AB} is a consequence of the exclusion of combined waves. Combined waves are only absent if all waves originating at one of the axes of the composition path grid have the same change (increase or decrease) of eigenvalue when travelling away from the axis. Hence, if wave 1 is a shock wave, wave 3 is a diffuse wave and *vice versa*. The same holds for wave 2 and 4.

The impact of the sign of the binary non-self interaction coefficient on wave 2 and the optimal point is large. Upon changing the sign of B_{AB} from negative to positive, the optimal point shifts to considerably larger m_2. The reason is that the boundary on m_2 is at $\lambda^{\min}(c_A^{II},0)$, which corresponds to the “distribution coefficient” of B, and which is strongly influenced by the concentration of A (cf. Figure 5). At positive B_{AB}, this eigenvalue increases, leading to a high m_2 at high c_A at the optimal point, and a lower m_2 at low concentration near the positive feed line. At negative B_{AB}, the situation is inverted: the eigenvalue decreases with increasing c_A, leading to an optimal point at m_2 below K^{og}_B.

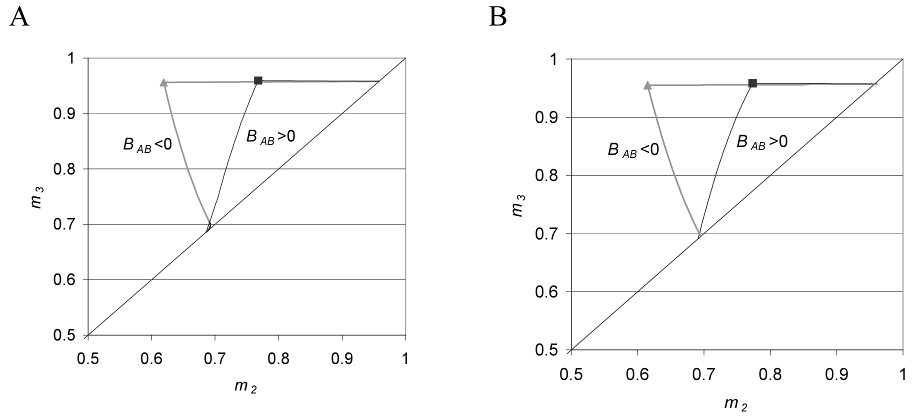

B_{AA} >0, B_{BB} >0, wave pattern = ssdd

B_{AA} <0, B_{BB} >0, wave pattern = dssd

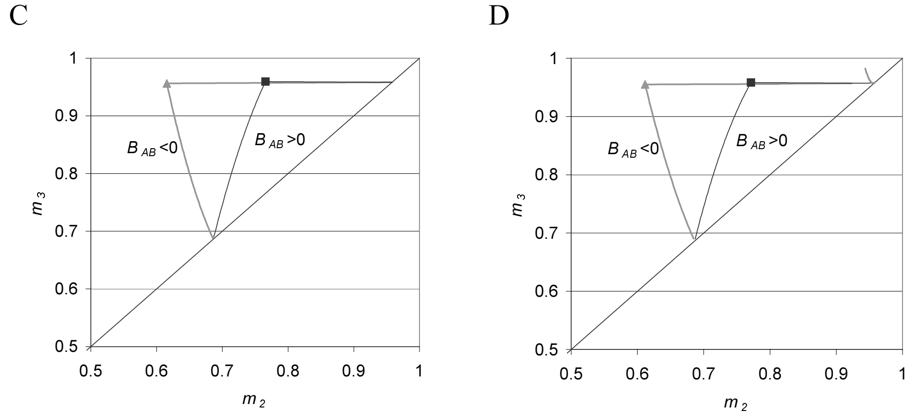

B_{AA} >0, B_{BB} <0, wave pattern = sdds

B_{AA} <0, B_{BB} <0, wave pattern = ddss

Figure 7. Effect of the interaction coefficients on the region of complete separation at $c_A^F = c_B^F = 5$ g/L.

In all four pictures of Figure 7, the boundary corresponding to wave 3 is more or less equal. This is an effect of the small A-molecule (r_A = 0.5 nm), which implies there is little sterical interaction between two like molecules, as well as interaction with the larger B molecule. As is shown in Figure 5, the isotherm is hardly influenced by the concentration of the two species. Hence, the slope and chord of the isotherm are almost the same, and the velocities of shock and diffuse waves are hardly different.

The boundaries corresponding to the diffuse waves 2 and 3 are equal in all figures (when existent). The limiting compositions of these waves are (c_A^{II},0) and (0,c_B^{III}); the corresponding limiting eigenvalues are only influenced by the magnitude of B_{AA} and B_{BB} respectively, and the cross-interaction coefficient does not play a role.

The boundaries corresponding to the shock waves 2 should be different, since both components A and B influence the eigenvalue of the shock wave. However, it is seen in Figure 7 that these boundaries seem to coincide, and also coincide with the boundaries corresponding to diffuse waves. This is explained by the very small change of the minimal eigenvalue over wave 2 at given B_{AB} and limiting concentrations. For instance, the eigenvalue ranges between 0.771 and 0.766 over wave II when all B_{ii} are positive. Similar figures are found at the other combinations of B_{ii}. Hence, shock and diffuse wave propagate at more or less the same velocity and the corresponding point on the two boundaries is equal. When travelling over the boundary, e.g. from the optimal point W to the positive feed line, the limiting (average) eigenvalue changes, so the boundary is at new point (m_2,m_3), but still the difference between shock and diffuse waves remains small.

Finally, let us look at the remarkable concentrations in and between the sections that are calculated during construction of the boundaries. We will itemize the observations:

- Whenever B_{AB} is negative, the concentration of B in section III at the optimal point exceeds the feed concentration. Also, the concentration in section III always exceeds the concentration of B at location β. This is a consequence of the increasing composition paths when going from composition c^F or c^γ to (0,c_B^{III}), see Figure 6.
- Similarly, the concentration c_A^{II} exceeds the concentration $c_A\gamma$ at positive B_{AB}.
- At negative B_{AB} and positive B_{BB}, the concentration c_B^{III} increases when the boundary corresponding to wave 2 is traveled from the optimal point towards the positive feed line. That the concentration c_B^{III} is high follows from the coherence of the shock wave 2. At the nearly constant K_A, the ratio (q_A^β-q_A^{II})/(c_A^β-c_A^{II}) equals K_A; the ratio (q_B^β)/(c_B^β) only equals the same value at high c_B^β.

- Similarly, when $B_{AA}<0$ and $B_{AB}>0$, c_A^{II} and c_A^{γ} increase when the boundary corresponding to wave 3 is traveled from the optimal point to the positive feed line.

The described concentration effects in sections II and III are favorable from an efficiency point of view, since these reduce the dilution of the product and hence reduce consumption of solutions, resin and effort necessary for concentrating the product in later production stages.

Conclusions

The isotherms observed during gelfiltration of concentrated mixtures of proteins are curved instead of linear, as is commonly assumed. Both convex and concave isotherm shapes are described in literature. Using Wills' description of these isotherms (Wills *et al.*, 1995), azeotropy is predicted to occur. Azeotropy is the situation where the fronts of both components move at the same velocity. Secondly, composite waves are predicted. These waves are partly shock and partly diffuse of shape. A third prediction is that a pure product may not be obtained chromatographically, as the composition path starting at some feed concentrations asymptotically approaches the pure product composition. In the fourth place, the distribution coefficients may reach values exceeding unity. To our best knowledge, these four phenomena have not yet been described in case of gelfiltration separations.

With respect to azeotropy phenomena, it is concluded that the common term "reversal of selectivity" should not be used in chromatography context. Depending on the wave shape, there are four possibilities by which the two waves in a binary system have the same velocity. By "reversal of selectivity", only one of these is covered. The term azeotropy, covering all possibilities, is preferred.

A novel procedure for flow rate selection in SMBs based on this separation mechanism is developed. The procedure is based on wave theory, where the latest paper in the "robust design" series (Migliorini *et al.*, 2000) is taken as basis. However, the current method does not impose a certain wave pattern (i.e. shock or diffuse waves at given positions in the system). The procedure may require a numerical determination of composition path grids. Restrictions to the starting compositions due to azeotropy are given. The current method is not yet

able to treat composite waves. This part of the theory should be developed shortly, since composite waves are likely to occur in case of the used isotherm.
The effect of the interaction between species (be it repulsive or attractive) on the region of complete separation of a fictive model system is shown. The results can be explained from e.g. the composition path grids. We think this method, in a future version that is extended to include composite waves, is a powerful tool to construct regions of complete separation for any situation, starting from any arbitrary isotherm.

Acknowledgements

This project was financed by the Dutch ministry of economic affairs through the program IOP-Milieu Preventie.

Notation

B_{ij}	two body interaction coefficient between species *i* and *j*	[L/mol]
c	concentration in the liquid phase	[mol/L]
$\mathbf{I}$	identity matrix	[-]
K	distribution coefficient (= q/c)	[-]
$\mathbf{M}$	matrix of partial derivatives ($\mathbf{M}_{i,j}=\partial q_i/\partial c_j$)	[-]
MW	molecular weight	[g/mol]
N_{av}	Avogadro's constant	[-]
q	concentration in the sorbed phase	[mol/L]
r	radius	[m]
R	gas constant	[J/mol·K]
T	temperature	[K]
z	distance	[m]

greek

α	interaction parameter	[-]
β	phase ratio (= (1-ε)/ε)	[-]
ε	porosity	[-]
ϕ	volume fraction of component	[-]
λ	eigenvalue	[-]
Λ	eigenvalue	[-]
μ	chemical potential	[J/mol]

super- and subscripts

f	fiber
L	in liquid phase
S	in sorbed phase
ex	excluded volume
og	Ogston

Literature

Bosma, J.C. and J.A. Wesselingh, “Partitioning and diffusion of large molecules in fibrous structures,” *J. Chromatogr.* **743**, 169 (2000).

Bosma, J.C., “More efficient process chromatography”, Ph-D. Thesis Groningen State University, the Netherlands (2001).

Fanti, L.A. and E.D. Glandt, “Partitioning of spherical particles into fibrous matrices,” *J. Coll. Int. Sci.* 135, 385 (1990).

Haynes, C.A., F.J. Benitez, H.W. Blanch and J.M. Prausnitz, “Application of integral-equation theory to aqueous two-phase partitioning systems”, A.I.Ch.E. J., **39**, 1539 (1993).

Helfferich, F.G. and G. Klein, “Multicomponent chromatography: theory of interference,” Marcel Dekker, New York (1970).

Helfferich, F.G. and R.D. Whitley, ” Non-linear waves in chromatography. II: Wave interference and coherence in multicomponent systems,” *J. Chromatogr*. **734**, 7 (1996).

Houwing, J., H.A.H. Billiet, J.A. Wesselingh and L.A.M. van der Wielen, “Azeotropic phenomena during separation of dilute mixtures of proteins by simulated moving bed chromatography,” *J. Chem. Technol. Biotechnol.,* **74**, 213 (1999), chapter 3 of this thesis.

Houwing, J., H.A.H. Billiet and L.A.M. van der Wielen, “Mass transfer effects during separation of proteins in SMB by size exclusion,” *A.I.Ch.E. J.,* **49**, 1158 (2003), chapter 2 of this thesis.

Hwang, Y.-L., “Wave propagation in Mass-transfer processes: from chromatography to distillation,” *Ind. Eng. Chem. Res.*, **34**, 2849 (1995).

Lazzara, M.H., D. Blankschtein and W.M. Deen, “Effects of multisolute steric interactions on membrane partition coefficients,” *J. Coll. Interf. Sci.,* **226**, 112 (2000).

Ma, Z. and N.-H. L. Wang, “Standing wave analysis of SMB chromatography: linear systems,” *A.I.Ch.E. J.*, **43,** 2488 (1997).

Neal, B.L. and A.M. Lenhoff, “Excluded volume contribution tot the osmotic second virial coefficient for proteins,” *A.I.Ch.E. J.*, **41**, 1010 (1995).

Ogston, A.G., "The spaces in a uniform random suspension of fibres," *Trans. Faraday Soc.*, **54**, 1754 (1958).

Rhee, H.-K., R. Aris and N.R. Amundson, "Multicomponent adsorption in continuous countercurrent exchangers," *Phil. Trans. Roy. Soc. Lond. A.*, **269,** 187 (1971).

Shearwin, K.E. and D.J. Winzor, "Thermodynamic nonideality in macromolecular solutions : evaluation of parameters for the prediction of covolume effects," *Eur. J. Biochem.*, **190**, 523 (1990).

Storti, G., M. Mazzotti, M. Morbidelli and S. Carrà, "Robust design of binary countercurrent adsorption separation processes," *A.I.Ch.E. J.*, **39**, 471 (1993).

Vilker, V.L., C.K. Colton and K.A. Smith," The osmotic pressure of concentrated protein solutions : effect of concentration and pH in saline solutions of bovine serum albumin*," J. Coll. Int. Sci.* **79**, 548 (1981).

Vonk, P., "Diffusion of large molecules in porous structures," Ph-D thesis Groningen State University (1994).

Wills, P.R., W.D. Comper and D.J. Winzor, "Thermodynamic nonideality in macromolecular solutions: interpretations of virial coefficients," *Arch. Biochem Biophys.*, **300**, 206 (1993).

Wills, P.R., Y. Georgalis, J. Dijk and D.J. Winzor, "Measurement of thermodynamic nonideality arising from volume-exclusion interactions between proteins and polymers", *Biophys. Chem.*, **57**, 37 (1995).

Wu, D.-J., Y. Xie and N.H.L. Wang, "Design of simulated moving bed chromatography for amino acid separations," *Ind. Eng. Chem. Res.*, **37**, 4023 (1998).

Appendix: coherence and composition path grid

A relation between the composition c^{γ} and $(c_A^{II},0)$ and $(0, c_B^{III})$ in diffuse waves can only be obtained from wave theory. Wave theory, as developed by Helfferich and Klein (1970) and Rhee, Aris and Amundson (1971), is well documented. In this paragraph, we'll only summarize the essentials by which the above mentioned relations are obtained; the reader is referred to the original papers for the details.

Essential to wave theory is the principle of coherence, which has been explained as follows (Helfferich and Whitley, 1996):

> The introduction of a feed of arbitrary composition into a column produces a wave… "This initial wave is non-coherent and is resolved into a set of coherent waves. The latter, by definition, travel without further breakup; they may sharpen or spread, but retain their integrity in all other respects".

Further, in the same paper:

> "Coherence requires all components that are locally present to have the same wave or shock velocity at any point in space and time within the wave".

From the wave equation, is then obvious that all species have the same wave velocity, which implies for diffuse waves (Helfferich and Whitley, 1996):

$$\frac{dq_i}{dc_i} = \lambda \qquad \text{where} \qquad dq_i = \frac{\partial q_i}{\partial c_1} dc_1 + \frac{\partial q_i}{\partial c_2} dc_2 + \frac{\partial q_i}{\partial c_3} dc_3 + ..$$

By rewriting these two equations in matrix form, the matrix equation (7) is obtained.

In order to maintain the coherence over the complete wave, the changes in concentration in a wave are restricted: any change to a concentration that is not in coherence to the previous would lead to the creation of more new coherent waves.

The allowed concentration changes are given by the eigenvectors of the matrix of partial derivatives. The allowed concentration changes are conveniently plotted as a composition path grid, a graph with the concentrations of the species on the axes and lines connecting the coherent compositions. The lines, also called "composition paths" are essential to the problem stated in the first lines of this appendix. Let us take wave 2 as an example. As this is one single wave, the compositions (c_A^{II},0) and c^{γ} should be coherent.

Starting from the extreme composition, the coherent composition are obtained by repeatedly:

- calculating the matrix of partial derivatives and the corresponding eigenvalues and eigenvectors at the current composition;
- selecting the eigenvector corresponding to the wave to be followed (the wave of minimum velocity corresponds to the wave of maximum eigenvalue);
- calculating a new current composition by following the selected eigenvector over a small distance. The direction is determined by the known change in concentration of one component, e.g. in wave 2, it is known that the concentration of B increases from zero in section II to c_B^{γ} between sections II and III.

Note that one concentration at the end point of the composition path (e.g. c_B^{γ}) has to be known; in our current application, this concentration is calculated from mass balances.

Outlook

The decision to look for the improvement of efficiency of chromatographic processes in Simulated Moving Bed (SMB) technology has proven to be just over the course of this Ph-D period. In this thesis, it is described how proteins can efficiently be purified in SMBs, based on size exclusion as well as ion exchange. In the latter case, the use of a salt gradient in the SMB has been shown to be able to reduce both resin and solvent use with orders of magnitude relative to isocratic operation.

Other groups have also realized the potentials of SMB chromatography. During the past eight years, more and more industrial processes have been based on SMB. Of these, separations of enantiomers have covered the majority of investigations, and industrial applications are now emerging (see Schulte and Strube (2001) for a review). Also, processes are being suggested that will lead to separation in multiple products, instead of a binary separation (e.g. Nicolaos *et al.*, 2001).

The issue of sanitary operation, which was regarded as a severe drawback of SMB compared to fixed bed separations in pharmaceutical industry is currently being tackled; the manufacturing companies of SMBs now advertise the SMB as being GMP-compatible. This opens the technology to efficient production of (chiral) drugs, even though a lot of validation and the establishment of a track record is still required. It should however be noted that current GMP applications are restricted to separations involving organic solvents; as far as we know, sanitary operation for separation of proteins has not been shown yet.

The success of SMB in industrial practice is largely due to the fact that its (computer aided) design is now well developed, certainly in case of binary separations obeying linear or Langmuir type isotherms. Also, more general methods for flow rate selection, without prior assumption of the isotherm are being developed, cf. chapter 7 of this thesis. Further research could imply expansion of this model, in order to be able to include composite waves, as well as separation of concentrated mixtures of proteins in gradient SMB.

With respect to further refinement of “triangle theory”, one should carefully consider its use. “Triangle theory” is based on the analogy between SMB and TMB, and is a simplification as such. Refinement of flow selection procedures is only apt when the analogy with TMB is justified. Hence, the sorbent bed should be subdivided sufficiently (which usually requires three to four columns per section (Hidajat *et al.*, 1986). This restriction certainly holds true for gradient SMB, as a small difference in modulator concentration may introduce a large change in affinity of components towards the resin. Consequently, the calculated region of complete separation may not be fully accessible as a result of small deviations in comparison to the TMB-approximation (Jensen *et al.*, 2003).

Future application studies of SMB are foreseen in the area of multicomponent mixtures, where multiple products are required. These include separations typical for biotechnology, where a feed containing many solutes is fractionated into a pure solution of the aimed component, as well as two products containing the more and less retained solutes. A major impediment for (industrial) application of multicomponent separations is the vast body of equilibrium data that is required before a detailed design can be made.

SMB-based industrial separations would gain economical benefit if more rigid matrices were developed that still allow a high mass transfer efficiency and that could conveniently be packed into (stainless steel) SMB columns. In this way, the optimization of throughput (as described in chapter 2 in this thesis) would lead to a highly productive separation. Possibly, monoliths can serve as a solution at this point (Schulte and Dingenen, 2001).

Literature

Hidajat, K., C.B. Ching and D.M. Ruthven, “Simulated countercurrent adsorption processes: a theoretical analysis of the effect of subdividing the adsobent bed,” *Chem. Eng. Sci.,* **41**, 2953 (1986).

T.B. Jensen, S.H. van Hateren, J. Houwing, H.A.H. Billiet and L.A.M van der Wielen, "Experimental Validation of Gradient Elution in SMB Chromatography," Chapter 3 in: *"Gradient SMB chromatography"*, Ph-D thesis T.B. Jensen, Delft University of Technology (2003).

Nicolaos, A., L. Muhr, P. Gotteland, R.M. Nicoud and M. Bailly, "Application of equilibrium theory to ternary moving bed configurations (four + four, five + four, eight and nine zones) I. Linear case," *J. Chromatogr.*, **908**, 71 (2001).

Schulte, M. and J. Strube, "Preparative enantioseparation by simulated moving bed chromatography," *J. Chromatogr.,* **906**, 399 (2001).

Schulte, M. and J. Dingenen, "Monolithic silica sorbents for the separation of diastereomers by means of simulated moving bed chromatography," *J. Chromatogr.,* **923**, 17 (2001).

Summary

This thesis describes the separation of mixtures of proteins by Simulated Moving Bed (SMB) chromatography. The research was initiated upon a demand for more efficient process chromatography, where the sorbent inventory and the consumption of solvent and salt are reduced in comparison to current fixed bed process scale chromatographic separations. Displacement, recycle, two way and SMB chromatography were considered as potential more efficient technologies. SMB chromatography was selected for further investigation, as it may lead to reduction of both sorbent, eluent and salt use. The emphasis of this research was laid on further development of the SMB chromatography rather than on its comparison with the conventional methodology.

SMB chromatography is a countercurrent separation technique, which leads to binary fractionation of a feed mixture. It makes use of differences in affinity of the feed components towards the chromatography resin. The weakly binding component predominantly moves in the direction of the liquid flow (“upward”), where as the strongly retained component predominantly moves in the direction of sorbent flow (“downward”). SMBs in Sorbex configuration are known from very efficient sugar and olefin separations, where both sorbent and eluent consumption are reduced. Only few applications of SMB systems in biotechnology, e.g. for separation of proteins are known. Procedures for design of SMBs lack or fall short for such separations.

In this project, SMB has been used for the separation of two proteins, Bovine serum albumin (BSA) and myoglobin, based on size differences. The so-called “triangle theory” can then be used straightforwardly for the design of the SMB in terms of liquid and sorbent flow rates that lead to complete separation. However, mass transfer limitations impeded complete separation in experiments where BSA and myoglobin were separated using an unfunctionalized Big Beads matrix. By reducing the particle diameter, mass transfer limitations decrease,

but pressure drop restrictions increase. Based on an analytical solution of the TMB mass balances, a particle size could be selected that leads to maximum throughput (i.e. feed flow rate per sorbent flow rate) at a given product purity and system contents.

During ion exchange separations of proteins in fixed bed, the salt concentration of the buffer can be used to control the affinity of the solutes towards the sorbent. Similarly, an affinity gradient can be introduced in the SMB. By the use of a feed and desorbent stream of a different salt concentration, a situation of high affinity in the top sections and low affinity in the bottom sections can be established. This is believed to increase the loading capacity and reduce the consumption of the salty eluent in comparison to the isocratic SMB, which is operated at a constant salt concentration.

When separating dilute mixtures of proteins in such gradient SMB's, azeotropic phenomena may occur. The distribution coefficients of two proteins (in dilute solutions) respond in a different extent to changes in salt concentration. At a certain critical salt concentration, the affinities of the two proteins equal, and the proteins cannot be separated. This azeotropy (i.e. "reversal of selectivity") is very commonly found in ion exchange of proteins. The gradient SMB only separates properly when all salt concentrations in the SMB are either above or below the above mentioned critical salt concentration.

The use of the gradient was evaluated on the basis of the separation of dilute solutions of BSA and a yeast protein on Q-Sepharose FF at pH 4.6. The throughput, the consumption of the (volume of) desorbent and the consumption of the (moles of) salt were optimized. The developed procedure determines the optimal flow rate ratios by an analytical procedure that includes azeotropy. By subsequent numerical optimization, the optimal salt concentrations in feed and desorbent are found. Feeds exactly at the salt concentration of selectivity reversal can only be separated in a gradient SMB with all salt concentrations exceeding that critical concentration. The consumption of both desorbent volume and salt mass can be reduced by three orders of magnitude in comparison to isocratic operation by the use of a gradient at salt concentrations below the concentration of reversal of selectivity. The recycle of both salt and "volume" of the liquid leaving the top of the SMB (section IV) as a desorbent is highly beneficial to reduce salt and desorbent consumption.

Sodium chloride, used for formation of the gradient during separation of BSA and myoglobin, appears to bind to the Q-Sepharose FF sorbent used. This interaction of salt and sorbent needs to be accounted for during the selection of the flow rate ratios. Only then, the affinity of the top sections (III and IV) exceeds the affinity in the bottom sections (I and II). Both “upward” and “downward” gradients can occur, depending on the direction of movement of the salt. In an upward gradient, the salt is primarily transported by the liquid, whereas it is predominantly transported by the sorbent in a downward gradient. Positioning of the salt gradient has been implemented in the “triangle theory” used for flow rate selection. The developed procedure has been verified by experiments.

The design of the gradient SMB for separation of a dilute mixture of two proteins involves imposing the correct direction of movement to all three interacting components (in our case BSA, myoglobin and salt) in all four sections. The interacting salt further restricts the operating region in comparison to a non-interacting salt. The regeneration of sorbent in section I and the regeneration of desorbent in section IV impose limits on the flow rate ratio in sections II and III. These additional constraints have been implemented in the procedure for designing the SMB. The positioning of the gradient as well as the directions of movement of the proteins observed during the experiments in a twelve column lab-scale SMB agreed well with the predictions based on the developed theory.

The reduced extent of dilution during size exclusion in SMB in comparison to pulse-wise fixed bed chromatography may lead to high protein concentrations, at which deviations from linearity of the size exclusion isotherm can occur. Both convex and concave isotherms are predicted, for attractive and repulsive interactions, respectively. Both are described by an equilibrium model based on osmotic virial expansion. A general procedure for selection of the flow rates during such separations has been developed on the basis of triangle theory. The flow selection method is able to handle both the attractive and repulsive interactions as well as the azeotropic phenomena that are predicted by this isotherm model. The effect of the binary interaction coefficient on the shape of the region of complete separation is shown for the case of a fictive model system.

Summary to: “Separation of proteins by simulated moving bed chromatography”,
Ph-D thesis Joukje Houwing, Delft University of Technology (2003).

Samenvatting

Dit proefschrift beschrijft de scheiding van mengsels van eiwitten met behulp van Simulated Moving Bed (SMB) chromatografie. De aanleiding voor het onderzoek was de lage efficiëntie van conventionele (proces)chromatografische scheidingen. Het beoogde resultaat was een chromatografische techniek waarbij het verbruik van zowel sorbens, buffers als zouten worden gereduceerd in vergelijking met conventionele kolomchromatografie. Displacement-, two-way-, recycle- en SMB-chromatografie werden initieel beschouwd als mogelijk meer efficiënte procesopties. SMB-chromatografie werd geselecteerd voor verder onderzoek, omdat alleen hiermee besparingen van zowel sorbens, zout als buffer waren te verwachten. Het onderzoek richtte zich meer op de verdere ontwikkeling van SMB-chromatografie en minder op de vergelijking ervan met de conventionele scheidingsmethode.

SMB-chromatografie is een tegenstrooms scheidingsproces, waarbij een voedingsstroom wordt gefractioneeerd in twee productstromen op basis van verschillen in affiniteit van de te scheiden componenten voor een chromatografisch sorbens. De zwak-bindende component beweegt voornamelijk in de richting van de vloeistofstoom (“omhoog”), terwijl de sterk-bindende component voornamelijk beweegt in de richting van de sorbensstroom (“omlaag”). SMBs in Sorbex-configuratie zijn bekend om hun zeer efficiënte toepassing in oleofine- en suikerscheidingen, waarbij zowel op sorbens- als op eluensverbruik aanmerkelijk wordt bespaard. SMB-systemen worden nog weinig gebruikt voor biotechnologische toepassingen als de scheiding van eiwitten. Procedures voor het ontwerp van een SMB voor dergelijke scheidingen ontbreken of schieten te kort.

In dit onderzoek is SMB chromatografie gebruikt voor de scheiding van twee eiwitten, Bovine Serum Albumin (BSA) en myoglobine, op basis van verschil in molecuulgrootte. De zogenaamde “triangle theory” kan dan worden gebruikt voor het ontwerp van het SMB, i.e. de selectie van de vloeistof- en sorbenssnelheden die leiden tot volledige scheiding in twee zuivere productfracties. Echter, bij de scheiding van BSA en myoglobine met behulp van een ongefunctionaliseerde Big Beads matrix belemmeren stofoverdrachtslimitaties de volledige scheiding. Door de deeltjesgrootte te verkleinen nemen stofoverdrachtslimitaties af, maar nemen druklimitaties toe. Met behulp van een analytische oplossing van de TMB massabalansen kan de optimale deeltjesdiameter worden gekozen waarbij de doorzet (i.e. ratio van voedingssnelheid tot de sorbenssnelheid) optimaal is bij een gegeven zuiverheid en systeeminhoud.

Bij de conventionele scheiding van eiwitten op basis van ionenwisseling wordt verandering van de zoutconcentratie gebruikt om de affiniteit van de eiwitten voor het sorbens te beïnvloeden. Op eenzelfde manier kan een affiniteitsgradiënt in het SMB worden toegepast. Men gebruikt dan een voedings- en desorbensoplossing met een verschillende zoutconcentratie. Daardoor ontstaat een hoge affiniteit in de bovenste secties van het SMB en een lage affiniteit in de onderste secties van het SMB. Naar verwachting wordt hierdoor de beladingscapaciteit verhoogd en het gebruik van het zoute eluens verminderd in vergelijking met het “isocratisch” SMB, dat bij constante zoutconcentratie wordt bedreven.

Bij het scheiden van verdunde mengsels van eiwitten in dergelijke gradiënt-SMB’s kunnen azeotropische fenomenen optreden. De verdelingscoëfficiënten van twee eiwitten zijn in verschillende mate afhankelijk van de zoutconcentratie. Bij een bepaalde kritische zoutconcentratie zijn de verdelingscoëfficiënten (in een verdund systeem met lineaire isothermen) gelijk aan elkaar, zodat de componenten niet meer van elkaar kunnen worden gescheiden. Dergelijke azeotropie (“omkering van de selectiviteit”) komt veelvuldig voor bij ionenwisseling van eiwitmengsels. Het gradiënt-SMB werkt alleen naar behoren als alle zout concentraties in het SMB óf boven óf onder de genoemde kritische zoutconcentratie liggen.

Het gebruik van gradiënt-SMBs is uitgewerkt voor de scheiding van een verdunde oplossing van BSA en een gist-eiwit op Q-Sepharose FF bij pH 4.6. De doorzet en het verbruik van het desorbens(volume) en van de hoeveelheid zout zijn geoptimaliseerd. Bij de ontwikkelde optimalisatie-procedure wordt eerst een analytische relatie bepaald tussen de optimale snelheidsverhoudingen van vloeistof en sorbens in alle secties en de zoutconcentraties in het SMB. Hierbij wordt rekening gehouden met azeotropie. Door daaropvolgende numerieke optimalisatie kunnen de optimale zoutconcentraties in de voeding en het desorbens worden vastgesteld. Een voeding die exact de kritische zoutconcentratie heeft waarbij omkering van de selectiviteit optreedt, kan alleen worden gescheiden in een gradiënt waarin alle zoutconcentraties boven die kritische zoutconcentratie liggen. In vergelijking met het isocratisch SMB (zonder gradiënt) kan het verbruik van zowel desorbens-volume als de hoeveelheid zout met drie ordegroottes worden gereduceerd wanneer een gradiënt wordt gebruikt waarin alle zoutconcentraties lager zijn dan de genoemde kritische zoutconcentratie. Het (partieel) hergebruiken van de vloeisof die de top van het SMB (sectie IV) verlaat als desorbens is erg gunstig voor de reductie van zowel zout- als eluensverbruik.

Keukenzout, gebruikt voor de vorming van de gradiënt bij de scheiding van BSA en myoglobine, blijkt te binden aan de ionenwisselaar, Q-Sepharose FF. Deze interactie van zout met de ionenwisselaar moet worden opgenomen in de procedure voor selectie van de snelheidsverhoudingen. Alleen dan is de affiniteit in de top-secties (III en IV) hoger dan in de onderste secties (I en II). Afhankelijk van de richting waarin het zout beweegt kunnen “opwaartse”en “neerwaartse”gradiënten ontstaan. In een “opwaartse gradiënt” wordt het zout voornamelijk met de vloeistof mee naar boven getransporteerd; in een “neerwaartse gradiënt” beweegt het zout voornamelijk met het sorbens naar beneden. Het positioneren van de zoutgradiënt is geïmplementeerd in de op golftheorie gebaseerde ontwerpprocedure. De ontwikkelde procedure is experimenteel geverifieerd.

Bij de selectie van de snelheidsverhoudingen in een gradiënt-SMB voor de scheiding van eiwitten moet aan alle drie de componenten (in ons geval BSA, myoglobine en zout) in alle vier de secties een gewenste bewegingsrichting worden opgelegd. Door de interactie van het zout met de matrix wordt het gebiedje waarin volledige scheiding mogelijk is beperkt ten opzichte van de situatie zonder interactie van zout en matrix. De regeneratie van de matrix in sectie I en de regeneratie van het desorbent in sectie IV zorgen voor extra limieten aan de snelheidsverhoudingen in sectie II en III. Deze additionele voorwaarden zijn geïmplementeerd in de ontwerpprocedure voor het SMB. De in een twaalf-koloms labschaal SMB geobserveerde bewegingsrichtingen kwamen goed overeen met de voorspellingen op basis van de ontwikkelde theorie.

Doordat in een SMB gebaseerd op gelfiltratie minder verdunning optreedt dan tijdens conventionele pulsgewijze kolomchromatografie, kunnen de eiwitconcentraties zo hoog oplopen dat afwijkingen van de doorgaans lineaire gelfiltratie-isotherm optreden. Zowel convexe als concave isothermen worden voorspeld, respectievelijk voor aantrekking en afstoting tussen moleculen. Beide worden beschreven door een evenwichtsmodel dat is gebaseerd op osmotische viriaal-expansie. Een algemene procedure voor de selectie van de snelheidsverhoudingen bij dergelijke scheidingen is ontwikkeld op basis van “triangle theory”. De ontwikkelde methode is bruikbaar voor zowel aantrekkende als afstotende interacties tussen componenten en houdt ook rekening met de azeotropische verschijnselen die door het evenwichtsmodel worden voorspeld. Het effect van de binaire interactie-coëfficiënt op de vorm van het gebied van volledige scheiding is gedemonstreerd aan de hand van een fictief modelsysteem.

Samenvatting bij: “Separation of proteins by simulated moving bed chromatography”,
proefschrift Joukje Houwing, Technische Universiteit Delft (2003).

Dankwoord

En dan eindelijk, na acht jaar, is het proefschrift af! In al die tijd hebben zoveel mensen op hun eigen wijze bijgedragen aan dit onderzoek, dat het onmogelijk is ze allemaal persoonlijk te bedanken. Daarom op deze zeer onpersoonlijke manier: allen hartelijk bedankt voor jullie input; ook al is deze misschien klein geweest, hij is zeer gewaardeerd!

Een aantal mensen heeft zoveel betekend voor het onderzoek, dat ik hen nog in het bijzonder wil noemen.

In de eerste plaats zijn dat de promotoren, Karel Luyben en Luuk van der Wielen, die mij de kans gaven te promoveren. Karels overzicht was zeer plezierig gedurende de eerste jaren van het project. En waar zou dit onderzoek zijn geëindigd zonder Luuks nimmer aflatende stroom van ideeën en zijn blijvend vertrouwen in een goede afloop?

Thomas Jensen, Hugo Billiet en Stef van Hateren, jullie hulp was onmisbaar. Thomas als sparring partner en brein achter het SMB, Hugo als chromatografiespecialist en Stef als experimentator, onvermoeibaar op zoek naar HAE (het alles omvattend experiment), elke AiO mag zich een samenwerking met mensen als jullie wensen.

Het "team" van het project MEP (Meer Efficiënte proceschromatografie) wil ik bedanken voor de prettige samenwerking. Met veel plezier heb ik met Jaap Bosma en Hans Wesselingh, onze Groningse collega's over wetenschap gediscussieerd en de verschillende MEP-cursussen opgezet en gegeven. De leden van de begeleidingscommissie, Gijs van Dedem (Diosynth), John Krijgsman (Gist-Brocades), Ard Tijsterman (Univalid), Wim de Rooij, Wim Bel, Matthijs Dekkers (Unilever), Theone Kon (Amersham Biosciences), Anton Sweere (DMV/Campina), Koen Wouterse, Yvette van Golstein-Brouwers en Anouska Versleijen (Senter) wil ik bedanken voor hun prettige (soms provocerende) input tijdens halfjaarlijkse voortgangsbesprekingen. In één adem wil ik Senter noemen, dat dit project heeft gefinancierd middels het programma IOP-milieutechnologie-preventie.

Veel dank ben ik de werkpaats van het Kluyverlab verschuldigd. Jullie zorgden voor het apparaat om proeven op te doen, en veel goede sfeer in 't lab! Joop Houwers, dank voor het ontwikkelen van de bioscada software.

Aan dit project werkten ook drie afstudeerders, twee research-praktikanten, één BODL-student/TwaiO en één “Birdie”. Freija van der Schot, Jeroen Meewisse, Francine van Dierendonck, Bart van Beek, John Nijenhuis, Linda Jacobs en Dirk Geerts: heel erg bedankt voor alles wat jullie hebben gedaan. Misschien is weinig van jullie werk direct terug te vinden in dit proefschrift, maar het heeft daar zeker aan ten grondslag gelegen!

Een spin-off van het MEP- project was het HSA-project. Jack Pronk, Hans van Dijken, Sander Worst en Erik de Hulster, bedankt voor jullie samenwerking op het gebied van het "groene soepje".

En dan zijn er nog al die mensen die op de achtergrond een hele belangrijke rol speelden in de ups en de downs van dit project. Collega’s van het Kluyverlab, als “smeerolie” (ik noem geen namen om niemand te kort te doen), Heit en Mem, als continue steun in de rug (ook al ging de wetenschap hun boven de pet), Fokje en Preben, als praatpaal (in de breedste zin) en logeeradres, Alco en Rik, als belangrijke hulptroepen in de diepe downs (en nog veel meer)…

Bedankt allemaal!

Curriculum Vitae

Joukje Houwing werd op 17 september 1971 geboren in Gorredijk. Na haar atheneum-opleiding, gevolgd aan het Drachtster Lyceum in Drachten, studeerde zij scheikunde en technische scheikunde aan de Rijksuniversiteit Groningen. Tijdens haar eerste afstudeeronderzoek in de vakgroep milieubiotechnologie bestudeerde zij de cometabole afbraak van trichlooretheen en tolueen door *Pseudomonas cepatia* G4. In haar tweede afstudeeronderzoek maakte zij kennis met het (opschalen van) chromatografie bij het Unilever Research Laboratorium in Vlaardingen.

In 1994 begon zij met het in dit proefschrift beschreven promotieonderzoek aan de Technische Universiteit Delft. Vier jaar later werd zij wetenschappelijk onderzoeker bij NIZO Food Research te Ede, waar zij onder andere. werkte aan membraanscheidingen en electromembraanfiltratie. In 2001 keerde zij terug naar de Technische Universiteit Delft, waar zij als postdoc onderzoek verrichtte naar de scheiding van bioactieve peptiden uit eiwithydrolysaten met behulp van Simulated Moving Bed Technologie op basis van gelfiltratie. Sinds juni 2002 is zij werkzaam als bioprocesspecialist influenza bij Solvay Pharmaceuticals in Weesp, waar zij zich onder andere bezig houdt met (chromatografische) scheidingsprocessen.

Publicaties

Mars, A.E., J. Houwing, J. Dolfing and D.B. Janssen, "Degradation of toluene and trichloroethylene by *Burkholderia cepacia* G4 in growth-limited fed-batch culture," *Appl. Environ. Microbol.*, **62**, 886 (1996).

Houwing, J., K.Ch.A.M. Luyben, and L.A.M. van der Wielen, "Development of large scale purification process for recombinant HSA using SMB technology," *Proc. A.I.Ch.E. Annual Meeting, Los Angeles* (1997).

Houwing, J., H.A.H. Billiet, J.A. Wesselingh and L.A.M. van der Wielen, "Azeotropic phenomena during separation of dilute mixtures of proteins by simulated moving bed chromatography," *J. Chem. Technol. Biotechnol.,* **74**, 213 (1999).

Houwing, J., G. Bargeman, I. Recio, M.P.J. Dohmen-Speelmans, D.J.J. Stoffels and H.C. van der Horst, "Electro-membrane filtration for selective isolation of peptides, " In: *Proc. "Conference on electro-membrane processes and bipolar membranes, Twente*", 52 (2000).

Houwing, J., S.H. van Hateren, H.A.H. Billiet and L.A.M. van der Wielen, "Effect of salt gradients on the separation of dilute mixtures of proteins by ion-exchange in simulated moving beds," *J. Chromatogr. A,* **952**, 85 (2002).

Houwing, J., H.A.H. Billiet and L.A.M. van der Wielen, "Optimization of azeotropic protein separations in gradient and isocratic ion exchange simulated moving bed chromatography," *J. Chromatogr. A,* **994**, 189 (2002).

Bargeman, G., J. Houwing, I. Recio, G.H. Koops and H.C. van der Horst, "Electro-membrane filtration for the selective isolation of bio-active peptides from an α_{s2}-casein hydrolysate," *Biotechnol. Bioeng.,* **80**, 599 (2002).

Houwing, J., H.A.H. Billiet and L.A.M. van der Wielen, "Mass transfer effects during separation of proteins in SMB by size exclusion," *A.I.Ch.E. J.,* **49**, 1158 (2003).

Houwing, J., T.B. Jensen, S.H. van Hateren, H.A.H. Billiet and L.A.M. van der Wielen, “Positioning of salt gradients in ion exchange SMB,” *A.I.Ch.E. J.*, **49**, 665 (2003)

T.B. Jensen, S.H. van Hateren, J. Houwing, H.A.H. Billiet and L.A.M van der Wielen, “Experimental Validation of Gradient Elution in SMB Chromatography,” Chapter 3 in: *“Gradient SMB chromatography”*, Ph-D thesis T.B. Jensen, Delft University of Technology (2003).

populair-wetenschappelijk:

Houwing, J. and L.A.M. van der Wielen, “Theoretische modelvorming moet proceschromatografie efficiënter maken,” *Chemisch magazine,* **11,** 423 (1998).

Bargeman, G., J. Houwing, M. Dohmen, M. Frank, A. Zwijnenburg and M. Wessling, “Capillaire membranen maken proceswaterhergebruik goedkoper,” *NPT procestechnologie*, **4**, 7(2001).

Houwing, J., G. Bargeman, M. Dohmen and H.C. van der Horst, “Bio-actieve ingrediënten goedkoper isoleren,” *Voedingsmiddelen technologie* **9**, 23 (2001).

Houwing, J., R. Jonker, G. Bargeman, J.G. van Doorn, M.A. Janssens, M. Dohmen-Speelmans and H.C. van der Horst, “Ontzouten en concentreren van carboxymethylinuline (CMI) met nanofiltratie”, *NPT procestechnologie* **3**, 23 (2001).

Bargeman, G., G.-H. Koops, J. Houwing, I. Breebaart and H.C. van der Horst, “The development of electro-membrane filtration for the isolation of valuable charged components,” Chemie Ingenieur Technik, **74**, 639-640.